THE UNIVERSITY OF CHICAGO

POWER SERIES CORRECTION TO SINGLE PARTICLE ELECTRON GREEN'S FUNCTION: APPLICATION TO 1D HOLSTEIN CHAIN

A DISSERTATION SUBMITTED TO
THE FACULTY OF THE DIVISION OF THE PHYSICAL SCIENCES
IN CANDIDACY FOR THE DEGREE OF
DOCTOR OF PHILOSOPHY

DEPARTMENT OF PHYSICS

BY
BIPUL PANDEY

CHICAGO, ILLINOIS
JUNE 2023

Dedication Text

To my wife Khushboo, my brother Biraj, and my parents Madhav and Gita. You are the wind behind my sails.

"Man's reach should exceed his grasp." - Robert Browning

TABLE OF CONTENTS

LIST OF FIGURES

ACKNOWLEDGMENTS

This manuscript is based on my research at the University of Chicago for my doctoral degree. First and foremost, I would like to heartily thank my advisor Peter B. Littlewood for giving me the opportunity, time, guidance, and encouragement to pursue this project. Your endless supply of encouraging words and nuggets of wisdom have helped me become not just a better scientist but also a better human being.

I would also like to thank my family and friends who have been by my side through this journey. Firstly, to the love of my life - my wife Khushboo, whom I met right before I started this journey - this truly would have been impossible without your patient and kind words on days when everything seemed to go awry. It is truly a privilege to have you by my side. My parents and my brother - I will never be able to thank you enough for bestowing me the privilege to pursue a non-conventional career path and cheering me on every step along the way. My roommates of 6 years - Ankur, Suhail, and Shobhit, I am glad we started our Ph.D. journeys together and I am glad we are ending our journeys together on a high note. I couldn't have asked for a better Chicago family than you all. Suhail Rehman, my roommate of six years and a dear friend, deserves a special mention for teaching me the basic principles of clean and efficient coding during his own adventures with Ph.D. in computer science.

Finally, I want to thank numerous friendly faces I have met during conferences, on GCIS and KPTC hallways, at Physics Department coffee hours, and at campus social events. Explaining my science and hearing yours helped me tremendously in crystallizing my arguments. Lastly, all of the errors in this manuscript are solely my doing. After all, to err is human.

ABSTRACT

Electrons in materials undergo numerous complex interactions among themselves, the external fields, as well as the constituent atomic lattice. The strength of such many-body interactions depends on various factors such as the electronic configuration of the host material, the presence of doping and defects, spins of carrier and lattice elements, etc. In the thermodynamic limit, these interactions are often treated as bosons that interact with the electrons in the system and manifest as side bands (replicas or satellites) in the electronic band structure seeping spectral weight and renormalizing the band structure obtained from purely electronic calculations.

In ab-initio calculations, when the strength of such electron-boson interaction is weak, it is not only justified to neglect these interactions completely but also pragmatic for reasons ranging from tractability to associated computational cost. This is because the effect of electron-boson interaction is minute compared to the electronic energy scale of the problem. However, in many systems, especially organic semiconducting materials, the bosonic vibrations (stretching modes) of the molecule are strongly coupled with the electron. Furthermore, the bosonic energy scale is comparable to the electronic energy scale in these problems. Hence, neglecting the effect of electron-boson interactions in electronic spectra in such systems is myopic at best and catastrophic at worst.

In the context of a single electron two orbital Holstein system coupled to dispersionless bosons, we develop a general method to correct single-particle Green's function and electronic spectral function using an integral power series correction (iPSC) scheme. We then outline the derivations of various flavors of cumulant approximation through the iPSC scheme and explain the assumptions and approximations behind them. Finally, we compute and compare iPSC spectral function with cumulant and exact diagonalized spectral functions and elucidate three regimes of this problem - two that cumulant explains and one where cumulant fails. We find that the exact and the iPSC spectral functions match within spectral broadening

across all three regimes.

In order to scale our method to large systems, we then develop an ODE-based Power series correction(dPSC) formalism that goes beyond the cumulant approximation. We implement it to a 1D Holstein chain for a wide range of coupling strengths in a scalable and inexpensive fashion at both zero and finite temperatures. We show that this first differential formalism of the power series is qualitatively and quantitatively in excellent agreement with exact diagonalization results on the 1D Holstein chain with dispersive bosons for a large range of electron-boson coupling strength. We also investigate carrier mass growth rate and carrier energy displacement across a wide range of coupling strengths. We also present a faster second differential formalism which is very much similar to self-consistent cumulant formalism. We show the regime where this method is applicable and where it diverges. Finally, we present a heuristic argument that predicts most of the rich satellite structure without explicit calculation.

CHAPTER 1

OVERVIEW: WHY ARE WE DOING WHAT WE ARE DOING

From the advent of the telegraph in the 1830s to the smartphones on everyone's hands today, moving electrons reliably from one point to another is a theme that has constantly driven and defined our modern world for the past 200 years. We first learned to communicate through telegraphy over long distances by moving electrons across the Atlantic. Then we learned to make it carry and disperse energy in filament bulbs (1879) and light our world at night. After vacuum tubes were invented (1904), we even learned to hold and process information by manipulating the flow of electrons. Many such adventures in taming the electron inside different materials and making it move on demand gave rise to the quantum revolution, the electronic age, and finally the current information age. So, have we understood all that is to be understood about moving electrons? The answer is far from a resounding 'Yes'. Given the variety of materials, the astronomical numbers of moving components (electrons, nuclei, defects, and external fields), and the interactions these moving components have amongst each other, understanding electronic motion, its energy-carrying limits and its reliability in doing so in any material is a Herculean task. So, we need to temper down our ambition and ask a little more specific questions.

1.1 The Quantum Many-Body Problem.

Given that moving electrons (or holes) from one part to another part of some material (say circuitry of a device) is at the heart of most electronic devices, our goal at the end of the day is to understand the effect the entire universe on this target electron (or hole) in question. For now, we will be satisfied with the entire universe being composed of a perfect lattice of this host material. Furthermore, we can construct a better framework for this problem by dividing this question into three sub-questions:

- What is the effect of electrons on electrons?
- What is the effect of everything else on everything else
- What is the effect of everything else on electrons?

Since this is a quantum mechanical problem and knowing the eigen-spectrum (wave functions and energy) of the total Hamiltonian is the first (and the most complicated) step in knowing every property of the carrier, we begin our journey by sketching a total Hamiltonian in terms of the three questions asked above.

$$H_{tot} = H_{el-el} \quad + H_{eth-eth} \quad + H_{el-eth} \tag{1.1}$$

Here, the first term on the right H_{el-el} captures the effect of electrons-electrons interactions (carrier-carrier interaction in general). The second term $H_{eth-eth}$ captures the effect of everything else (eth) on everything else. And finally, the last term H_{el-eth} captures the effect of electron (el) interacting with everything else (eth) and vice versa.

We understand how two electrons interact with each other. And therefore we assume for the sake of this thesis the electron-electron interaction problem, although a many-body problem of enormous complexity, is solvable. This is a reasonable thing to do because of the machinery built by the ab-initio community to solve this class of problems. There are methods ranging from simple tight-binding model-like theories to density functional theory to wave function-based methods that have been tried and tested to solve this electronic problem successfully on many classes of materials.

1.2 System's response = Collective Modes

But even after assuming that this electron-electron problem is solvable, we are left with a seemingly impossible task. We have chosen to sweep the complexity of the entire system

modulo the electrons by calling them "everything else". But given the number of moving parts, the variety of ways they can move, and the variety of materials, solving in detail to understand this effect on the carrier seems Sisyphean even with the aid of the most powerful computers. Therefore, rather than taking this detail-oriented approach which is impossible anyway, we take a different route by redefining what "everything else" means in our problem.

Since the interactions in these quantum systems are probabilistic anyway, it doesn't make sense to account for the detail of every single interaction of the lattice elements with the electrons. We want to study only those effects which happen in a statistically significant amount. The first of such effects one encounters when building a many-body electronic system from scratch is the plasmon in the jellium Hamiltonian. Jellium, simply put, is a gas of electrons kept in a box with an equal uniform positive charge smeared in the backdrop so that the box as a whole remains electrically neutral. Here, the oscillation of plasma (the electron gas) can be bosonized and looked at as a collective motion of the system. The target electron, in this case, interacts with this quantized collective mode- termed plasmon (1) and, behaves differently than a free electron depending on how strong the coupling between the plasmon and the electron is.

Similarly, in crystals where the nuclei are bound to the lattice site with a "spring-like" harmonic force, the motion of electron through the crystal can cause the nuclei to start vibrating as a response to the attractive force between the negative charge of electron and the positive charge of nuclei. These bosonic vibrations termed phonons in turn modify the ambient environment of the electron usually making it harder to drive the electron through the system. In extreme cases, they can even localize the electron completely, screen its long-range effects and transmute it into a phonon-electron hybrid particle called 'polaron'. Another example where phonon plays a crucial role is in superconductivity where the dynamics of two electrons separated by large distances (10-100 nm) are strongly correlated through the vibrations of the ambient lattice. These electron pairs, termed Cooper pairs,

are at the heart of the BCS theory of superconductivity.

In crystals of quantum magnets (atoms or molecules with non-zero spin angular momentum), the passage of electron can cause oscillations of these quantum magnets about their lattice sites. These oscillations conspire with each other to form another type of long-ranged collective mode called a magnon- the elementary spin wave. These bosonic spin waves have been shown to interact with and shorten the lifetime of charge carriers in the material as well as produce novel features in the band structure (2; 3).

1.3 (Why) Are Collective Modes Important?

It has been established through experiments that electrons (or holes) in a solid suffer dynamical scattering from aforementioned collective modes (e.g. phonons, magnons, and plasmons)(4; 2; 5). These scattering processes have been shown to renormalize the carrier(electron or hole) particle's energy, effective mass, and lifetime transmuting this particle into a quasiparticle. An analogy of this is presented in figure 1.1. Another hallmark of carrier-boson coupling is the presence of satellite shake-offs in the electronic spectra(6). These satellites drain spectral weight from the quasiparticle and somewhat resemble the quasiparticle band structure. Hence they are also termed replica bands.

However, these collective modes are often overlooked in the ab-initio modeling of materials. And in many cases, there are good reasons for it. Oftentimes, the electronic part of the problem takes the front seat in governing macroscopic material properties. These bosonic collective excitations of the system merely result in small corrections to the carrier properties.

Hence, they take a back seat regardless of their origin (plasma oscillation, spin waves, molecular stretching, etc). In such systems, it is not only justifiable but also pragmatic to take into account only the electronic part of the problem in modeling and predicting material properties such as the effective mass of the carrier, energy levels, lifetimes, etc. This is

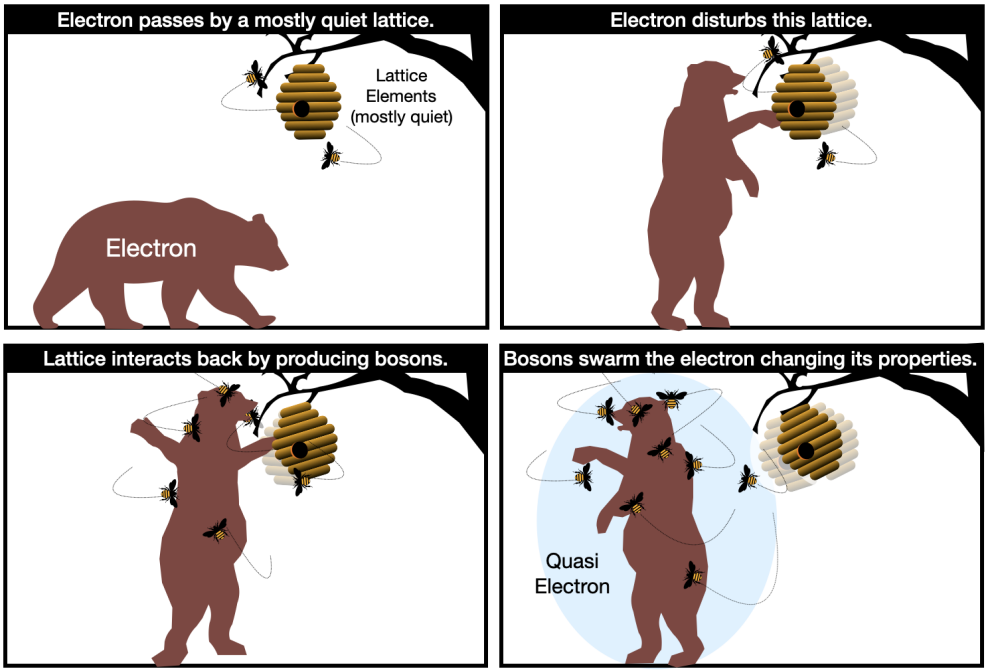

Figure 1.1: Electron perturbs the lattice while moving through it. The lattice interacts back by dressing the electron with boson cloud, turning it into a quasi-electron and changing its properties.

because of the associated overhead cost of incorporating bosonic degrees of freedom which are extremely expensive but ultimately insignificant in the actual system and predictions thereof. For this reason, the development of efficient and accurate methods to handle electronic problems has been a topic of great interest for more than half a century. This has led to the development of myriads of methods from families of Density functional-based methods (7; 8) to families of Green's function-based methods such as GW (9; 10) that have proven their worth in computing the charged electronic excitation spectra and predicting properties across a wide variety of materials.

Although at very weak coupling the quasiparticle renormalization due to the collective modes is negligible, with stronger coupling a proportional renormalization of the quasiparticle occurs. Hence forgetting about the collective mode outside of the very weak coupling limit can lead to erroneous electronic band structure and incorrect predictions of material properties. To handle the weak carrier-boson coupling limit when the bosonic corrections

to the carrier are small, non-self-consistent post-processing methods called cumulant expansions (11; 12; 13; 14) have been developed that wrap around GW methods and produce bosonic satellites at roughly the right energy. In recent years, this has proven successful in incorporating plasmonic as well as phonon effects in the electronic band structure. However, cumulant methods are *ad hoc* by construction and it has been shown that attempts to incorporate higher order corrections or introduce self-consistency in cumulant-based methods result in divergence or artifacts (15; 16) of the correction function. On the other hand, going the route of Monte Carlo approach (17) or any basis-dependent method like exact diagonalization (18), coherent basis expansion (19), although stable, is extremely expensive and thus unscalable to large systems.

There are physical systems where the coupling is not small. As an example, in photoemission spectra of strontium titanate, this coupling manifests as a significant shift in quasiparticle energy, a significant decrease in lifetime and intensity of quasiparticle features, strong shake-off features, as well as a strong carrier mass enhancement (20; 21; 22; 23; 24). Strong electron-phonon coupling is also visible in electronic spectra in metallic cuprates (25; 26) and the metal-insulator transition in undoped cuprates (27), and other correlated metals, for example, $FeSe/SrTiO_3$ epitaxial layers (28).

Recent advances in organic (polymeric) semiconductors such as poly(3-hexylthiophene) (P3HT) (29; 30; 31) show that, in these long-chain systems with vibrational modes (stretching) encompassing huge numbers of sites, bosonic effects on the carrier are significant for two reasons. Firstly, these bosonic stretching modes themselves are highly energetic in nature with energies (0.2 eV in P3HT) comparable to electronic energy scale (0.6 - 1 eV in P3HT). Secondly, these modes are strongly coupled to the electronic degrees of freedom (32). This has also been observed in proteins (33; 34; 35) where the electronic degrees of freedom and the collective modes are intimately intertwined. Strong electron phonon coupling is also observed in correlated metals such as cuprates (26; 27; 36), the iron pnictide

high-temperature superconductors (37; 38), the colossal magneto-resistance manganites, and nickelates (39; 40; 41).

At extreme values of coupling constant, strong electron-boson coupling can completely self-trap (25) and localize electrons creating polaronic states. This severely modifies carrier mobility in the material, and is of particular interest in material design for photovoltaics and electronics (42; 43; 44). Sometimes such large electron-phonon coupling conspires with strong correlation physics to produce metal-to-insulator or metal-to-bad metal phase transitions.

In calculations, the interaction strengths between collective excitations and particles are modeled as tunable electron-boson coupling parameters. In experiments, this coupling tunability is achieved by introducing doping and defects (22; 45). This fine control over doping has allowed for the advent of plasmonic devices (46; 47; 43) where plasmons (plasma oscillations) and their coupling to the carrier is leveraged for tasks ranging from sensing to energy capture and harvest. Another recent advent is the field of phonovoltaics (48; 49) where the carriers excited after gulping modulated phonon quanta are collected and used for energy generation. At extreme values of carrier-boson coupling, the carrier becomes strongly self-trapped and localized creating polaronic states with properties very different than free carriers(50; 4).

Finally, in the presence of multiple boson species, there can be competition between their effect on the carrier which creates novel phase crossovers in materials (50). A proper understanding and quantification of the effects of collective modes on charge carriers is vital in understanding and designing novel materials with useful engineering applications. Therefore focusing solely on the electronic problem in these systems is myopic at best and catastrophic at worst because of the strong modulation of carrier's energy levels, mobility, masses, and lifetimes by bosons.

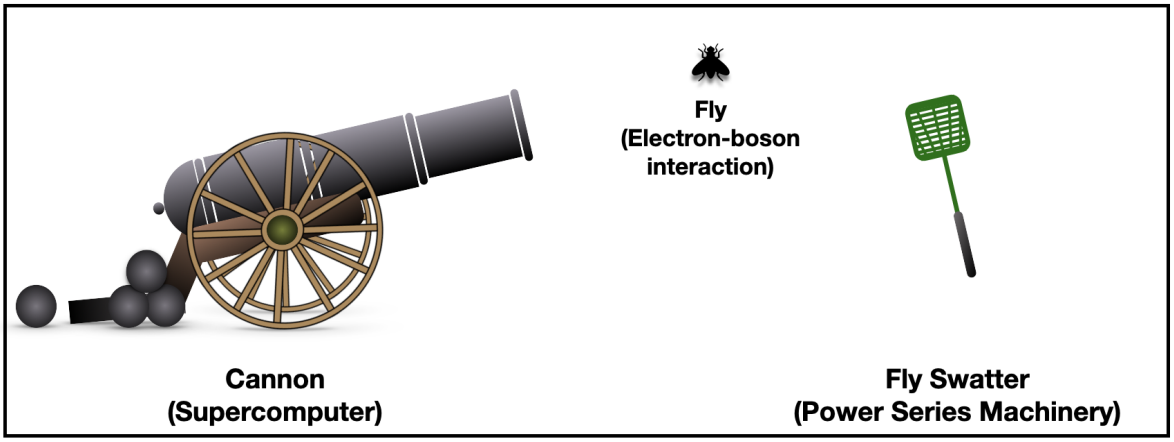

Figure 1.2: What is the best way to kill the fly? A) Cannon? B) Fly Swatter?

1.4 Goal of This Thesis

The work presented in this thesis is based on the two papers we have written (51; 52) and talks we have given during the March meetings 2021, 2022, and 2023. We hope that by now we have convinced the reader that often times the collective modes strongly modify the electronic properties inside a material. Regardless of the origin of these modes, they follow Bose-Einstein statistics and hence can be treated as baths of bosons. Our goal, in general, is to include the effect of these bosons in the electronic spectra. One can always use a cannon to kill a fly. But is it necessary? Or can we just use a fly swatter instead? Given the speed and storage of modern supercomputers, a mindless approach (*the cannon*) to this is to throw the problem into a supercomputer, let it simulate the system in time, and wait for the result. But there are drawbacks to this approach. This is an inherently slow and really expensive calculation because of the sheer number of particles (electrons and bosons) and therefore dynamical equations involved in the system. Furthermore, this is a very opaque calculation with no intuition and insight gained as to what is happening in the system unless the one running the calculation is also the one who wrote the entire algorithm. And even then, it is not immediately clear which physics (electronic, bosonic, or interaction) is dominant in the system. And after days of calculation, it might turn out that bosons just do not play a

significant role in the system in question.

Our approach will be different in the sense that we will take two separate physics(spectra) - the non-interacting electronic and the bosonic. We will consider that the best starting picture is the non-interacting electronic physics. Then we will self-consistently sprinkle the bosonic physics (*the fly*) over the electronic physics (electronic spectra) through power series machinery (*the fly swatter*) that we construct. This is a much more transparent way of solving this many-body problem as we can literally compare the properties of a final interacting electronic system to the non-interacting electronic system and gauge the effect of bosons firsthand.

At extreme coupling between electrons and bosons, our approach obviously breaks down. This is because we have started with an assumption that the appropriate starting picture is the non-interacting electronic physics which no longer remains true. In such cases, one often resorts to using a different formalism altogether. This is a case we will not discuss in this thesis. But we hypothesize that a similar power series-based treatment is possible where we correct the bosonic physics by self-consistently sprinkling the electronic physics.

CHAPTER 2

THE 1D HOLSTEIN CHAIN

2.1 The Holstein Chain

Consider a single (or many independent electrons) hopping around in a one-dimensional chain of N vibrating atomic sites with inter-site distance 'a'. The vibration of the sites (vibrons or phonons) are bosonic in nature and are coupled to the electron. Thus the electron can be thought of as being submerged in a bath of bosonic vibration at the site where it is located. We take this chain and glue together the ends to construct a periodic (Born-von Karman) system in order to have correspondence with perfectly crystalline systems. In this thesis, we are especially interested in the case of $N = 2$ - the Holstein dimer and the limit of $N \to \infty$ case - the 1D Holstein chain.

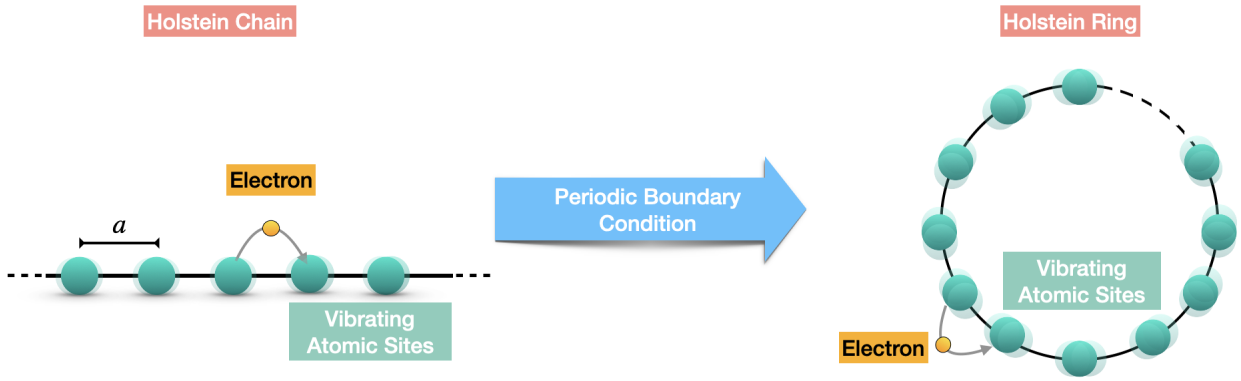

Figure 2.1: Holstein chain to Holstein Ring transformation through the use of periodic(Born-von Karman) Boundary condition

2.2 Why Holstein Hamiltonian?

2.2.1 1D Holstein Hamiltonian- a Perfect Proving Ground

Given that this Hamiltonian has a clear electronic part and a clear bosonic part both of which are clear, simple, and exactly solvable, and a complicated electron-boson interaction part which is creating the mixing of states, the 1D Holstein Hamiltonian provides a perfect proving ground to construct, test and benchmark approximation schemes. Furthermore, once in second quantized form, all of the details of the origin of electronic as well as bosonic degrees of freedom neatly get absorbed into the energy scales associated with the problem. Therefore, the general problem then becomes agnostic of the details of the electronic and the bosonic physics in the system allowing us to construct a method general enough to take into account electron-boson physics for technically any type of boson- be it plasmon, phonon, vibron, magnon, etc. What matters then is the energy scales associated with each of the three pieces and we can smoothly tune this Holstein system from regimes where the electron-boson interaction is negligibly small to regimes where it is the dominant physics. This allows us to systematically test the foundational assumptions we have made to construct our machinery and pin-point regimes where our method is exact to regimes where our method breaks down.

Another reason why Holstein Hamiltonian is a perfect candidate is that we can systematically access the exact energies of the interacting system through an exact diagonalization procedure in a finite boson basis even though there is no exact analytical solution. Doing so not only helps validate our method but also gives us a sense of how resource efficient and fast our method is compared to this standard technique.

2.2.2 1D Holstein Hamiltonian in Real Systems

As discussed in the previous chapter, the 1D Holstein chain is the model Hamiltonian to study organic semiconductors such as poly(3-hexylthiophene) (P3HT) and proteins (32). In

these long chained systems with vibrational modes (molecular stretching) encompassing a huge number of sites, the bosonic modes themselves are highly energetic (0.2 eV in P3HT) and almost comparable to the carrier's energy scales(0.6 - 1 eV in P3HT). On top of this, there is also a strong coupling between the carrier and the bosonic modes. Because of these two reasons, a proper accounting of the effect of electron-boson interaction on the overall physics of the interacting system must be done. Therefore, this whole study is more than an exercise in method building and the results shown in this thesis are a stepping stone to modeling and understanding the physics in these real systems.

2.3 Quick Primer on Second Quantization:

In order to motivate further discussion, we quickly introduce the concept of second quantization. This section is meant to serve only as a refresher to the main idea necessary for us in the later section and is not intended to be a substantial resource to understand second quantization. We direct the reader to references that treat this topic more thoroughly (53; 54; 55).

The main reason why the second quantization technique was introduced is because of the inability of the first quantization formalism to change particle number. Furthermore, in the second quantization, the detailed mechanism of the problem also gets packaged nicely into the energy scales of the problem, and therefore, many problems which differ in details of their mechanism in the first quantization boil down to the same class of problem. This is especially true in our case where we intend to create a method that is agnostic of the individual fermionic and bosonic mechanisms in the system. With this in mind, we introduce the creation and annihilation operators (ladder operators) which respectively create and destroy particles in a system by mapping between Hilbert spaces ($\mathcal{H}$) of different particle

numbers$(N, N-1)$.

$$\begin{aligned} \hat{c}_i^\dagger \quad &: \mathcal{H}(N-1) \rightarrow \mathcal{H}(N) \\ \hat{c}_i \quad &: \mathcal{H}(N) \qquad \rightarrow \mathcal{H}(N-1) \end{aligned} \tag{2.1}$$

Here, $\hat{c}_i^\dagger$ creates a particle at some site 'i' thereby mapping the $(N-1)$ particle Hilbert space $\mathcal{H}(N-1)$ to a N particle Hilbert space $\mathcal{H}(N-1)$. Similarly, $\hat{c}_i$ destroys a particle at some site 'i' thereby mapping the N particle Hilbert space $\mathcal{H}(N)$ to a $(N-1)$ particle Hilbert space $\mathcal{H}(N-1)$. For our purposes, we use $\hat{c}^\dagger/\hat{c}$ for fermion ladder operators and $\hat{b}^\dagger/\hat{b}$ for boson ladder operators. The main difference between these fermionic and bosonic ladder operators is their commutation relation due to the symmetry constraints on their respective many-body wave-functions under particle exchange - i.e fermion many-body wave-functions are anti-symmetric and boson many-body wave-functions are symmetric under two particle exchange. For example, in site basis where i and j represent i^{th} and j^{th} atomic sites the non-zero fermion anti-commutation relation and the non-zero boson commutation relation are as follows:

$$\begin{aligned} \{\hat{c}_i, \hat{c}_j^\dagger\} &= \hat{c}_i\hat{c}_j^\dagger + \hat{c}_j^\dagger\hat{c}_i = \delta_{i,j} \quad \text{Anti-commutation relation for fermions} \\ [\hat{b}_i, \hat{b}_j^\dagger] &= \hat{b}_i\hat{b}_j^\dagger - \hat{b}_j^\dagger\hat{b}_i = \delta_{i,j} \quad \text{Commutation relation for bosons} \end{aligned} \tag{2.2}$$

All other fermion anti-commutation relations are zero and similarly, all other boson commutation relations are zero. Finally, we review the conversion of first-quantized operators to second-quantized operators in many-body Hamiltonians. Mainly, we are concerned with the conversion of first quantized single particle and local two-particle operators but extension to higher order operators follows naturally. Then any operator $(\hat{\mathcal{O}})$ that is a sum of operators acting only on the coordinates of a single fermion (or boson) is called a single particle operator. A good example of this is the total kinetic energy operator in the many-body Hamiltonian which just is the sum of the individual kinetic energy operators of the constituent fermions and bosons. An operator $(\hat{\mathcal{V}})$ that is a sum of operators acting on the

coordinates of two different particles is called a local two-particle operator. The term "local" here means that the action of this operator depends only on the coordinates involved and not on any other hidden third coordinate. A good example of this type of operator is the total Coulomb potential energy which is a sum of two-particle Coulomb potential energies in the system.

$$\begin{aligned} \hat{\mathcal{O}} &= \sum_{m=0}^{N} \hat{O}(\vec{x}_m) && \text{Single Particle Operator} \\ \hat{\mathcal{V}} &= \sum_{\substack{m,n=0 \\ m\neq n}}^{N} \hat{V}(\vec{x}_m, \vec{x}_n) && \text{Local two particle Operator} \end{aligned} \tag{2.3}$$

Suppose we have some appropriate and complete single particle basis set $\{\phi_i \to |i\rangle\}_{i=1}^{\infty}$. Here the word "appropriate" signifies the ease of use in practical implementation - i.e. a basis set that diagonalizes some repeating single-particle motif of the system. But in theory, any complete basis set works. Then, using this basis set, these operators in equation 2.3 can be expressed in second quantization as:

$$\begin{aligned} \hat{\mathcal{O}} = \sum_{m=0}^{N} \hat{O}(\vec{x}_m) &= \sum_{i,j}^{\infty} \langle i| \hat{O} |j\rangle \hat{c}_i^{\dagger} \hat{c}_j \\ \text{where, } \langle i| \hat{O} |j\rangle = O_{ij} &= \int \phi_i^*(\vec{x}) \hat{O}(\vec{x}) \phi_j(\vec{x})\, d\vec{x} \end{aligned}$$

$$\begin{aligned} \hat{\mathcal{V}} = \sum_{\substack{m,n=0 \\ m\neq n}}^{N} \hat{V}(\vec{x}_m, \vec{x}_n) &= \sum_{i,j,k,l}^{\infty} \langle i,j| \hat{V} |k,l\rangle \hat{c}_i^{\dagger} \hat{c}_j^{\dagger} \hat{c}_k \hat{c}_l \\ \text{where, } \langle i,j| \hat{V} |k,l\rangle = V_{ijkl} &= \iint \phi_i^*(\vec{x}) \phi_j^*(\vec{y})\, \hat{V}(\vec{x},\vec{y})\, \phi_k(\vec{x}) \phi_l(\vec{y})\, d\vec{x} d\vec{y} \end{aligned} \tag{2.4}$$

Similar transformations hold true for bosonic single and two-particle operators.

2.4 Derivation of 1D Holstein Hamiltonian - First Quantization

2.4.1 The Electronic Hamiltonian: Tight Binding Model

We start our discussion with a single ionic site single electron system - a basic model of a mono-electronic atom (Hydrogen atom). Given that the electronic mass(m) is much smaller than the nuclear mass(M), we assume that in this otherwise blank universe with a single Hydrogen atom, the nucleus due to its heaviness is static (or it moves at a time scale much slower) compared to the electron. Thus, the Hamiltonian for this simple system consists of the kinetic energy (T) term of the electron at position vector ($\vec{r}$) from the nucleus and a coulomb potential energy(U) term due to the attractive interaction between the nucleus and the electron. We furthermore assume that we have solved for the eigenvectors (atomic wave functions $\left|\psi^{(n)}\right\rangle$) and the eigenvalues (atomic energy levels ϵ_n) of this system.

$$\begin{aligned} H_{at} = T + U(\hat{r}) \ &= \frac{\hat{p}^2}{2m} + U(\hat{r}) \\ H_{at}\left|\psi^{(n)}\right\rangle = \epsilon_n \left|\psi_n\right\rangle \qquad &\forall n \in \mathbb{Z} \end{aligned} \tag{2.5}$$

So far, nothing interesting has happened in this universe. So with the knowledge of the atomic energy levels and atomic wave functions, we go forward to a universe where we have a lattice ring of N such identical Hydrogen nuclei with lattice constant a with a single electron free to hop around as shown in figure 2.1. We will still assume that these atomic sites are static (Born-Oppenheimer Approximation) due to the fact that $M \gg m$. This chain's Hamiltonian (H_c) now was N separate electron-nucleus potential energy terms because of the N different nuclei. We can also nucleus-nucleus Coulomb interaction terms. But since we have physically pinned the nuclei into the underlying lattice, such terms will only add a

constant to the Hamiltonian and thus will be ignored for the current discussion.

$$H_c \quad = T + \sum_{i=1}^{N} U_i(\hat{r}) \quad = \frac{\hat{p}^2}{2m} + \sum_{i=1}^{N} U_i(\hat{r}) \tag{2.6}$$

We now want to construct the ground state of this problem. Armed with the intuition that in the limit of $a \to \infty$, where each nucleus is infinitely far away from any other nucleus, the electron has to pick one nucleus and localize around it to form an "atom" with the Hamiltonian given by 2.5, we postulate that we can construct a ground state wave function ($\left|\Psi_g\right\rangle$) with energy eigenvalue E_o for this system using a linear combination of atomic ground state orbitals ($\left|\psi_i^{(o)}\right\rangle \equiv |i\rangle$) for each atom i. This is the famous **Linear Combination of Atomic Orbitals** (LCAO) method (56).

$$\begin{aligned} \left|\Psi_g\right\rangle &= \sum_{i=1}^{N} a_i \left|i\right\rangle \\ H_c \left|\Psi_g\right\rangle &= E_o \left|\Psi_g\right\rangle \end{aligned} \tag{2.7}$$

Here, a_i are coefficients to be determined and we don't know E_o yet. But we know that if $\left|\Psi_g\right\rangle$ indeed is the ground state, it should have the lowest possible energy eigenvalue. Variationally, this means that, given any general state $|\Phi\rangle$ of this system,

$$\begin{aligned} & E_o \leqslant \frac{\langle\Phi| H_c |\Phi\rangle}{\langle\Phi|\Phi\rangle} \qquad \text{with equality only when } |\Phi\rangle = \left|\Psi_g\right\rangle \\ \text{i.e. } & E_o \left\langle\Psi_g|\Psi_g\right\rangle = \left\langle\Psi_g\right| H_c \left|\Psi_g\right\rangle \\ & E_o \Big[\sum_{i,j}^{N} a_i^* a_j \langle i|j\rangle \Big] = \Big[\sum_{i,j}^{N} a_i^* a_j \langle i| H_c |j\rangle \Big] \end{aligned} \tag{2.8}$$

We get the last expression above by substituting $\left|\Psi_g\right\rangle$ from equation 2.7 into 2.8. Finally,

after some redefinition we get the following equation.

$$\begin{aligned} \langle i|j\rangle \equiv S_{ij} \quad \text{and} \quad \langle i|\, H_c\, |j\rangle \equiv H_c^{ij} \quad \text{, we get:} \\ E_o \sum_{i,j}^{N} a_i^* a_j S_{ij} = \sum_{i,j}^{N} a_i^* a_j H_c^{ij} \end{aligned} \tag{2.9}$$

The overlap integral S_{ij} with $S_{ii} = 1$ accounts for the fact that the individual atomic orbitals centered around nuclei i and j might not be perfectly orthogonal to each other and could have regions of overlap which are especially relevant for nearby nuclei as in the limit of small lattice constant a. Since we are looking for a_l and a_l^* that minimize E_o, we proceed by setting the partial derivative of E_o with respect to these coefficients as zero.

$$\begin{aligned} \frac{\partial}{\partial a_l^*}\Big[E_o \sum_{i,j}^{N} a_i^* a_j S_{ij}\Big] &= \frac{\partial}{\partial a_l^*}\Big[\sum_{i,j}^{N} a_i^* a_j H_c^{ij}\Big] \qquad \forall l \\ \frac{\cancel{\partial E_o}^{\,0}}{\cancel{\partial a_l^*}}\Big[E_o \sum_{i,j}^{N} a_i^* a_j S_{ij}\Big] + E_o\Big[\sum_{i,j}^{N} \frac{\cancel{\partial a_i^*}^{\,\delta_{il}}}{\cancel{\partial a_l^*}} a_j S_{ij}\Big] &= \sum_{i,j}^{N} \frac{\cancel{\partial a_i^*}^{\,\delta_{il}}}{\cancel{\partial a_l^*}} a_j H_c^{ij} \\ \therefore E_o \sum_{j}^{N} a_j S_{lj} &= \sum_{j}^{N} a_j H_c^{lj} \\ \text{i.e} \quad E_o \mathbf{S}\vec{a} &= \mathbf{H}\vec{a} \end{aligned} \tag{2.10}$$

The last equation in 2.10 is a **generalized eigenvalue equation**. Here **S** and **H** are the overlap matrix and the Hamiltonian matrix in the basis of single particle ground states and $\vec{a}$ is the coefficient vector in LCAO ground state equation 2.7. Since $\langle l|j\rangle = \langle j|l\rangle^*$, **S** just like **H** is a Hermitian matrix. Furthermore, the diagonal elements of **S** are ones, and the off-diagonal elements S_{lj} get vanishingly small for larger $|l - j|$ because of the increasing distance between l^{th} and j^{th} nucleus. This allows us to make the nearest neighbor (or n-nearest neighbor approximation if necessary) where we say that the non-diagonal($l \neq j$)

overlap integral S_{lj} is non zero and small ($\eta \ll 1$) only if $j = l \pm 1$.

$$\begin{aligned} S_{lj} &= \langle l|k\rangle \\ &= \delta_{l,j} + \eta[\delta_{l,j+1} + \delta_{l,j-1}] \qquad \text{where } \eta \ll 1 \end{aligned} \tag{2.11}$$

Similarly, we can also make a similar approximation to the Hamiltonian matrix and say that potential energy operator from other sites can only make the electron hop between the nearest neighbor (or n-nearest neighbor if needed) sites with hopping energy '$-t$'.

$$\begin{aligned} H_c^{lj} = \langle l|\, H_c\, |j\rangle &= \langle l|\ T + U_j(\hat{r})\, |j\rangle + \langle l|\ \sum_{i\neq j}^{N} U_i(\hat{r})\, |j\rangle \\ &= \quad \epsilon_o \cancelto{S_{lj}}{\langle l|j\rangle} \quad + \langle l|\ \sum_{i\neq j}^{N} U_i(\hat{r})\, |j\rangle \end{aligned}$$

Case 1: $j = l$

$$H_c^{ll} = \quad \epsilon_o \cancelto{1}{S_{ll}} \quad + \langle l|\ \sum_{i\neq j}^{N} U_i(\hat{r})\, |l\rangle \quad = \epsilon_o + V_d \tag{2.12}$$

Case 2: $j \neq l$

$$\begin{aligned} H_c^{lj} &= \quad \epsilon_o\ S_{lj} \quad + \langle l|\ \sum_{i\neq j}^{N} U_i(\hat{r})\, |j\rangle \\ &= \epsilon_o\eta[\delta_{l,j+1} + \delta_{l,j-1}] - t[\delta_{l,j+1} + \delta_{l,j-1}] \\ &= [-\tilde{t} + \epsilon_o\eta][\delta_{l,j+1} + \delta_{l,j-1}] \end{aligned}$$

Here, V_d in case 1 is called the 'direct term' the hopping of an electron back to the same site due to the potential energy gain from all other sites and the term with prefactor of '$-\tilde{t}$' in case 2 is called the 'exchange term' and it describes the hopping of electron to the nearest neighbor site due to potential energy gain from all other sites. Replacing the overlap matrix elements and the Hamiltonian matrix elements from 2.11 and 2.12 in the generalized eigenvalue equation 2.10 and making some small parameter arguments, we can find a good

approximation for E_o without having to solve the full eigenvalue equation.

$$
\begin{aligned}
E_o S_{ll} a_l + E_o \sum_{j \neq l}^{N} S_{lj} a_j &= H_c^{ll} a_l + \sum_{j \neq l}^{N} H_c^{lj} a_j \\
\text{i.e } E_o S_{ll} a_l &= H_c^{ll} a_l + \sum_{j \neq l}^{N} (H_c^{lj} - E_o) S_{lj} a_j \\
E_o\, a_l \quad &= [\epsilon_o + V_d] a_l + [-\tilde{t} + (\epsilon_o - E_o)\eta]\,[\delta_{l,j+1} + \delta_{l,j-1}] a_j
\end{aligned}
$$

Assuming, $n \ll 1$ such that $(\epsilon_o - E_o)\eta \approx \Delta \ll 1$

$$
E_o\, a_l \quad = [\epsilon_o + V_d] a_l \quad + [-\tilde{t} + \Delta]\,[\delta_{l,j+1} + \delta_{l,j-1}] a_j \tag{2.13}
$$

Redefining, $\epsilon_o + V_d \equiv \varepsilon_o$ and $-\tilde{t} + \Delta = -t$, we get,

$$
\begin{aligned}
E_o\, a_l \quad &= \quad \varepsilon_o a_l \quad - t[\delta_{l,j+1} + \delta_{l,j-1}] a_j \\
E_o\, a_l \quad &= \quad \Big[\varepsilon_o \delta_{lj} \quad - t[\delta_{l,j+1} + \delta_{l,j-1}]\Big] a_j
\end{aligned}
$$

$$
\begin{aligned}
i.e \quad E_o\, \vec{a} \;&= H_{TB}\, \vec{a} \qquad\qquad \big[\textbf{Regular Eigenvalue Equation}\big] \\
\text{where,} \quad H_{TB}^{lj} \;&= \Big[\varepsilon_o \delta_{lj} \quad - t[\delta_{l,j+1} + \delta_{l,j-1}]\Big]
\end{aligned}
$$

We have now successfully written our generalized eigenvalue equation 2.10 into a regular eigenvalue equation and in the process converted the chain Hamiltonian H_c into an effective tight-binding Hamiltonian H_{TB} that takes into account the approximations of the overlap matrix as well as nearest neighbor interaction.

2.4.2 The Bosonic Hamiltonian: The Harmonic Chain

Although most many body electronic calculations traditionally are done either with completely static nuclei (the frozen nuclei approximation) or at least at a limit where the nuclei

are so massive that their motion happens in a time scale orders of magnitude slower than the lighter electron. This is the famous Born-Oppenheimer approximation (57). For most practical applications in systems with phonons, this is a fairly adequate treatment. However, in this thesis, we will treat nuclear motion more generally by not making any order of magnitude arguments. Although in most crystalline systems, this is a definite overkill and will result in minimal improvement of the calculated electronic spectral function, for molecular systems, this is not the case. Vibrational modes of the molecules often play a central role in their electronic structure and spectra. These modes can split electronic levels and often manifest new replicas of pure electronic levels thereby draining spectral weight (probability of an electron being at that energy level) as well as significantly shifting and distorting the purely electronic energy levels. A semi-classical example of this is the increase in resistance of conductors when temperature steadily rises. The electron can no longer flow freely in the wire because of the obstruction caused by atoms in the lattice starting to vibrate faster around their lattice sites. In quantum many-body language, this is often called the "dressing" of the particle (electron or hole) with the boson(vibron in this case) and this dressing effectively turns the particle into a quasiparticle with larger effective mass and slower dynamics.

Therefore, in order to model the vibrating nuclei, we start our discussion with the quantum harmonic oscillator. Let us imagine a single nucleus of mass M in 1 dimension tied to its lattice location with some harmonic potential $\hat{U}$. The Hamiltonian for this simple quantum spring-mass problem with spring constant 'k' (and $\hbar = 1$)is ;

$$\begin{aligned} H_b = T + U &= \frac{\hat{p}^2}{2M} + \frac{1}{2}k\hat{x}^2 \\ &= \frac{\hat{p}^2}{2M} + \frac{1}{2}m\omega_o^2\hat{x}^2 \qquad\qquad \text{where, } \omega_o = \sqrt{\frac{k}{M}} \end{aligned} \tag{2.14}$$

Since both terms in this Hamiltonian are quadratic, we have some hope of factorizing this

Hamiltonian. Let's define the factors as follows;

$$\begin{aligned}\hat{b}^\dagger &= \sqrt{\frac{M\omega_o}{2}}\Big(\hat{x} - \frac{i}{M\omega_o}\hat{p}\Big) \\ \hat{b} &= \sqrt{\frac{M\omega_o}{2}}\Big(\hat{x} + \frac{i}{M\omega_o}\hat{p}\Big)\end{aligned} \tag{2.15}$$

These factors can always be recombined to get representation in terms of the position and momenta operators- $hatx$ and $\hat{p}$ respectively for the nucleus.

$$\begin{aligned}\hat{x} &= \frac{1}{\sqrt{2M\omega_o}}(\hat{b}^\dagger + \hat{b}) \\ \hat{p} &= \frac{1}{\sqrt{2M\omega_o}}(\hat{b}^\dagger - \hat{b})\end{aligned} \tag{2.16}$$

If we multiply these two possible from equation (2.15) we get the following;

$$\begin{aligned}\hat{b}^\dagger\hat{b} &= \Big[\sqrt{\frac{M\omega_o}{2}}(\hat{x} - \frac{i}{M\omega_o}\hat{p})\Big]\Big[\sqrt{\frac{M\omega_o}{2}}(\hat{x} + \frac{i}{M\omega_o}\hat{p})\Big] \\ &= \frac{1}{\omega_o}\Big[\frac{1}{2M}\hat{p}^2 + \frac{1}{2}M\omega_o^2\hat{x}^2\Big] - \frac{i}{2}[\hat{x}\hat{p} - \hat{p}\hat{x}] \\ &= \frac{1}{\omega_o}H_b \quad - \quad \frac{i}{2}[\hat{x}\hat{p} - \hat{p}\hat{x}]\end{aligned} \tag{2.17}$$

The factorization is close but not exact. We get a cross term $[\hat{x}\hat{p} - \hat{p}\hat{x}]$. Imagine we have a boson wave packet $|\psi\rangle$. The first term in this cross term when applied to this wave function measures the momenta of this wave packet followed by a measurement of position. The second term in this cross term, in the same case, measures the position of this wave packet followed by a measurement of momenta. This cross-term quantifies the difference between these two switched orders of operations. This term is often referred to as the commutator of the two operators (here $\hat{x}$ and $\hat{p}$).

This difference in the classical case is actually zero because we have an infinite and independent resolution of the position and momenta of any particle. So classically, this is an exactly factorizable problem. However, in the quantum realm, because of the position-

moment quantum uncertainty principle, this cross-term does not vanish. This is one of the fundamental postulates of quantum mechanics.

$$[\hat{x}\hat{p} - \hat{p}\hat{x}] \equiv [\hat{x}, \hat{p}] = i$$

Substituting this postulate in (2.17), we get;

$$H_b = \omega_o \Big[\hat{b}^\dagger \hat{b} + \frac{1}{2}\Big] \tag{2.18}$$

We can solve this Schrodinger's equation exactly and know the exact wave functions and energies. We will quote the standard result for eigen wave functions and associated eigen energies below.

$$\begin{aligned} |n\rangle \equiv \Psi_n(x) &= \frac{1}{\sqrt{2^n n!}} \Big(\frac{\alpha}{\pi}\Big)^{\frac{1}{4}} . \mathcal{H}_n(\alpha x) . e^{-\frac{(\alpha x)^2}{2}} \qquad \text{where, } \alpha = m\omega_o \\ E_n &= \Big(n + \frac{1}{2}\Big)\omega_o \\ \mathcal{H}_n(x) &= (-1)^n e^{x^2} \frac{d^n}{dx^n} e^{-x^2} \qquad \text{(Hermite Polynomials)} \end{aligned} \tag{2.19}$$

The eigen energy levels, associated wave functions, as well as the probabilistic position of this single nucleus in this harmonic potential, can be visualized as shown in figure 2.2. The state $ketn$ is interesting in that any state $|n\rangle$ contains 1 quantum of energy more than state $|n\rangle$. The operators in (2.15) are called ladder operators because they add or take away one quantum of energy from any eigen state $ketn$ thus effectively raising it to $|n+1\rangle$ or lowering it to $|n-1\rangle$.

$$\begin{aligned} \hat{b}^\dagger |n\rangle &= \sqrt{n+1}\ |n+1\rangle \\ \hat{b} |n\rangle &= \sqrt{n}\ |n-1\rangle \\ \hat{b}^\dagger \hat{b} |n\rangle &= n\ |n\rangle \qquad \text{(number operator)} \end{aligned} \tag{2.20}$$

The number operator $\hat{n} \equiv \hat{b}^\dagger \hat{b}$ counts the number of quanta of ω_o in any given wave function

$|n\rangle$ without altering the wave function. Here, 'n=0' is the lowest eigen energy and it corresponds to a state with zero bosons although it has finite energy. The state with '$n = 1$' is the single boson state with energy $\hbar\omega_o$ over the '$n = 0$' state. In our analysis, we already subtract the $n = 0$ energy from our Hamiltonian and set '$\hbar = 1$'. Therefore, state '$n = 0$' in this new picture has zero energy, and any n^{th} state corresponding to n bosons in the system has '$n\omega_o$' quanta of energy.

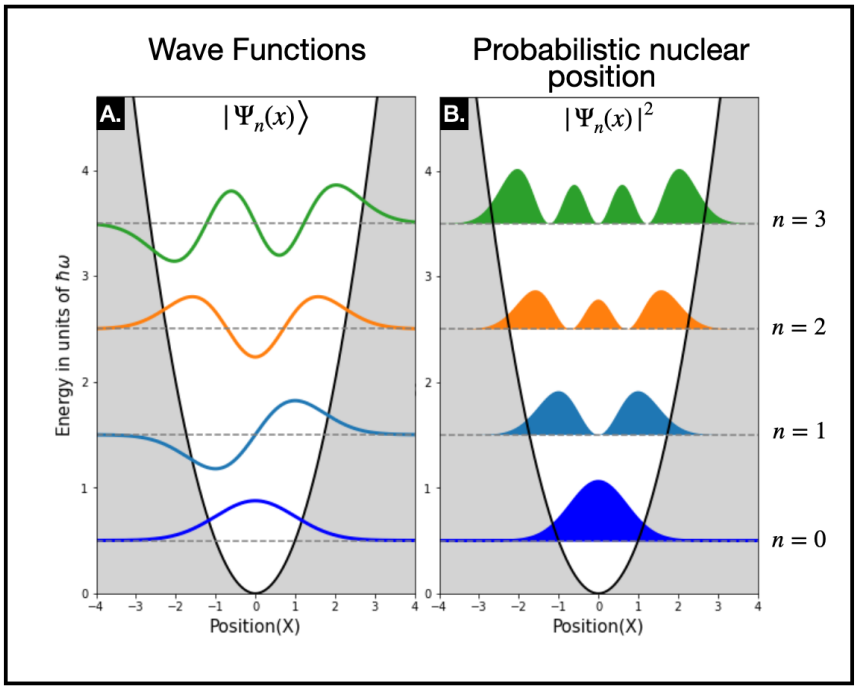

Figure 2.2: Eigen energies, eigen wave functions as well as probabilistic nuclear position for a single nucleus in a 1D harmonic trap. Here, n is the index of increasing eigen energy.

We now have an effective language to describe the quantized nuclear vibrations. Let's now go to a problem with 'N' different sites. Rather than talking about what each nucleus is doing, we can take about the problem in terms of the number 'n_i' of vibration quanta ω_o at any given site 'i' and the vibrational wave function of that site $|n_i\rangle$. We can also let the vibrational quanta travel from site 'i' to its nearest neighbor with some hopping energy 't_d'. This now boils down to the tight binding problem discussed previously with the on-site boson creation energy ω_o and hopping energy t_d. We can do the entire tight binding calculation

with LCAO approximation as shown in equation (2.7) in subsection 2.4.1.

$$H_b^{lj} = \Big[n_l \omega_o \delta_{lj} \quad + t_d[\delta_{l,j+1} + \delta_{l,j-1}] \Big] \tag{2.21}$$

2.5 The Electron Boson Interaction, The Holstein Paradox and The Molecular Crystal

This piece is the most subtle part of this Hamiltonian that is also at the heart of why this problem is of physical relevance. Suppose we are at a single atom limit with a single electron and a single positively charged site - a hydrogen atom.

We make a claim that an electron responds to the motion of the nucleus and the system's total energy changes. Say the energy change due to this interaction is 'Γ'. let $\hat{X}$ be the position operator of the nucleus.

Claim:

$$H_{int} \stackrel{?}{=} \Gamma \hat{X} = \frac{\Gamma}{\sqrt{2M\omega_o}}(\hat{b}^\dagger + \hat{b}) = g(\hat{b}^\dagger + \hat{b}) \tag{2.22}$$
$$\text{where, } g \equiv \frac{\Gamma}{\sqrt{2M\omega_o}}$$

Say the nucleus is vibrating left(negative) and right(positive) of its equilibrium. If what we claim is true, then the interaction decreases the system's overall energy by g when the nucleus moves left and increases the system's overall energy by g when the nucleus moves right as shown in 2.3. But this does not make sense because for a single hydrogen atom sitting in an empty 1D universe, the nucleus going left or right should be equivalent. So we end up with a paradox which I call the **"Holstein paradox"**. A more correct interpretation of this kind of interaction warrants a more complicated structure of the nucleus. The nucleus should be more negative on one side and more positive on the other side for its motion to make any difference for the electron cloud. In other words, the 'nucleus' isn't really a nucleus

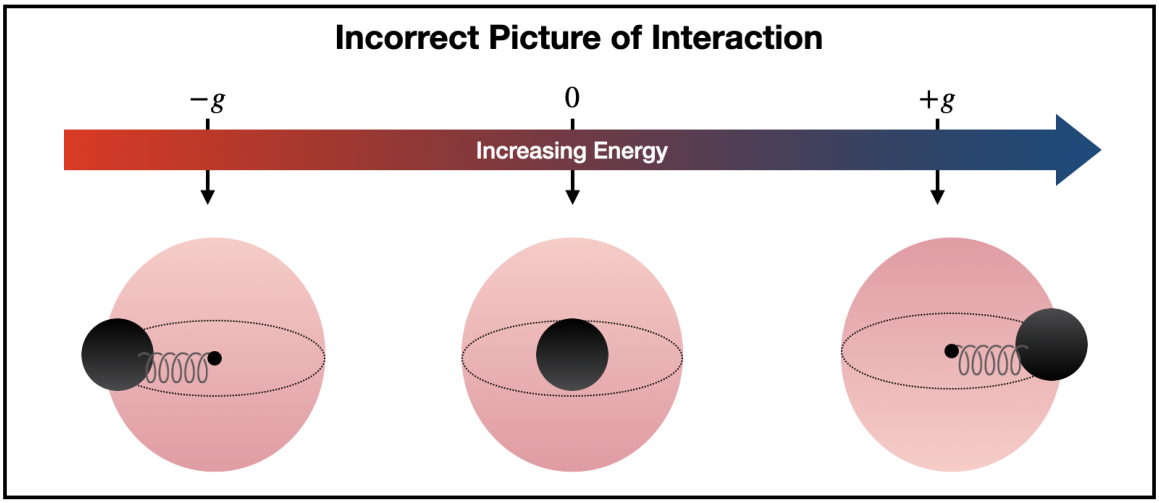

Figure 2.3: A naive interpretation of electron-boson interaction with Hydrogen-like intact nucleus and an electron cloud leads to a paradox in Holstein model

but rather an elongated polar ion with a net charge of $+e$. Doing so will lead to a decrease in the system's energy when the partially negatively charged part ($\delta-$) of the polar ion is pushed out of the electron cloud during 'nuclear' oscillation and an increase in the system's energy when the partially positively charged part $\delta+$ part is pushed out of the electron cloud as shown in figure 2.4.

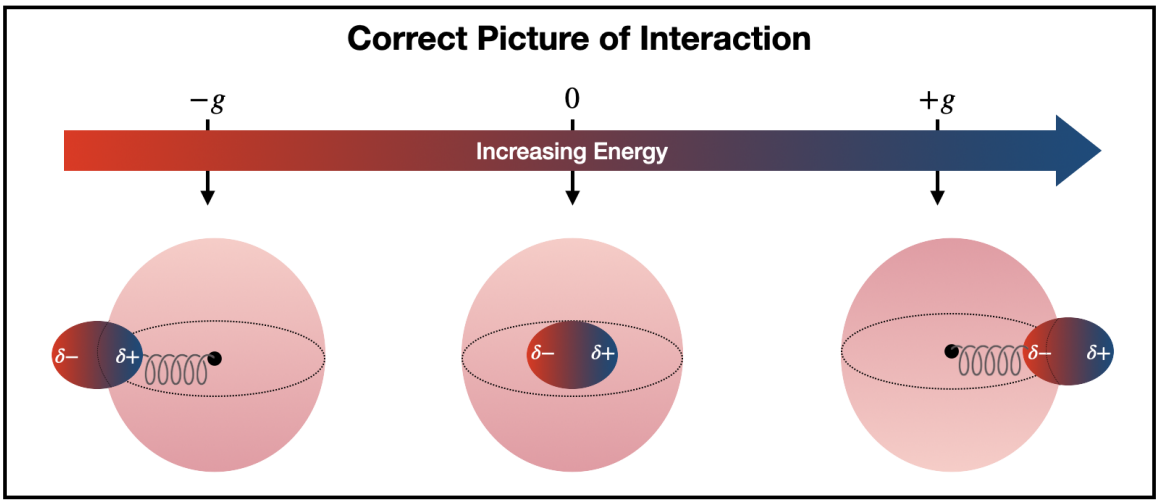

Figure 2.4: Correct way to interpret electron boson interaction in the Holstein model requires a polar ion as the nucleus.

2.5.1 The Molecular Crystal

We now scale this system with a polar nucleus up to get a chain of polar molecules sitting on some uniform lattice as shown in figure 2.5(i). These molecules can vibrate about their respective lattice sites as shown in figure 2.5(ii). The interaction of electron with nuclear vibration is on-site -i.e. happens only at the site where the electron currently resides. Therefore, the vibration of sites without electron does not matter regardless of how many sites are vibrating. Hence for this N-site chain, our electron-boson Hamiltonian has the following

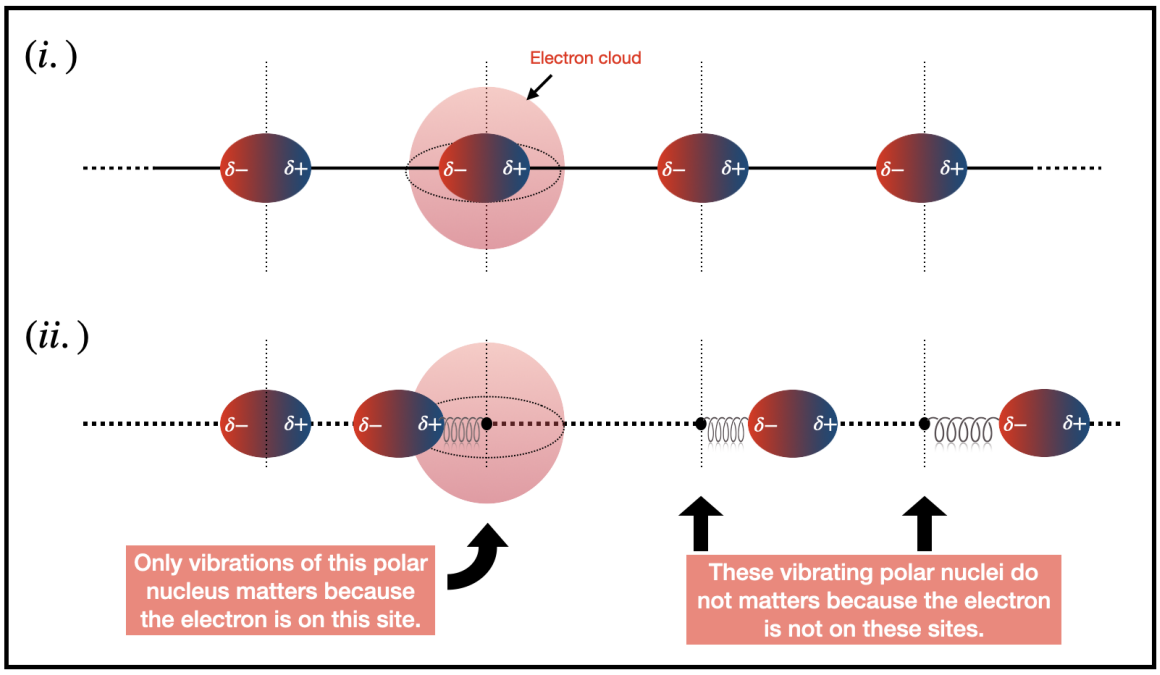

Figure 2.5: A model of 1D molecular crystal with the polar nucleus and a single electron. (i) crystal with no vibrations. (ii) crystal with vibrating sites.

form;

$$H_{int} = \Gamma \sum_{i=1}^{N} N_i.\hat{X}_i = \frac{\Gamma}{\sqrt{2M\omega_o}} \sum_{i=1}^{N} N_i(\hat{b}_i^\dagger + \hat{b}_i) = g \sum_{i=1}^{N} N_i(\hat{b}_i^\dagger + \hat{b}_i)$$

$$\text{where, } N_i = \begin{cases} 1 & \text{if electron is in site 'i'} \\ 0 & \text{if electron is not in site 'i'} \end{cases} \tag{2.23}$$

Here we have packaged the parameters of the original problem and defined the interaction energy g.

2.6 1D Holstein Hamiltonian in Second Quantization:

Although the first quantized language is useful in understanding the mechanism of the process, oftentimes it obfuscates the understanding of the process because of its complicated form. Therefore, in this section, we will translate the pieces of Holstein Hamiltonian derived in the first-quantized language into the second-quantized language. We will use the second quantized Hamiltonian (as well as language) for the rest of the thesis.

2.6.1 Electronic Hamiltonian in Second Quantization

We can now convert the effective tight-binding Hamiltonian from equation 2.13 into a second quantized form using the second-quantization rule for single particle operators described in equation 2.4. Since we have not specified that our chain is finite, the sum here runs to ∞ and not to N -the number of sites in our chain.

$$H_{TB} = \sum_{ij}^{N} {H_{TB}}^{ij} \hat{c}_i^\dagger \hat{c}_j = \varepsilon_o \sum_{i}^{N} \hat{c}_i^\dagger \hat{c}_i \quad - t \sum_{i}^{N} [\hat{c}_{i+1}^\dagger \hat{c}_i + \hat{c}_{i-1}^\dagger \hat{c}_i] \tag{2.24}$$

The first term here (with prefactor ε_o) is called the on-site energy because it accounts for the electron hopping from a site back to the same site. The second term (with prefactor $-t$) is called the hopping energy because it accounts for the electron hopping from a site i to its neighboring sites $i \pm 1$.

2.6.2 Bosonic Hamiltonian in Second Quantization

Since the nuclear vibrations also boiled down to a tight binding form, the bosonic Hamiltonian for a Holstein chain with N sites is;

$$H_b = \sum_{ij}^{N} H_b{}^{ij} \hat{b}_i^\dagger \hat{b}_j = \omega_o \sum_{i}^{N} \hat{b}_i^\dagger \hat{b}_i \quad + t_d \sum_{i}^{N} [b_{i+1}^\dagger \hat{b}_i + \hat{b}_{i-1}^\dagger \hat{b}_i] \tag{2.25}$$

The term 't_d' is commonly referred to as the boson dispersion. It quantifies the hopping of vibration from one site to another. Although most calculations in literature are done in $t_d = 0$ limit explicitly, we add this to our Hamiltonian to make the problem more general.

2.6.3 Electron-Boson Hamiltonian in Second Quantization

The interaction Hamiltonian from equation (2.23) for the most part is already in the second-quantized language. The tern N_i counts the electron at any given site 'i'. Analogous to the bosonic case shown in equation 2.20, we can define a number operator for the electron as well in terms of $\hat{c}_i^\dagger / \hat{c}_i$ - the electron creation and annihilation operators for site 'i'.

$$\hat{N}_i = \hat{c}_i^\dagger \hat{c}_i \qquad \text{Electron number operator}$$

Using this relation, the interaction Hamiltonian can be written in a second quantized language.

$$H_{int} = g \sum_{i=1}^{N} \hat{c}_i^\dagger \hat{c}_i (\hat{b}_i^\dagger + \hat{b}_i) \tag{2.26}$$

Putting together all three pieces- the electronic, the bosonic, and the interaction, we

finally get our general Holstein Hamiltonian.

$$\begin{aligned} H &= H_{el} + H_b + H_{int} \qquad \text{where,} \\ H_{el} &= \varepsilon_o \sum_i^N \hat{c}_i^\dagger \hat{c}_i \quad - t \sum_i^N [\hat{c}_{i+1}^\dagger \hat{c}_i + \hat{c}_{i-1}^\dagger \hat{c}_i] \\ H_b &= \omega_o \sum_i^N \hat{b}_i^\dagger \hat{b}_i \quad + t_d \sum_i^N [b_{i+1}^\dagger \hat{b}_i + \hat{b}_{i-1}^\dagger \hat{b}_i] \\ H_{int} &= g \sum_{i=1}^N \hat{c}_i^\dagger \hat{c}_i (\hat{b}_i^\dagger + \hat{b}_i) \end{aligned} \tag{2.27}$$

2.7 From a general many-body Hamiltonian to 1D Holstein chain

In this section, we start with a 1-dimensional general many-body Hamiltonian and approximate it to a 1D Holstein chain. Consider a 1-dimensional chain of N_e electrons and N_i number of atomic sites (ions). The many-body Hamiltonian can be written in terms of position and momenta operators of the electrons and the ions as follows;

$$\begin{aligned} H_{tot} &= H_{el} + H_{ion} + H_{el-ion} \qquad \text{where,} \\ H_{el} &= \sum_i^{N_e} \Big[\frac{\hat{p}_i^2}{2m} \quad + \frac{1}{2} \sum_{j:j\neq i}^{N_e} V(|\hat{r}_i - \hat{r}_j|) \Big] \\ H_{ion} &= \sum_I^{N_i} \Big[\frac{\hat{P}_i^2}{2M} \quad + \frac{1}{2} \sum_{J:J\neq I}^{N_i} V(|\hat{R}_i - \hat{R}_j|) \Big] \\ H_{el-ion} &= \sum_i^{N_e} \sum_I^{N_i} V(|\hat{R}_I - \hat{r}_i|) \end{aligned} \tag{2.28}$$

The purely electronic part H_{el} of the Hamiltonian consists of the kinetic energy of the electron (first term) as well as the coulomb interaction between two different electrons (hence $j : j \neq i$). The coulomb interaction term only depends on the distances between the two charges in question (hence the absolute value of the position operator) and also has a factor of 1/2 upfront so as not to double count the interaction as both indices i and j are running

from 1 to N_e. The ionic part $Hion$ is very similar to the electronic part in that it consists of the kinetic energy of the vibrating ions in the lattice as well as the coulomb interaction between these ions. The major difference then comes from the fact that the mass of an electron is much less than that of the ion ($m < M$) which is the foundational argument for the Born-Oppenheimer approximation.

Finally, the electron-ion interaction piece consists of coulomb interaction between the positively charged ions and the negatively charged electrons at positions R_I and r_i respectively. So far, this Hamiltonian, although in 1D, is very general. We can transform this into a Holstein problem with the following three simplifications:

1. Assume that the electrons are independent.

2. Linearize H_{el-ion}.

3. Assume ions and electrons interact when they are at or less than a unit cell away.

The first simplification is fairly straightforward. All we do there is we assume that

$$V(|\hat{r}_i - \hat{r}_j|) = 0 \qquad \text{which results in,} \qquad H_{el} = \sum_i^{N_e} \frac{\hat{p}_i^2}{2m} \tag{2.29}$$

This simplification results in a massive simplification of the whole system by decoupling the eigenvectors (wave functions) in the space of electronic degrees of freedom. All this means is that the electrons don't see each other as their dynamics evolve in time. At first glance, although this approximation looks drastic, there are numerous many-body methods such as Density functional theory (58) and variational tight-binding models (59) which successfully treat the effect of electrons on one another at mean-field level and beyond. Thus, we trudge forward with this approximation keeping in mind the fact that a more sophisticated treatment of electron-electron interaction is always possible.

The second simplification would not be necessary if the ions were pinned to the lattice. In this case, this term would only result in a constant ionic potential submerging the electron.

However, in real systems, ions oscillate around their equilibrium position (lattice sites). For our purposes, we suppose that any given ion $\vec{R}_I$ is undergoing a simple harmonic oscillation with displacement $\vec{X}_I$ which allows us to linearize H_{el-ion} about the equilibrium point $\vec{R}_I^{(o)}$. Although this problem is in 1 dimension, we use vector notations here to denote that the displacement vector $\vec{X}_I$ is changing in magnitude and direction (sign) around the equilibrium position i.e $\vec{R}_I = \vec{R}_I^{(0)} + \vec{X}_I$. We replace this in coulomb interaction potential in H_{el-ion}, Taylor expand it and linearize.

$$\begin{aligned} V(|\vec{R}_I - \vec{r}_i|) &= V(|\vec{R}_I^{(0)} + \vec{X}_I - \vec{r}_i|) \\ &= V(|\vec{R}_I^{(0)} - \vec{r}_i|) \ + \ \vec{X}_I.\vec{\nabla}V(|\vec{R}_I^{(0)} - \vec{r}_i|) \ + \ \mathcal{O}(|\vec{X}_I|^2) \\ &\approx V(|\vec{R}_I^{(0)} - \vec{r}_i|) \ + \ \vec{X}_I.\vec{\nabla}V(|\vec{R}_I^{(0)} - \vec{r}_i|) \end{aligned} \tag{2.30}$$

The very first term in this expansion is the potential landscape of the frozen(static) lattice interacting with the electron at r_i. We can combine this with the equation (2.29) which gives us a sum of N_e basic electronic tight binding Hamiltonians- one for each independent electron in this problem.

$$\begin{aligned} H_{TB} &= \sum_i^{N_e} \frac{\hat{p}_i^2}{2m} + \sum_i^{N_e}\sum_I^{N_i} V(|\vec{R}_I^{(0)} - \vec{r}_i|) \\ &= \sum_i^{N_e} \Big[\frac{\hat{p}_i^2}{2m} + \sum_I^{N_i} V(|\vec{R}_I^{(0)} - \vec{r}_i|)\Big] \\ &= \sum_i^{N_e} H_{TB}^i \end{aligned} \tag{2.31}$$

The ionic Hamiltonian is already in the form we have discussed before in section 2.4.2. In fact, we actually have a more general version of the problem where the nearest neighbor ions interact with each other in the second quantized formalism in the preceding section.

We now direct our attention to the linear term in equation (2.30). The term $\vec{\nabla}V(|\vec{R}_I^{(0)} - \vec{r}_i|)$ is nothing but Coulomb force between the ion at the equilibrium position $\vec{R}_I^{(0)}$ and an

electron at location $\vec{r_i}$. At any given moment, the electron in question is in some unit cell around the K^{th} ion at equilibrium position $\vec{R}_K^{(0)}$. We can define the position of this electron inside this unit cell 'K' centered around the equilibrium ion position as $\vec{r}_i^0$ - i.e $\vec{r_i} = \vec{R}_K^{(0)} + \vec{r}_i^0$. Putting this information back in the potential, we get;

$$\begin{aligned} \vec{\nabla} V(|\vec{R}_I^{(0)} - \vec{r_i}|) &= \vec{\nabla} V(|(\vec{R}_I^{(0)} - \vec{R}_K^{(0)}) - \vec{r}_i^0|) \\ &\propto \frac{1}{|(\vec{R}_I^{(0)} - \vec{R}_K^{(0)}) - \vec{r}_i^0|^2} \end{aligned} \tag{2.32}$$

By the nature of Coulomb interaction, this quantity is significant only when $(\vec{R}_I^{(0)} - \vec{R}_K^{(0)})$ goes to zero i.e the electron 'i' is actually in the unit cell centered at $\vec{R}_I^{(0)}$. We will therefore use our third approximation and say that interaction between an electron and a nucleus more than a unit cell away is zero a nucleus less than or equal to a unit cell is some constant Γ. With this the linear term in the H_{el-ion} becomes;

$$\begin{aligned} H_{el-ion} &= \sum_i^{N_e} \sum_I^{N_i} \vec{X}_I . \vec{\nabla} V(|\vec{R}_I^{(0)} - \vec{r_i}|) \\ &\approx \sum_i^{N_e} \sum_I^{N_i} \vec{X}_I . \Gamma . \hat{N}_I^i \\ &= \Gamma \sum_I^{N_i} \Big[\sum_i^{N_e} \hat{N}_I^i \Big] . \vec{X}_I \\ &= \Gamma \sum_I^{N_i} \Big[\hat{N}_I . \vec{X}_I \end{aligned} \tag{2.33}$$

$$\text{where,} N_I^i = \begin{cases} 1 & \text{if electron 'i' is in Unit cell around } \vec{R}_I^{(0)} \\ 0 & \text{if not.} \end{cases}$$

Here N_I^i is the number operator for i^{th} independent electron and N_I is the total electron number operator that checks how many electrons are present at site I. With this, our

problem has boiled down to a form very similar to what we described in section 2.5 and in (2.27).

Although we had to make approximations to the real many-body problem in order to get the Holstein Hamiltonian, this Hamiltonian still carries the bare minimum components that have a complexity similar to the real problem as well as practical relevance in polar molecules. Given we have clean descriptions of electronic and bosonic physics where the first-quantized parameters have been appropriately packaged, Holstein Hamiltonian provides us a suitable playground to build methods to understand and account for electron-boson interactions in many body systems.

2.8 Summary:

In this section, we derived the Holstein Hamiltonian from the first principles and elucidated the necessary underlying approximations in the three main components of this Hamiltonian. Furthermore, we discussed the Holstein paradox and developed the idea of a polar ion nucleus. We then described this system in the second-quantized language. Finally, we took the real many-body Hamiltonian and through a series of well-justified arguments boiled it down to the Holstein problem.

CHAPTER 3

MATHEMATICAL DETOUR: GREEN'S FUNCTION, SELF-ENERGY AND OTHER QUANTITIES OF INTEREST

3.1 An Introductory Problem: Goldfish in an Aquarium

Imagine a five-second memory having goldfish in an aquarium. This goldfish really likes jumping through two hoops that we have put in this aquarium- a red one and a blue one as shown in figure 3.1. So we assign some probability of this goldfish interacting with each of these hoops.

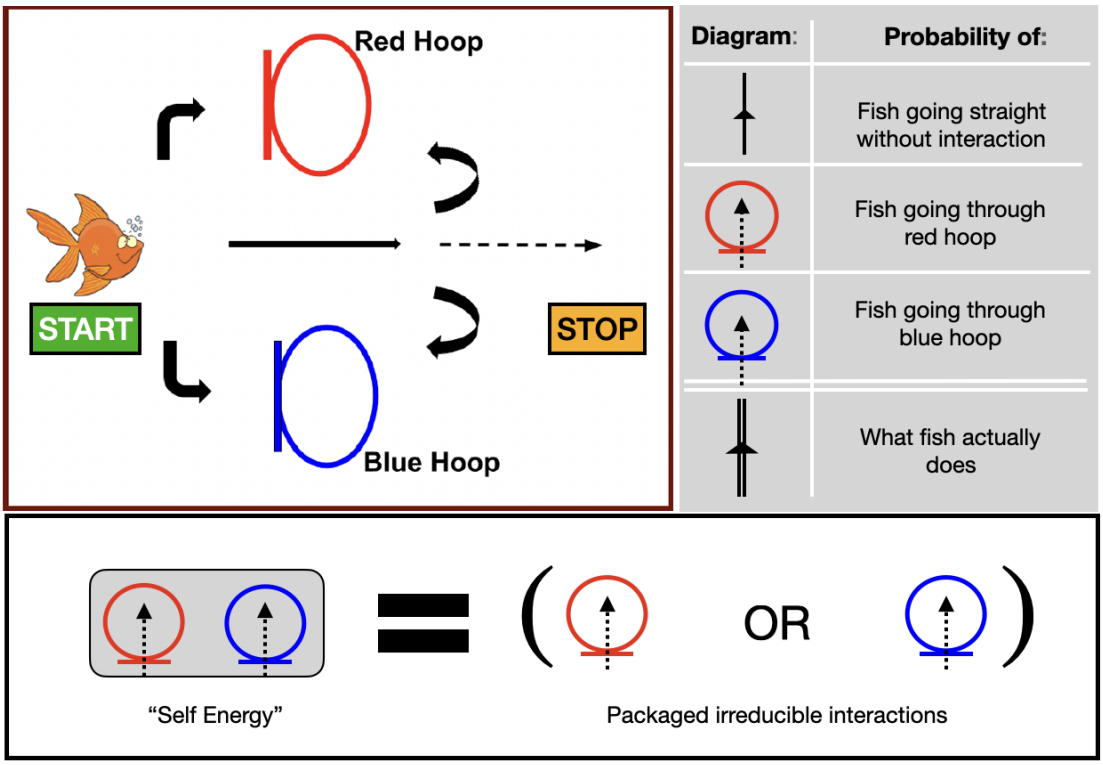

Figure 3.1: Goldfish in an aquarium (top left). Diagrammatic representation of probabilities is presented on the top right. The bottom panel shows the definition of self-energy

Suppose we wanted to know what is the probability of this goldfish going from one end of the aquarium marked 'start' to another end of the aquarium marked 'stop'. If there were

no hoops, the goldfish simply swims from one end to another end. But the presence of hoops complicates the motion of the goldfish. Since it lacks memory, it can interact with the hoops in any combination for as many times as it likes. But at any given moment in time, while interacting with the hoops, it can either go through the red hoop or the blue hoop once. Going through any one of these two hoops once is the most basic or irreducible interaction of goldfish. We can package this information about the irreducible together and construct an effective interaction probability for any given moment in time as shown in figure 3.1. We call this packaged interaction the 'self-energy' of this goldfish.

With the diagrammatic representation and the self-energy shown in figure 3.1, we can begin to write(draw) the first few cases for this goldfish's motion as shown in figure 3.2.

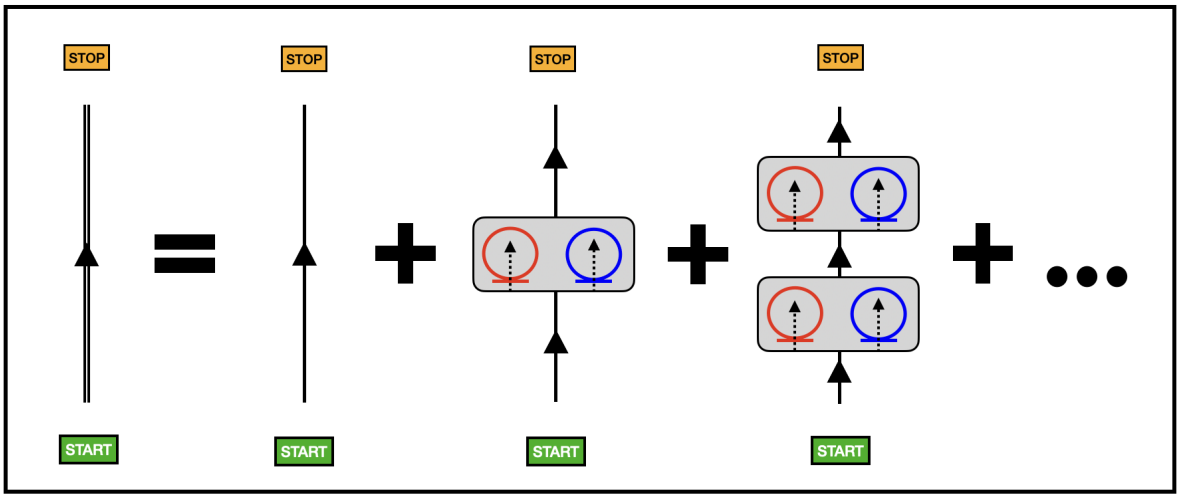

Figure 3.2: First few cases of goldfish motion

We now notice that the actual motion of the goldfish is nothing but a series expansion in the self-energy. Hence, we can write this more compactly as shown in figure 3.3. This is a self-consistent equation because the left and the right side both have the same quantity P - the actual probability of goldfish going from start to stop.

In the quantum case, the story is analogous. The only major difference is that we do not talk about the probability but rather the probability amplitude - the Green's function. This is because the fundamental quantity for a particle's location in space-time in quantum

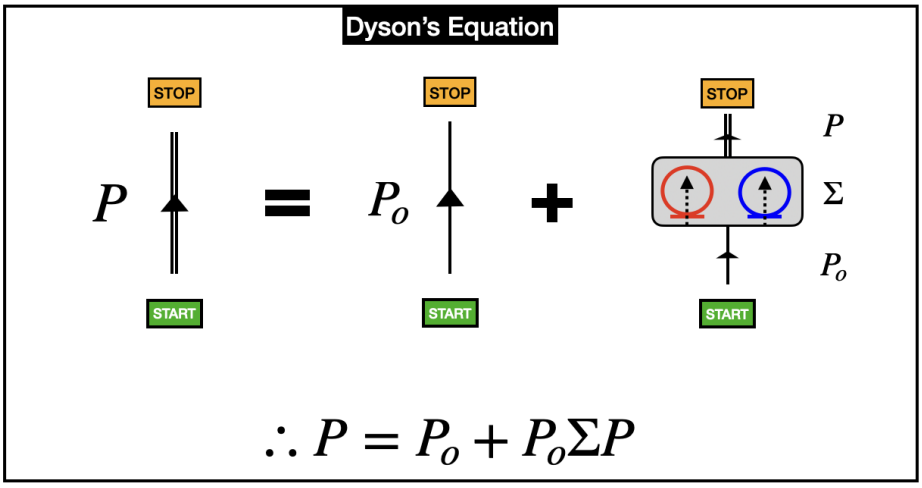

Figure 3.3: Dyson's equation for goldfish's dynamics as it goes from start to stop. Σ here represents the self-energy.

mechanics is not the probability but rather the wave function.

3.2 The Electron Green's Function

The electron Green's function is the tool at hand to study the effect of interaction on the propagation of electron from one state to another. States here could be the actual spatiotemporal location in the bulk or energy-momenta states. In fact, we can use any appropriate single particle basis say k_i, k_f to define the addition or removal of particles.

$$-iG(k_f, t_f; k_i, t_i) = \text{Probability amplitude for finding a particle in state } k_f \text{ at time } t_f$$
$$\text{if a particle in state } k_i \text{ was added to this system at time } t_i$$

In either case, the electron Green's function contains all possible interactions that the electron could undergo while propagating from one state to another. Knowledge of the electron Green's function, therefore, provides all the knowledge about the possible interactions in and the energy levels of the material. For a non-interacting system, once we know the dispersion relation, writing the electron Green's function or the bare Green's function(G_o) is

trivial. States are long-lived due to the infinite lifetime because of no interaction. Hence, the spectrum is just a series of delta functions at the energy eigenvalues(ε_k) of the Hamiltonian. However, once the interactions are switched on, there is an exchange of energy and momenta between states, the clumping of particles and holes to form quasi-particles, and the onset of long-range modes due to the response of the system. The interacting Green's function(G) therefore is no longer simple. However, if we know the kinds of irreducible interactions that the electron can undergo and we package it together and call it the self-energy $\Sigma(k,\omega)$, then we can write the Green's function using Dyson's equation in frequency(ω) space analogous to figure 3.3.

$$\begin{aligned} G(k,\omega) &= G_o(k,\omega) + G_o(k,\omega)\Sigma(k,\omega)G_o(k,\omega) + G_o\Sigma G_o\Sigma G_o + ... \\ &= G_o(k,\omega) + G_o(k,\omega)\Sigma(k,\omega)\big(G_o + G_o\Sigma G_o + ...\big) \\ &= G_o(k,\omega) + G_o(k,\omega)\Sigma(k,\omega)G(k,\omega) \end{aligned} \tag{3.1}$$

$$\therefore G(k,\omega) = \frac{1}{G_o(k,\omega)^{-1} - \Sigma(k,\omega)}$$

Of course, there are different conventions on writing the Green's function and various interpretations of the result. The time-ordered(TO) Green's function chooses to have time run in the positive direction for particles (electrons) and the negative direction for holes. This is because in this convention, the unperturbed system with a quiet fermi surface is the ground state. The Fermi surface (Energy = μ) is considered to be zero of the energy scale (the Fermi vacuum). Any new particle added is added above this fermi surface -at a positive energy state. Any hole added (particle removed) is removed from below the fermi surface - from a negative energy state. Because the two objects- particles and holes have positive and negative energies respectively, their propagation in time is also considered to be in either a positive or negative direction to make sure that the energy-time uncertainty principle can

be equivalently defined in both cases.

Hence the Green's function is defined piece-wise, once for particles and once for holes. Because of this reason, the same Green's function cannot smoothly vary from a particle to a hole state and vice versa due to the difference in functional structure for particles ($\epsilon_k > \mu$) and holes ($\epsilon_k < \mu$). If $|0\rangle$ is the unperturbed system with fermi level's energy at μ, and Θ is the Heaviside step function, for particle Green's function, we first add a particle above the fermi level at time t', let the system evolve, remove this particle at time t and compare this new system to the original Fermi vacuum $|\Psi_o\rangle$. For hole Green's function, we first remove an electron from below the fermi level at time t, let the system evolve, add back this electron at time t', and compare this new system to the original Fermi vacuum $|\Psi_o\rangle$.

With $c_k^\dagger/c_k$ the particle ladder operators, time-ordered Green's function is defined as follows.

$$G^{TO}(k,t;k',t') = -i\left\langle |\Psi_o|\, \mathbf{T}\{c_k(t), c_{k'}^\dagger(t')\}\, |\Psi_o\right\rangle \tag{3.2}$$

Here $\mathbf{T}\{\}$ is the time ordering operator which orders the ladder operators differently for particles and holes.

$$\mathbf{T}\{A(t_1)B(t_2))\} = \begin{cases} A(t_1)B(t_2) & \text{if}\, t_1 > t_2 \\ -B(t_2)A(t_1) & \text{if}\, t_2 > t_1 \end{cases} \tag{3.3}$$

If the system is non-interacting, the added particle or hole of energy $\varepsilon_{k'}$ and momenta k' does not change its energy or momenta during the system's evolution in time. Hence, the non-interacting Green's function is;

$$\begin{aligned} G_0^{TO}(k,t;k',t') &= -i\left\langle \Psi_o|\, \mathbf{T}\{c_k(t), c_k^\dagger(t')\}\, |\Psi_o\right\rangle \delta_{k,k'} \\ &= -ie^{-\epsilon_{k'}(t-t')}\delta_{k,k'}\Big[\Theta(t-t')\Theta(\epsilon_{k'}-\mu) - \Theta(t'-t)\Theta(\mu-\epsilon_{k'})\Big] \end{aligned} \tag{3.4}$$

Given the binomial term with step functions in this expression, clearly, there are two branches of this Green's function - one for holes with $(t' < t)$ and the other for particles with $(t' > t)$.

A different convention for constructing Green's function is the retarded time (RT) Green's function in which time runs forward for both electrons and holes. Here the energy eigenvalues ε_k are with respect to the actual vacuum with zero particles. This actual vacuum is also called the Fock vacuum. Hence, there is no real need to make a distinction between electrons and holes. The retarded-time interacting and non-interacting Green's function is defined as;

$$\begin{aligned} G^{RT}(k,t;k',t') &= -i\langle 0|\,\mathbf{T}\{c_k(t), c^{\dagger}_{k'}(t')\}\,|0\rangle \\ G^{RT}_{o}(k,t;k',t') &= -ie^{-\varepsilon_k(t-t')}\delta_{k,k'}\Theta(t-t') \end{aligned} \tag{3.5}$$

As discussed above, this Green's function has a single branch. It is worth discussing the differences between these two formalisms of Green's function. The time-ordered Green's function starts from a large complicated system and defines the unperturbed system as zero. And because it counts excitations below and above the fermi energy, it is a good tool to have in order to talk about excitations that are localized around the fermi energy. This is because if we started counting from an actual vacuum, for a reasonably complex system with a large number of core electrons, we will have to count up to a very high number of states just to define the Fermi level. This becomes extremely tedious very fast and is not an efficient way to represent higher excitations. However, if we are talking about deeper excitations or systems with fewer electrons, to begin with, the Retarded time formalism gives a complete picture of excitations without having to separate them into two classes and make electrons and holes interact with each other separately.

Since our system is a single electron system, it is better (easier) to talk about the excitations of the system as adding that electron to a vacuum rather than start with a Fermi level at a single electron and talk about removing it. Therefore, we will use retarded-time Green's function for the rest of this thesis.

3.3 The Non-Interacting Boson Green's Function

Here too we will use the retarded time formalism. Unlike electrons, there can be many bosons in a given momenta state $\vec{q}$. Furthermore, the boson energy is independent of the direction of boson momenta $\omega_q = f(|\vec{q}|)$. We can think of this as the vibration of an atomic site in an isotropic having the same effect on the system's energy regardless of the direction in which it vibrates. So the addition (or removal) of bosons of momenta $+q$ or $-q$ will have the same effect on the overall system's energy. This idea is better encapsulated by the quantity A_q which removes a quantum of boson with energy ω_q from the system as A_{-q} which adds a quantum of boson with energy ω_q to the system. Therefore, the boson Green's function is defined as;

$$\begin{aligned} \mathcal{D}(q,t) &= -i\theta(t)\langle 0|\left[A_q(t), A_{-q}\right]|0\rangle \\ &= -i\theta(t)\langle 0|\, A_q(t)A_{-q} + A_{-q}A_q(t)\,|0\rangle \quad \text{where,} \\ A_q(t) &= b_q(t) + b^{\dagger}_{-q}(t) \end{aligned} \tag{3.6}$$

For non-interacting bosons, the A_q operator and the Green's function becomes;

$$\begin{aligned} A_q(t) &= b_q e^{-i\omega_q t} + b^{\dagger}_{-q} e^{i\omega_q t} \\ \mathcal{D}_o(q,t) &= -i\theta(t)[e^{-i\omega_q t} - e^{i\omega_q} t] \end{aligned} \tag{3.7}$$

3.4 The Electron-Boson interaction and Feynman diagrams

Using the non-interacting electron and boson Green's function, we will build our very first approximation of the interaction. Feynman diagrams are helpful tools to visualize these interactions. So we will briefly discuss the relevant ideas on Feynman diagrams and refer the reader to more formal resources on the topic.

We already built a primitive version of the Feynman diagram technique for the goldfish in figure 3.1 and 3.3. It was easy there because the interactions themselves (the hoops) were static and did not change the fish's state in any way. However, the microscopic reality of

electron-boson interaction is complicated because the electrons do change momenta when absorbing or emitting bosons. Therefore, there are some extra rules two of which are especially important for us. Firstly, each interaction vertex contributes a factor of $-ig$ (the coupling).

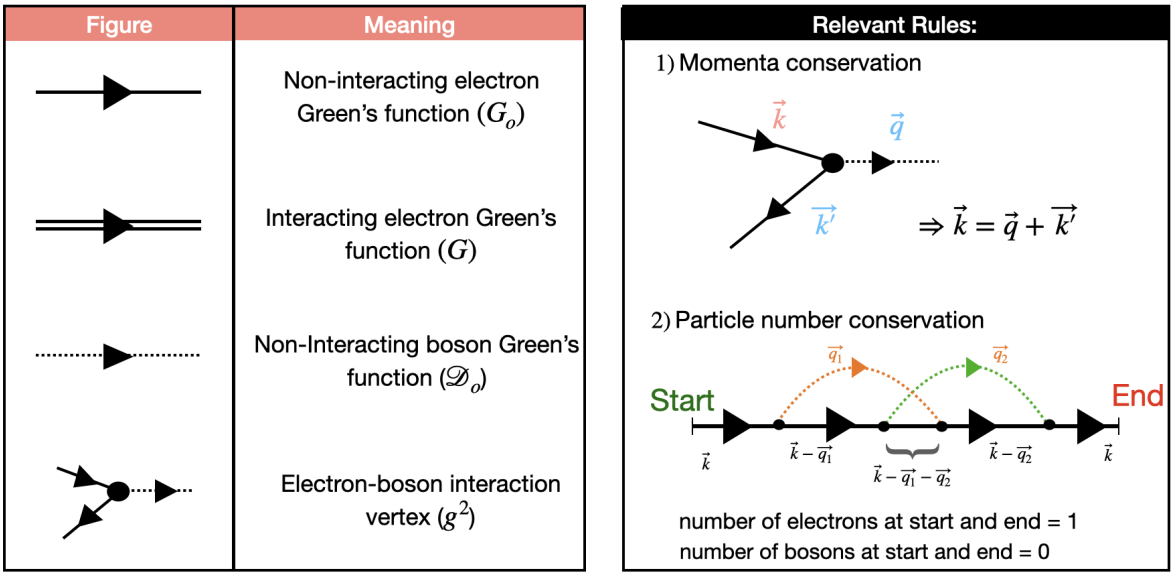

Figure 3.4: On left, Feynman Diagram dictionary for the Holstein problem. On the right are two relevant diagram rules for our approach.

This basically quantifies how often such interactions take place in the probability amplitude expansions. Furthermore, momenta are conserved at the vertices. Since all Green's functions have a direction arrow (in time), we assume that to be the direction of momenta flow. We then enforce the condition that the sum of incoming momenta to a vertex is equal to the sum of outgoing momenta from that vertex.

The second rule is regarding the conservation of particle number between the starting configuration and the end configuration. The number of electrons and bosons should be the same between the start and the end configuration. These numbers can however change as the system is evolving between these two times. Any newly created particle gets a new momenta variable and the equations are summed over the possible intermediate values of this new momenta variable. Both of these rules are summarized in figure 3.4.

There are other rules that are more technical and relevant for numerical applications such

as the conservation of energy variables. For these rules, we refer the reader to (60; 53; 54).

3.5 The Electron self-energy

Now, we will construct a very crude self-energy by making the non-interacting electrons and non-interacting bosons interact at the vertex. Although it sounds counter-intuitive, all we are saying is that these electrons and bosons only communicate instantaneously at the vertex, change momenta and go out of the vertex as non-interacting electrons and bosons again. This approximation simplifies the calculation by giving a clear framework to start the approximation. The first-order interaction is the simplest interaction between an electron and a boson at two points in time. This is shown in figure 3.5 A.

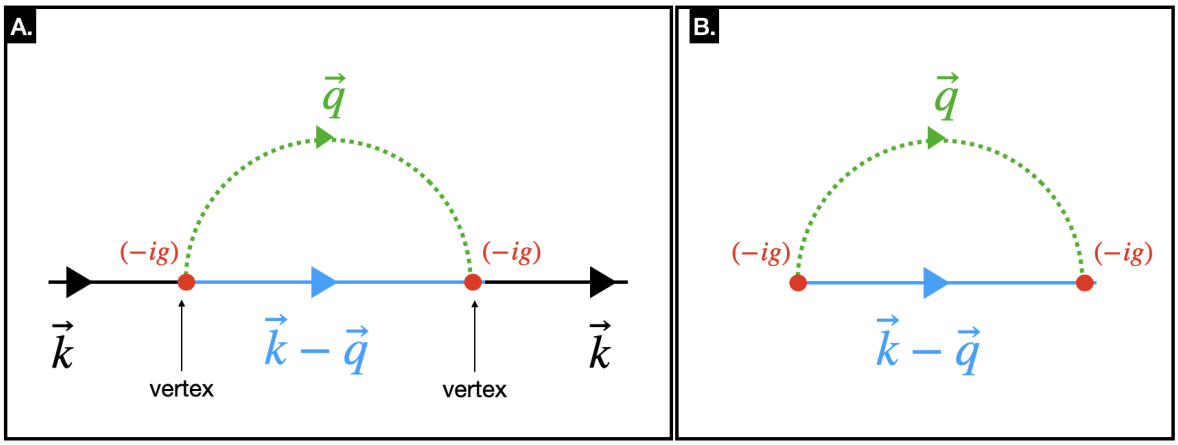

Figure 3.5: A. First order electron-boson interaction diagram. B. First order self-energy from diagram A.

The self-energy governing the process above (or any higher order process) is the part of diagram between the very first and the very last vertex . But we only care about the irreducible self-energy- those self-energy diagrams which cannot be constructed out of a combination of lower order self-energy diagrams. The first order self-energy for electron incoming at momenta 'k' $\Sigma(k,t)$ and is shown in figure 3.5 B. All we need to do is average over the possible boson momenta. This means that boson of any momenta can be excited

by this electron and this boson interacts back with the electron. Assuming the first vertex occurs at the time elapsed between the two vertices is t, we can write the expression for first order self-energy.

$$\begin{aligned} i\Sigma(k,t) &\equiv (-ig)^2 \frac{1}{N} \sum_{q=0}^{N} G_o(k-q,t)\mathcal{D}_o(q,t) \\ \therefore -i\Sigma(k,t) &= \frac{g^2}{N} \sum_{q} G_o(k-q,t)\mathcal{D}_o(q,t) \end{aligned} \tag{3.8}$$

Here, the factor of $1/N$ comes from the average over the boson momenta.

3.6 The Spectral Function

In our work, the photo-emission spectral function $A(m,n;\omega)$ evaluated on the frequency axis is defined as;

$$A(k,\omega) = \frac{1}{\pi}|\mathrm{Im}G(k,\omega)|$$

This absolute valued definition of spectral function differs from the traditional definition and is necessary in numerical application because of the finiteness of the time axis. We explain this further in this section. The retarded time bare electron Green's function in frequency space is defined as;

$$\begin{aligned} G_o(k,\omega) &= \lim_{\eta\to 0^+} \frac{1}{\omega - \varepsilon_k + i\eta} \\ &= \mathcal{P}\Big[\frac{1}{\omega-\varepsilon_k}\Big] - i\pi\delta(\omega-\varepsilon_k) \end{aligned} \tag{3.9}$$

Here, $\mathcal{P}$ represents the principal value of the function it is acting on. We see that the imaginary part of this $G_o(k,\omega)$ has the poles at the energy eigenvalues ε_k of the non-interacting part of Hamiltonian. From this, the traditional definition of the spectral function emerges;

$$A_o(k,\omega) = -\frac{1}{\pi}\mathrm{Im}(G_o(k,\omega) \tag{3.10}$$

Assuming a smooth transition from non-interacting to interacting system, we can extend this expression's validity to define interacting system's spectral function;

$$A(k,\omega) = -\frac{1}{\pi}\mathrm{Im}(G(k,\omega) \tag{3.11}$$

In the context of Dirac Delta function we often use the following relationship:

$$\begin{aligned} \lim_{\eta\to 0^+} \frac{1}{x \pm i\eta} &= \lim_{\eta\to 0^+} \frac{x}{x^2+\eta^2} \quad \mp \quad \lim_{\eta\to 0^+} i\pi \frac{\eta}{\pi(x^2+\eta^2)} \\ &= \quad \mathcal{P}\Big[\frac{1}{x}\Big] \quad \mp \quad i\pi\delta(x) \end{aligned} \tag{3.12}$$

The delta function in the imaginary part originates from the limit-definition (Sokhotski-Plemelj Theorem or Kramers Kronig Relations) of the function in the line right above it and hence is an idealization when it comes to numerical implementation. This is because in numerical implementation, explicitly demanding that η must go to zero only from the positive side of the number line (since we demand $\eta \to 0^+$) for a continuous function (bare electron green's function) is notoriously difficult. On top of this, the negative side then requires a sign flip in the definition of the delta function. Now, we no longer have a unified definition of the delta function but rather a piece-wise definition. This is still manageable when we have a single delta function i.e. bare electron Green's function in any one half of the real line. But when we use the bare electron Green's function to compute actual Green's function in the symmetric time domain and convert it back to the frequency domain, we now notice that we need to enforce this piece-wise definition of Green's function at every given frequency point. Furthermore, since there is a cutoff (t_{max}) in time, this manifests as oscillations in the frequency space in the order of t_{max}^{-1}. We are now at an impasse. We need a large t_{max} (ideally $t_{max} \to \infty$) to properly capture the Green's function decay. But t_{max} needs to be some large finite value for numerical implementation which manifests as violent small energy oscillation. In order to bypass this and reproduce the correct answer for

non-interacting as well as interacting fermionic systems, we can redefine the limit-definition of the function with an absolute value as follows;

$$\begin{aligned} \lim_{\eta\to 0}\frac{1}{x\pm i\eta} &= \lim_{\eta\to 0}\frac{x}{x^2+\eta^2} \quad \mp \quad \lim_{\eta\to 0} i\pi\left|\frac{\eta}{\pi(x^2+\eta^2)}\right| \\ &= \mathcal{P}\Big[\frac{1}{x}\Big] \quad \mp \quad i\pi\delta(x) \end{aligned} \tag{3.13}$$

Doing so, we now get a consistent single definition of the delta function on both sides of the number line. This manifests in our definition of the spectral function.

$$A(k,\omega) = \frac{1}{\pi}|G(k,\omega)| \tag{3.14}$$

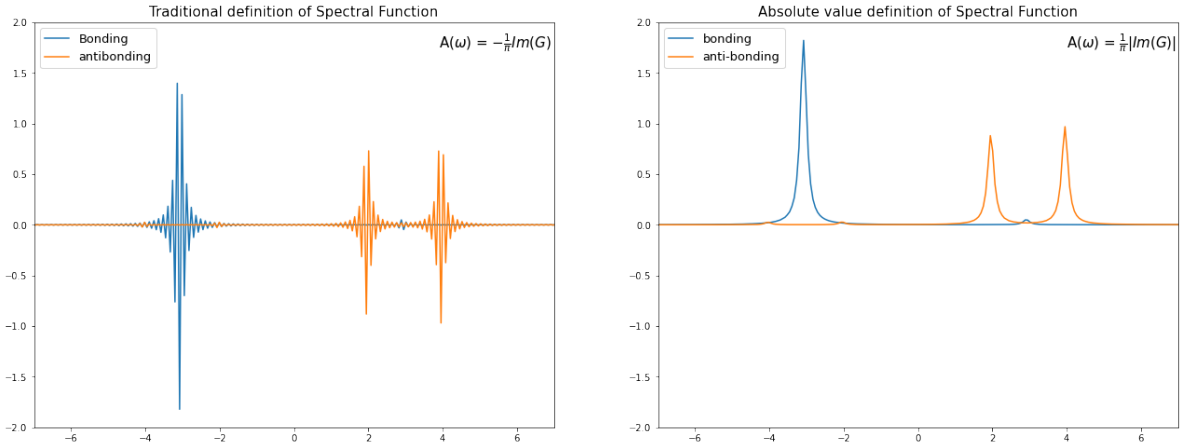

(a) Traditional definition from equation (3.10) (b) Absolute value definition from equation (3.14)

Figure 3.6: Two Definitions of Spectral Function for $g = 1$, $\varepsilon_{\pm} = \mp 3$ and $\omega_o = 6$

3.7 Migdal's Theorem and Cumulant Expansion

In the context of the Holstein problem, when the bosonic energy scale ω_o is much smaller than the electronic energy scale Δ, the interaction between the electron and the boson does not cause severe modification of electronic energy because the boson does not have enough kick to change the electronic energy. Hence, taking only the first-order self-energy and computing

the interacting Green's function gives a good enough description of the electronic properties. This is called the Migdal's theorem(61).

A better approximation to Migdal's approach is the cumulant approximation where we assume that the non-interacting electron Green's function maps to the interacting Green's function through some exponential correction (62; 11).

$$G(k,t) = G_o(k,t)e^{C(k,t)} \tag{3.15}$$

This ansatz is used in the Dyson's equation along with the first-order self-energy to compute the correction $C(k,t)$. This correction is put back in equation (3.15) and the interacting Green's function is computed. We will discuss the varieties of cumulant expansions in a later section in detail. But we would like to show the diagrammatic differences between the Migdal's approach and the cumulant approximation. Upto 2 vertex diagrams (order g^2), the

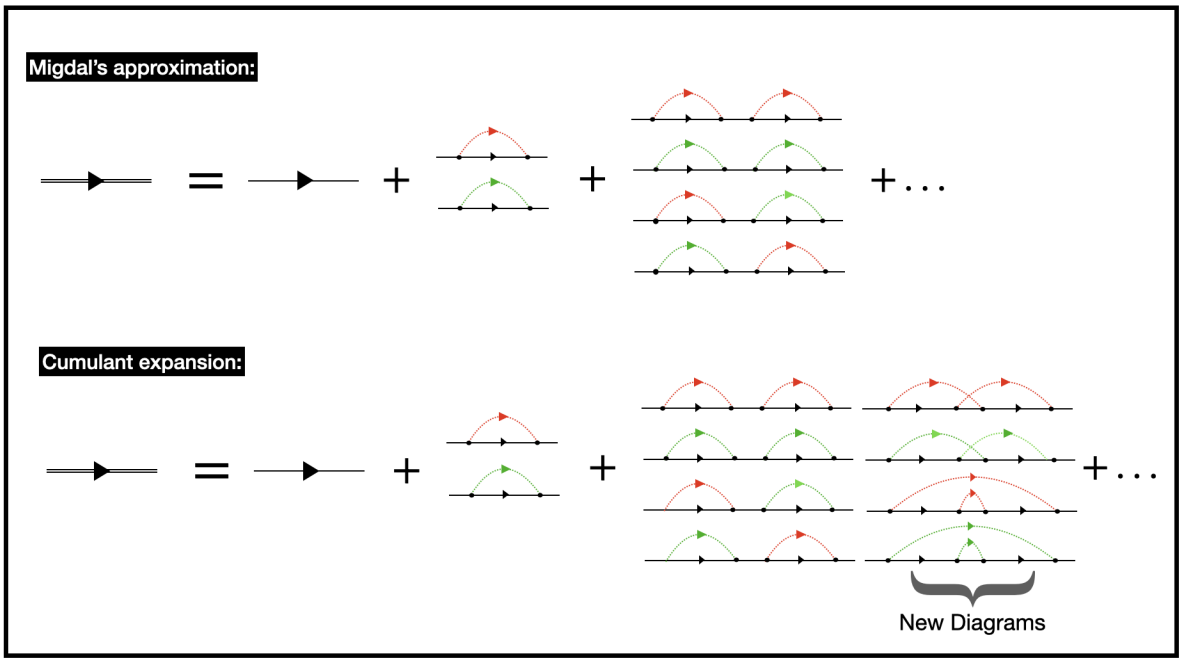

Figure 3.7: Electron interacting with two different bosons (red and green). Cumulant expansion produces more diagrams in the 2nd order compared to Migdal's approximation.

cumulant expansion and the Migdal's approximation produce the same diagrams as shown

in figure 3.7. However, at 4 vertices and more, cumulant produces novel diagrams (rainbow and overlap) along with the diagrams produced by Migdal's approximation. Hence, cumulant expansion provides a better approximation of the electronic Green's function from the same first-order self-energy as compared to Migdal's approximation.

3.8 Summary:

In this section, we discussed the main mathematical objects we use in this thesis. The Green's function, the electronic self-energy as well as the spectral function were intuitively discussed along with their equations. We also sketched the basic rules for the Feynman diagram and finally discussed the Migdal's approximation as well as cumulant expansion in terms of diagrams. Cumulant expansion as well as its varieties will be looked at again in more detail in the later chapters.

CHAPTER 4

DERIVATION AND BENCH-MARKING OF INTEGRAL POWER SERIES FORMALISM IN HOLSTEIN DIMER

4.1 The Holstein Dimer

Holstein dimer is a quantum volleyball match between two vibrating nuclei with a single electron. The quintessential example of this type of system is the dihydrogen cation (H_2^+) which occurs in hydrogen clouds (H I region) in space when atomic hydrogen is ionized by cosmic rays forcing it to share an electron with unionized atomic hydrogen.

Dihydrogen cation historically was one of the earliest models to have been investigated in the early days of the quantum revolution (1927) once quantum mechanics had successfully proved itself in the solution of energy levels of Hydrogen atom (63). However, because of the complexity of this problem, it was studied in clamped/frozen nuclei approximation (an early predecessor of the Born-Oppenheimer approximation). This approximation, by pinning the nuclei to their location, completely stops nuclear vibrations, which in real systems, are coupled to the electronic degree of freedom and thus affect the electron's dynamics. This becomes especially relevant when the coupling constant between the electronic and nuclear vibrational degree of freedom is large and when we are in the limit of a large number of vibrations per unit time when we can effectively treat these vibrations as baths of bosons - 'vibrons' in molecules and phonons in crystals.

The Holstein dimer is a perfect system to build the power series approximation scheme and test it because of its simplicity as well as clear identification of different energy scales of the problem. Furthermore, there is no known exact analytical solution but the exact numerical solution can be constructed using the exact diagonalization technique. Apart from this, the approximation methods previously used either give incorrect boson satellites (GW) or are *ad hoc* and unsystematic and incorrect at strong coupling (cumulant).

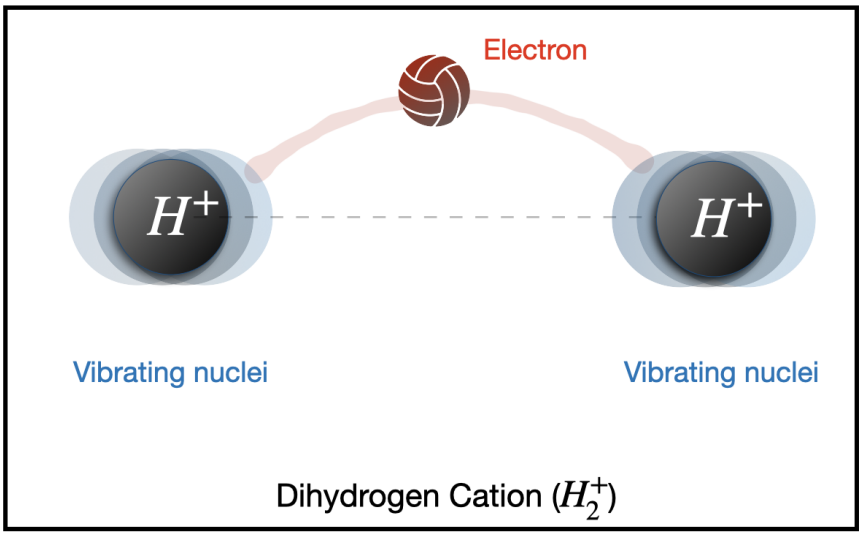

Figure 4.1: Dihydrogen Cation: An example of Holstein Dimer

In this chapter, we start by discussing the dimer's Hamiltonian and the three energy scales of this problem. We will then derive power series approximation in the context of the Holstein dimer and highlight two distinct parts of this correction. This will be followed by a derivation of various flavors of cumulant formalism through power series. Through this exercise, we will exactly point out what part of this problem is being ignored by these cumulant expansions. Finally, we will benchmark our method as well as GW and cumulant against Exact diagonalization and identify the three regimes of this problem.

4.2 Holstein Dimer's Hamiltonian

Imagine a system of two identical sites with an electron hopping between these two sites. Let $c_i^\dagger/c_i$ be the electron creation and annihilation operators for these two sites labeled by 'i' ($i = 1, 2$). let ϵ_o be the on-site energy for the electron when it is at any one of these two sites. The on-site energy is the same for both sites because they are identical. Let $-t$ be the hopping energy for the electron when it hops from one site to another. The real space

electronic Hamiltonian is;

$$H_{el} = \epsilon_o(c_1^\dagger c_1 + c_2^\dagger c_2) + (-t)(c_1^\dagger c_2 + c_2^\dagger c_1) \tag{4.1}$$

For the bosonic part of this problem, let us assume that each site can vibrate on its own without any effect on the other site. Therefore there are two distinct bosons (vibrons) in this problem - one for the vibration of each site. Let $b_i^\dagger / b_i$ be the vibron associated with the vibration of site i. Since both sites are identical to each other, the boson energy (commonly called boson frequency) for both of these vibrons is equal. Let this boson energy be ω_o. The boson dispersion is the measure of boson-boson interaction. Since the vibration of each site is independent of the other, the bosons are also dispersionless. We will explore a more complicated case with boson dispersion in a later chapter. The real space bosonic Hamiltonian is;

$$H_{bos} = \omega_o(b_1^\dagger b_1 + b_2^\dagger b_2) \tag{4.2}$$

Finally, let g be the electron-boson coupling constant that couples the electron at site 'i' to the vibration creation and annihilation at site 'i'. The real space electron-boson interaction Hamiltonian is;

$$H_{e-bos} = g(c_1^\dagger c_1)(b_1^\dagger + b_1) + g(c_2^\dagger c_2)(b_2^\dagger + b_2) \tag{4.3}$$

The real space Hamiltonian for this problem is the sum of the above three pieces.

$$H = H_{el} + H_{bos} + H_{el-bos} \tag{4.4}$$

We can transform this Hamiltonian from real space to orbital space (momenta space for crystals) by constructing bonding and antibonding combination of real-space ladder operators

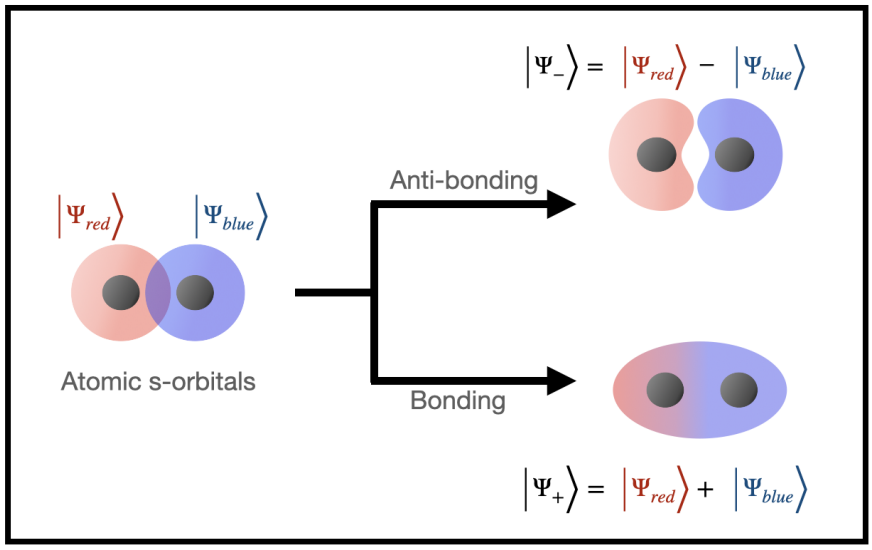

Figure 4.2: Combining atomic orbitals to form bonding(+) and anti-bonding(−) orbitals. The bonding orbital is the lower energy state among the two.

for the electron and the bosons (12).

$$c_\pm = \frac{c_1 \pm c_2}{\sqrt{2}} \quad \text{and} \quad b_\pm = \frac{b_1 \pm b_2}{\sqrt{2}} \tag{4.5}$$

Here, the fermionic ladder operators are $c_+/c_+^\dagger$ and $c_-/c_-^\dagger$ for bonding and anti-bonding orbitals respectively. The bosonic ladder operators for $(\pm)$ bosons are $b_\pm/b_\pm^\dagger$. In this bonding-antibonding basis, the dimer Hamiltonian transforms to the following:

$$\begin{aligned} H &= H_o + H_+ + H_- \quad \text{where,} \\ H_o &= \sum_{i=\pm} \varepsilon_\pm c_i^\dagger c_i \qquad \text{where, } \varepsilon_\pm = \epsilon_0 \mp t \\ H_+ &= \omega_o b_+^\dagger b_+ + \frac{g}{\sqrt{2}}(c_+^\dagger c_+ + c_-^\dagger c_-)(b_+^\dagger + b_+) \\ H_- &= \omega_o b_-^\dagger b_- + \frac{g}{\sqrt{2}}(c_+^\dagger c_- + c_-^\dagger c_+)(b_-^\dagger + b_-) \end{aligned} \tag{4.6}$$

The system in this representation has two orbitals - bonding/anti-bonding with respective energies $\varepsilon_+/\varepsilon_-$ such that their difference is Δ. This system is in baths of two dispersionless

boson species ($\pm$). The bosons are quantized packets of energy ω_o that the electron can interact with. Interaction of electron with $(-)$ bosons causes the electron's inter-orbital transition. The $(+)$ boson does not cause any electronic transition upon interaction.

The electron-boson interaction strength is controlled by the coupling constant g. The factor of $\sqrt{2}$ dividing g is a result of normalization for there being two sites and not really the part of interaction strength. The Hamiltonian for this problem is separable into three distinct pieces. H_o is the non-interacting part of the Hamiltonian. H_+ has $(+)$ bosons and doesn't cause inter-orbital transitions. H_- has $(-)$ bosons and governs inter-orbital transitions. We will show that the coupling of electron to $(\pm)$ bosons becomes crucial when $\Delta \approx \omega_o$. Vibronic couplings in this regime can cause inter-band transitions and severely renormalize the energy levels in the molecule (64; 65; 66).

4.3 Green's function and self-energy for Zero Temperature Holstein Dimer

The retarded-time(RT) formalism is better suited to handle problem with interacting electrons and holes because it treats both of them on equal footing as particles (11). Since there is a single electron in this problem, the ground state, therefore, is an absolute vacuum (fock vacuum). The excited state describes of addition of bosons or/and an electron to this vacuum. For the Holstein problem (4.6) with fock vacuum $|0\rangle$ as the ground state and $\{\ ,\ \}/[\ ,\ ]$ as the anti-commutator/commutator, The electron Green's function $G(n,t)$ for each orbital 'n' and the boson Green's function $\mathcal{D}(N,t)$ for each boson species 'N' in RT formalism is;

$$\begin{aligned} G(n=\pm,t) &= -i\theta(t)\langle 0|\{c_n(t), c_n^\dagger\}|0\rangle \\ \mathcal{D}(n=\pm,t) &= -i\theta(t)\langle 0|[b_n(t), b_n^\dagger]|0\rangle \end{aligned} \tag{4.7}$$

For the non-interacting electron boson system, the story is quite simple. The electronic and the bosonic parts of the problem do not talk to each other. The non-interacting Hamiltonian is, therefore, (4.6) in the limit $g = 0$. The Green's function defined in this limit for the electron as well as the two distinct boson species are called the bare Green's function or the non-interacting Green's function. For non-interacting electrons and dispersionless bosons with energy ω_o, the bare electron green's function G_o and a bare boson green's function $\mathcal{D}$ are,

$$\begin{aligned} G_o(\pm, t) &= -i\theta(t)e^{-i\varepsilon_\pm t} \\ \mathcal{D}(\pm, t) &= -i\theta(t)e^{-i\omega_o t} \end{aligned} \tag{4.8}$$

At zero coupling ($g = 0$), the energy eigenvalues $\varepsilon_\pm$ of (4.6) are real and the states have infinite lifetime owing to the lack of interaction between the orbitals. However, upon switching on the boson-mediated interaction ($g \neq 0$) between orbitals, the exchange of energy and momenta between states through boson exchange causes the clumping of electrons and holes to form quasiparticles. Because of time-translational invariance, we can package this interaction information together and call it the self-energy.

$$-i\Sigma(t) = g^2 \sum_{N,n=\pm} \mathcal{D}(N,t)G(n,t) = g^2 \sum_{n=\pm} -i\Sigma(n,t) \tag{4.9}$$

Each orbital's self-energy $\Sigma(n,t)$ is complex-valued, unlike the bare energy. This gives rise to spectral peak broadening - an indication of a finite quasiparticle lifetime. A properly constructed self-energy also incorporates boson-mediated inter-orbital transitions, produces satellite peaks at the correct boson frequencies, and redistributes the spectral weight from the quasiparticle to the satellites. For the very first interacting system approximation, we replace the interacting Green's function in this self-energy with their non-interacting counterparts (4.8).

4.4 Derivation of Integral Power Series Formalism

4.4.1 The Power Series Ansatz

In order to derive the power series correction, we first assume that the non-interacting electron's Green's function (G_o) for any orbital m can be adiabatically mapped to the interacting Green's function (G) for that orbital smoothly using a general power series($\mathcal{P}$) in the electron-boson coupling constant g^2 in the time domain. Mathematically, this means:

$$\begin{aligned} &G(m,t) = G_o(m,t)\mathcal{P}(m,t) \qquad \text{where,} \\ &\mathcal{P}(m,t) = 1 + g^2 C_1(m,t) + g^4 C_2(m,t) + g^6 C_3(m,t) + ... \end{aligned} \tag{4.10}$$

This is the Power series Ansatz. We assume no relationship between the functions appearing at different orders of g^2. The power series by construction is unity when '$g' = 0$. Hence, power series guarantees adiabaticity in the limit of $g \to 0$. However, we also need smooth deformation in time. Here, we use the retarded Green's function formalism starting at $t = 0$ and in this formalism, the particle always travels forward in time. Without loss of generality, we, therefore, switch on the interaction as well as the particle's evolution at $t = 0$. For smooth forward evolution in time, we must also enforce smooth forward temporal mapping from non-interacting to interacting system. For this reason, we enforce the following condition;

$$\begin{aligned} &C_i(m, t = 0) = 0 \qquad \forall i \qquad \text{[temporal adiabaticity condition]} \\ &\Rightarrow G(n, t = 0) = 1 \end{aligned} \tag{4.11}$$

Now, the system truly starts at the non-interacting limit and smoothly deforms to interacting system with coupling constant g^2 as time evolves.

4.4.2 Temporal Contraction Relation

For the bare m^{th} orbital electron Green's function, has the temporal fragmentation relation that,

$$iG_o(m, t - t_o) = \frac{1}{t - t_o} \int_{-\infty}^{\infty} dt_1 (iG_o(m, t - t_1))(iG_o(m, t_1 - t_o)) \tag{4.12}$$

This just means that the actual bare Green's function is the average of all possible time-fractured bare Green's function. Let us assume that the same relation also holds true for the actual (measured) Green's function in that it must also be the average of all possible time-fracturing. i.e,

$$iG(m, t - t_o) = \frac{1}{t - t_o} \int_{-\infty}^{\infty} dt_1 (iG(m, t - t_1))(iG(m, t_1 - t_o)) \tag{4.13}$$

If we replace the power series ansatz on both sides in this relation, we get;

$$iG_o(m, t - t_o)\mathcal{P}(m, t - t_o) = \frac{1}{t - t_o} \int_{-\infty}^{\infty} dt_1 (iG_o(m, t - t_1))(iG_o(m, t_1 - t_o)). \\ \left[\mathcal{P}(m, t - t_1)\mathcal{P}(m, t_1 - t_o\right] \tag{4.14}$$

The simplest relation that one could think of to make all three equations above to be true would be if;

$$\mathcal{P}(m, t - t_o) = \mathcal{P}(m, t - t_1)\mathcal{P}(m, t_1 - t_o) \qquad \forall \ t_o < t_1 < t \tag{4.15}$$

Although this contraction property of the power series corrections seems quite trivial, implementing this contraction property in actual calculations is absolutely essential because this gives rise to the bosonic crossing diagrams in the diagrammatic series expansion. Without such contraction, the core-hole cumulant expression cannot be derived from the power series machinery. This contraction relation isn't valid between power series pieces for different

orbitals.

4.4.3 Power Series Corrected self-energy

As the particle (electron or hole) evolves in time, it undergoes interaction with the ($\pm$) bosons. The irreducible part of this interaction between the particle and the boson is packaged in self-energy as described in the previous chapter. The overall evolution of the electron's Green's function is given by the Dyson's equation - repeated application of this self-energy on the particle Green's function. The particle is evolving in time as it interacts with the boson, there is a piece of particle's Green's function wedged inside the self-energy. Since we are correcting the overall Green's function, we must also correct this piece of Green's function inside the self-energy. Furthermore, in order to make sure that the interacting Green's function given by Dyson's equation smoothly transforms to non-interacting Green's function in the limit of $g \to 0$, the self-energy also gets a factor of g^2 in front of it. In the language of the Feynman diagram, this factor is colloquially called 'the vertex' and encodes the probability amplitude of the occurrence of interaction between the particle and the boson. In the context of Holstein dimer, If $G(m,t)$ and $G_o(m,t)$ are the particle's interacting and non-interacting Green's functions when it is in the m^{th} orbital and $D(N,t)$ is the N^{th} boson's Green's function (N=$\pm$), the self-energy can be written as;

$$\begin{aligned} -i\Sigma(t) &= g^2 \sum_{\substack{m=\pm \\ N=\pm}} G(m,t)\mathcal{D}(N,t) \\ &= g^2 \sum_{\substack{m=\pm \\ N=\pm}} G_o(m,t)\mathcal{P}(m,t)\mathcal{D}(N,t) \\ &= g^2 \sum_{m=\pm} -i\Sigma(m,t)\mathcal{P}(m,t) \end{aligned} \tag{4.16}$$

This is the power series corrected self-energy. Here, we have replaced the particle's interacting Green's function with the power series ansatz from (4.10) in the second step. This is followed

by a regrouping of terms and the definition of m^{th} orbital's self-energy $\Sigma(m,t)$.

4.4.4 The Dyson's equation with Power Series Correction

The next step is to replace both power series corrected particle's Green's function(4.10) and power series corrected (4.16) into Dyson's equation in the time domain. Without loss of generality, we take the initial time t_i as 0 and the final time t_f as t.

$$\begin{aligned} G(m,t_f-t_i) &= G_o(m,t_f-t_i)+\int_{t_i}^{t_f}dt_2\int_{t_i}^{t_f}dt_1 G(m,t_1-t_i)\Sigma(t_2-t_1)G_o(m,t_f-t_2) \\ \therefore G(m,t) &= G_o(m,t)+\int_0^t dt_2\int_0^t dt_1 G(m,t_1)\Sigma(t_2-t_1)G_o(m,t-t_2) \\ G_o(m,t)\mathcal{P}(m,t) &= G_o(m,t)+\int_0^t dt_2\int_0^t dt_1 G_o(m,t_1)\mathcal{P}(m,t_1)\Sigma(t_2-t_1)G_o(m,t-t_2) \end{aligned} \tag{4.17}$$

We now expand the non-interacting Green's function and use the following composition rule for the non-interacting Green's function to simplify the above expression.

$$\begin{aligned} G_o(m,t_1)G_o(m,t-t_2) &= (-ie^{-i\varepsilon_m t_1})\Theta(t_1)\,(-ie^{-i\varepsilon_m(t-t_2)})\Theta(t-t_2) \\ &= (-ie^{-i\varepsilon_m t})\Theta(t)\,(-ie^{-i\varepsilon_m(t_1-t_2)})\Theta(t_2-t_1) \\ &= G_o(m,t)\,(-ie^{i\varepsilon_m(t_2-t_1)})\Theta(t_2-t_1) \end{aligned} \tag{4.18}$$

Here we used the time-ordering enforced by the Heaviside functions in the non-interacting retarded electron Green's function outside and inside the self-energy in the rightmost integral of (4.17). The Green's function inside the self-energy enforces $t_1 \leqslant t_2$ and the Green's functions outside enforce $0 \leqslant t_1$ and $t_2 \leqslant t$. Hence the total time ordering is $0 \leqslant t_2 \leqslant t_1 \leqslant t$. Once this relation is established, we can now generate appropriate Heaviside functions that satisfy the time-ordering and set the limits for the integral. Replacing equation (4.18) in the

last term of (4.17) and canceling the factor of $G_o(m,t)$ on both sides, we get;

$$\mathcal{P}(m,t) = 1 + (-i)\int_0^t dt_2 \int_0^{t_2} dt_1 e^{i\varepsilon_m(t_2-t_1)}\Sigma(t_2-t_1)\mathcal{P}(m,t_1)$$

Finally, we replace the power series corrected self-energy (4.16) in the equation above and redefine $t_2 - t_1 = \tau$.

$$\mathcal{P}(m,t) = 1 + (-ig^2)\sum_{n=\pm}\int_0^t dt_2 \int_0^{t_2} d\tau e^{i\varepsilon_m\tau}\Sigma(n,\tau)\mathcal{P}(n,\tau)\mathcal{P}(m,t_2-\tau)$$

This expression can be further simplified by using the temporal contraction relation (4.15) when $n = m$. The final expression is;

$$\begin{aligned}\mathcal{P}(m,t) = 1 + (-ig^2)\int_0^t dt_2 \int_0^{t_2} d\tau e^{i\varepsilon_m\tau}\Sigma(m,\tau)\mathcal{P}(m,t_2) + \\ (-ig^2)\sum_{n\neq m}\int_0^t dt_2 \int_0^{t_2} d\tau e^{i\varepsilon_m\tau}\Sigma(n,\tau)\mathcal{P}(n,\tau)\mathcal{P}(m,t_2-\tau) \quad (4.19)\end{aligned}$$

This is the integral power series correction equation. The initial condition here is $\mathcal{P}(m, t = 0) = 1$ which is a consequence of the assumption that Green's function smoothly evolves forward in time in response to turning the interaction on at $t = 0$ as described in subsection 4.4.1.

4.4.5 Recursive Relation for Power Series

Since we are asserting that the perturbative expansion holds true, we can compare terms of the same order in the coupling constant g^2 on both sides. This immediately yields a recursive relation between the corrections with the starting correction being 1. Hence, we now are able to compute corrections to any order given that the series converges fast enough. A necessary condition for this is that the contribution of the higher-order terms must be smaller and

limiting to zero than the lower-order terms or else the sum diverges. We can write the recursive relation more explicitly. For the x^{th} correction term;

$$C_x(m,t) = (-i)\int_0^t dt_2 \int_0^{t_2} d\tau e^{i\varepsilon_m \tau}\Sigma_o(m,\tau)C_{x-1}(m,t_2)+ \\ (-i)\sum_{n\neq m}\sum_{y=0}^{x}\int_0^t dt_2\int_0^{t_2} e^{i\varepsilon_m\tau}\Sigma_o(n,\tau)C_y(n,\tau)C_{x-1-y}(m,t_2-\tau) \quad (4.20)$$

The initial condition for these equations is $C_x(m,t=0)=1$ for all orbital m.

4.4.6 Two distinct families of correction within Power Series:

The final power series equation (4.19) is composed of two distinct types of correction terms - the self correction(P_{SC}) and the inter-orbital correction (P_{IC}). This distinction arises from the enforcement of temporal contraction relation to compress power series pieces between the same orbital when $m=n$ and not doing so when $n\neq m$ in (4.19). This is also observed in the recursive formalism (4.20) between the first and the second integral term on the right-hand side.

$$\begin{aligned} \mathcal{P}(m,t) &= 1 + P_{SC}(m,t) + P_{IC}(m,t) \qquad \text{where,} \\ P_{SC}(m,t) &= (-ig^2)\int_0^t dt_2 \int_0^{t_2} dt_1 e^{i\varepsilon_m\tau}\Sigma(m,\tau)\mathcal{P}(m,t_2) \\ P_{IC}(m,t) &= (-ig^2)\sum_{n\neq m}\int_0^t dt_2\int_0^{t_2} dt_1 e^{i\varepsilon_m\tau}\Sigma(n,\tau)\mathcal{P}(n,\tau)\mathcal{P}(m,t_2-\tau) \\ \mathcal{P}(m,t=0) &= 1 \quad \forall m \qquad \text{(Initial condition)} \end{aligned} \quad (4.21)$$

The self-correction term incorporates the effects of (+) bosons which makes the electron hop from an orbital to the vibrational states originating from the same orbital. The inter-orbital correction term incorporates the effects of (−) bosons which when absorbed make the

electron jump from orbital m to the vibrational states originating from a different orbital n. Without making this distinction through the use of temporal contraction relation, we can only generate $2/3^{rd}$ of the interactions associated with self-hopping. This will be discussed in detail in a later section where we explore the diagrammatic interpretation of the Power series.

4.5 Derivation of Cumulant formalisms from Power Series

4.5.1 Simplest case: Instantaneous scattering by a static external potential

Consider a single (or isolated) band system with the band's bare energy ε. If we subject such a system to a static external potential V with particle-potential coupling parameter g^2, we know that there is a rigid shift in the band's energy by g^2V such that $\varepsilon \to \varepsilon + V$ in the limit of $g^2 \to 1$. We can explicitly show this result by using our formalism. With the bare and the corrected Green's function as defined in (4.8) and (4.10), our self-energy is given by;

$$\Sigma(t) = g^2 V\delta(t) = g^2\Sigma_o(t)\mathcal{P}(t)$$

Since we have a single band, our equation (4.21) boils down to the self-correction term. We can write the correction equation as;

$$\begin{aligned}\mathcal{P}(t) &= 1 + (-ig^2)\int_0^t dt_1 \int_0^{t_1} d\tau e^{i\varepsilon\tau}\Sigma_o(\tau)\mathcal{P}(t_1) \\ &= 1 + (-ig^2V)\int_0^t dt_1 \mathcal{P}(t_1)\end{aligned}$$

If we start the recursion with $C_0 = 1$, we find that $C_1 = -iVt$, $C_2 = (-iVt)^2/2!$ and so on. In general,

$$C_n(t) = -iV \int_0^t dt_1 C_{n-1}(t) = \frac{(-iVt)^n}{n!}$$

$$\begin{aligned}
\mathcal{P}(t) &= 1 + \sum_{n=1}^{\infty} g^{2n} C_n(t) = 1 + \sum_{j=1}^{\infty} \frac{(-ig^2Vt)^n}{n!} \\
&= e^{-ig^2Vt} \\
\therefore G(t) &= G_o(t)\mathcal{P}(t) = -ie^{-i(\varepsilon + g^2V)t}\theta(t)
\end{aligned}$$

We now have retrieved the right shift solution for not just $g^2 = 1$ but also for all possible values of g^2. We notice that the energy changes smoothly from bare energy when we tune the coupling parameter g^2 starting from 0.

4.5.2 The Core hole Cumulant from Power Series

Now we consider a single band of electrons of bare energy ε_o in a bath of dispersionless bosons (vibrons) of frequency ω_o. Although in real systems, dispersion of bosons is inevitable, the advantage of keeping them dispersionless is that this model is exactly solvable (62; 12). In fact, the solution to this problem is termed the core-hole cumulant which lies at the heart of all other cumulant approximations.

If we define the electron and boson creation/annihilation operators as $c^\dagger/c$ and $b^\dagger/b$ respectively the Hamiltonian for the problem is as follows;

$$H = \varepsilon_o c^\dagger c + \omega_o b^\dagger b + g(b^\dagger + b)(c^\dagger c - 1) \tag{4.22}$$

This is a more physical problem if one considers a well-separated band of electron that is far away from other valence bands and far below the Fermi level. Such bands model the core

electron/hole states which are isolated and do not interact strongly with other bands and can be qualitatively mapped to x-ray photo-emission data. The bosons in such multi-electronic systems could be plasmons (collective oscillation of valence electrons) without damping. This problem serves as a good physical model to elucidate the coupling of core states with these plasmons when such levels are probed using x-ray photo-emission techniques. The energetic electron that leaves the system in such experiments leaves behind a hole and the electron cloud responds to the imbalance of Coulomb forces by undergoing quantized long-range plasma oscillations at multiples of ω_o which here is the plasma(boson) frequency.

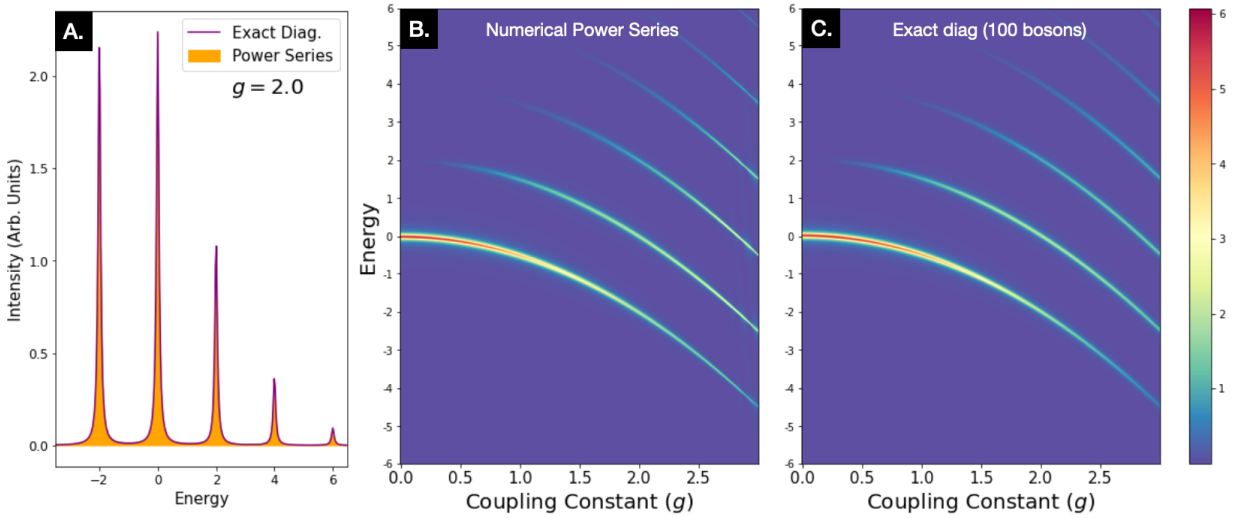

Figure 4.3: Electron spectral function for a core electron problem coupled to a boson bath as a function of coupling strength g using integral power series and exact diagonalization show exact agreement. Here, $\epsilon_o = 0$ and $\omega_o = 2$

We first show that power series can indeed solve this problem numerically at all g. In panel A. of figure 4.3, we show a self-consistent integral power series solution, as well as the exact diagonalization result with 100 bosons for $g = 2$. Both these results are in exact agreement. In panels B. and C., we show power series results and exact diagonalization results respectively for a wide range of coupling constant. Here too, we see exact agreement between the two methods.

We will now show the analytical derivation of core-hole cumulant result using integral

power series formalism. The bare Green's function with bare energy ε_o and the corrected Green's functions are defined as (4.8)] and (4.10). Here too, we suppress the momenta variable. The self-energy for this case with power series corrected internal Green's function is;

$$\begin{aligned} -i\Sigma(t) &= g^2 G(t).\mathcal{D}_o(t) = g^2.G_o(t)\mathcal{P}(t).\mathcal{D}_o(t) \\ &= g^2\big[-e^{-i(\varepsilon_k-\omega_o)t}\theta(t)\big]\mathcal{P}(t) \\ &= -ig^2\Sigma_o(t)\mathcal{P}(t) \end{aligned} \tag{4.23}$$

Since there is a single band, we only have a self-correction term in equation (4.21).

$$\begin{aligned} \mathcal{P}(t) &= 1 + (-i)g^2 \int_0^t dt_1 \int_0^{t_1} d\tau e^{i\varepsilon_k\tau}\Sigma_o(\tau)\mathcal{P}(t_1) \\ &= 1 + (-ig)^2 \int_0^t dt_1 \int_0^{t_1} d\tau e^{i\omega_o\tau}\mathcal{P}(t_1) \\ &= 1 + (-ig)^2 \int_0^t dt_1 \mathcal{P}(t_1)\Big[\frac{e^{i\omega_o t_1}-1}{i\omega_o}\Big] \end{aligned}$$

We now insert Power series ansatz on both sides and compare terms of the same order in g^2 in the equation above.

$$\begin{aligned} 1 + g^2C_1(t) + g^4C_2(t) + ... &= 1 + g^2(-i^2)\int_0^t dt_1\big[1 + g^2C_1(t_1) + g^4C_2(t_1) + ...\big]\Big[\frac{e^{i\omega_o t_1}-1}{i\omega_o}\Big] \\ \therefore C_n(t) &= (-i^2)\int_0^t dt_1 C_{n-1}(t_1)\Big[\frac{e^{i\omega_o t_1}-1}{i\omega_o}\Big] \end{aligned} \tag{4.24}$$

We can then start with $C_0 = 1$ to generate the higher order corrections.

$$C_1(k,t) = -\int_0^t d\tau\ 1.\left[\frac{e^{i\omega_o\tau}-1}{i\omega_o}\right] = \left[\frac{e^{i\omega_o t}-i\omega_o t-1}{\omega_o^2}\right]$$
$$\implies dC_1(k,t) = \left[\frac{e^{i\omega_o t}-1}{-i\omega_o}\right]dt$$

Using this relation in the original equation 4.24 to get;

$$\begin{aligned} C_n(t) &= \int_0^t dt_1 C_{n-1}(t)\, dC_1(k,t) = \frac{C_1(k,t)^n}{n!} \\ \therefore \mathcal{P}(k,t) &= e^{g^2 C_1(k,t)} \qquad \text{and,} \\ G(k,t) &= G_o(k,t)e^{g^2 C_1(k,t)} \end{aligned} \tag{4.25}$$

This is the exact result for the core hole problem with a dispersionless boson with an added advantage of a smoothly tunable coupling parameter g.

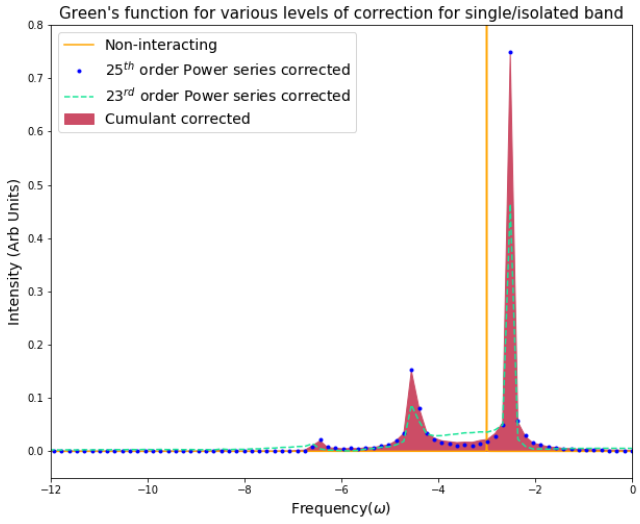

Figure 4.4: Spectral function for a core hole. Notice how the satellites are on the other side as compared to the electron problem shown in figure 4.3. Here, $\varepsilon_o = -3$ units, $\omega_o = 2$ units, and $g^2 = 1$, the power series corrected Green's function approaches the cumulant corrected Green's function computed on the same time-grid with increasing order of correction.

With added iterations of the self-consistent cycle of power series, our corrected Green's function gets closer to the exact answer given by cumulant ansatz found in (62). The number of cycles required to converge is inversely related to the proximity of boson frequency to quasiparticle energy. We see in the above figure 4.4 that as we increase the number of self-consistent iterations from 23 to 25, the power series smoothly deforms to exactly capture the cumulant spectra. No change is observed with added iterations once the converged solution is reached.

4.5.3 The Retarded-Time Cumulant from Power Series

In the original formalism of time-ordered cumulant applied to GW band structure, (12; 67), since electrons and holes are described by different branches of a piece-wise Green's function, there is no interaction between an electron state (above Fermi level) and a hole state (below Fermi level). Some fraction of the inter-band effect between holes alone and between electrons alone is accounted for by this method. Later, Kas et al. (11) extended the method and showed that by using a retarded time cumulant formalism, some fraction of inter-band effects between all states can be accounted for. But a clear justification of just how much inter-band effect is accounted for by the method is missing. Furthermore, the idea of systematically improving the method is also absent in both formalisms.

Our method can successfully recreate the expressions of retarded cumulant by improving the assumptions on interaction. Rather than doing this derivation in a crystalline setup with multiple bands, we will do this in a Holstein dimer because of two reasons- the simplicity of the system and a clear Hamiltonian. But the idea still carries over and we will discuss this in the later chapters. We will also make this Holstein dimer Hamiltonian more elaborate by artificially assuming that the electron-boson coupling constant is different for different boson species - i.e, $g_{\pm}$ respectively in $H_{\pm}$. This assumption effectively converts the Holstein system to Frohlich-type Hamiltonian thus allowing us to extend our method to a larger class

of electron-boson coupling problems. Converting this back to the Holstein system is a matter of setting $g_+ = g_-$. This artificially constructed Frohlich-type Hamiltonian in orbital space is then;

$$\begin{aligned} H &= H_o + H_+ + H_- \quad \text{where,} \\ H_o &= \sum_{i=\pm} \varepsilon_\pm c_i^\dagger c_i \qquad \text{where, } \varepsilon_\pm = \epsilon_0 \mp t \\ H_+ &= \omega_o b_+^\dagger b_+ + \frac{g_+}{\sqrt{2}}(c_+^\dagger c_+ + c_-^\dagger c_-)(b_+^\dagger + b_+) \\ H_- &= \omega_o b_-^\dagger b_- + \frac{g_-}{\sqrt{2}}(c_+^\dagger c_- + c_-^\dagger c_+)(b_-^\dagger + b_-) \end{aligned} \tag{4.26}$$

If we treat the corrections as being explicitly independent of the orbital (orbital index $m = \pm$), then we can reproduce the retarded cumulant. This assumption physically means that the orbital energy gap(Δ) is small and thus orbitals bands are almost equal to each other everywhere such that $\varepsilon_m \approx \varepsilon_n$ for all $m \neq n$. In this limit of $t \to 0$, the retarded cumulant ansatz approached the true correction. Physically, this means that the hopping energy required for the electron to hop from one to another site is almost zero because the sites are extremely close to each other. If these conditions are not true, then the retarded cumulant ansatz generates the inter-band interactions only partially.

For dispersion-less boson of frequency ω_o and two orbitals with bare energies ε_+(lower) and ε_-(upper), if the above assumptions about explicit orbital independence of corrections hold true, we can compute the correction series exactly. The orbital self energies with power series corrected internal green's function in retarded time formalism are:

$$\begin{aligned} \Sigma(+,t) &= \frac{g_+^2}{2} \sum_{n=\pm} G_o(n,t)\mathcal{P}(n,t)\mathcal{D}(+,t) \\ \Sigma(-,t) &= \frac{g_-^2}{2} \sum_{n=\pm} G_o(n,t)\mathcal{P}(n,t)\mathcal{D}(-,t) \end{aligned} \tag{4.27}$$

Here, $\Sigma(\pm,t)$ captures the effect of $(\pm)$ bosons respectively and hence contains the respective

boson's Green's function $\mathcal{D}(\pm, t)$. We now define a dummy constant g such that $g_+ \rightarrow g_+/g$ and $g_- \rightarrow g_-/g$ and expand our power series correction in terms of g^2 rather than $g_\pm^2$. We will set $g = 1$ at the very end. Thus far, the total self-energy without making any approximation of orbital independence is;

$$\begin{aligned}\Sigma(t) &= \Sigma(+,t) + \Sigma(-,t) \\ &= g^2\Big[\frac{g_+^2}{2g^2}\sum_{n=\pm} G_o(n,t)\mathcal{P}(n,t).\mathcal{D}(+,t) + \frac{g_-^2}{2g^2}\sum_{n=\pm} G_o(n,t).\mathcal{P}(n,t)\mathcal{D}(-,t)\Big]\end{aligned} \tag{4.28}$$

Given our assumptions hold true, let $\mathcal{P}(t)$ be the (explicit orbital independent) correction to the bare Green's function G_o. The total self-energy $\Sigma(t)$ for such a system given orbital self energies $\Sigma(m,t)$ is;

$$\begin{aligned}-i\Sigma(t) &= -i\Sigma(+,t) + -i\Sigma(-,t) \\ &= g^2\Big[\frac{g_+^2}{2g^2}\sum_{n=\pm} G_o(n,t)\mathcal{D}(+,t) + \frac{g_-^2}{2g^2}\sum_{n=\pm} G_o(n,t)\mathcal{D}(-,t)\Big]\mathcal{P}(t) \\ &= g^2\Big[\quad \frac{g_+^2}{2g^2}(-i\Sigma_o(+,t)) \qquad + \qquad \frac{g_-^2}{2g^2}\,(-i\Sigma_o(-,t)) \quad\Big]\mathcal{P}(t) \\ &= -i\,g^2\,\Sigma_o(t)\,\mathcal{P}(t)\end{aligned} \tag{4.29}$$

The power series correction comes out of the summation in 4.29 as compared to 4.28 because of this approximation. This is equivalent to saying that for the electron in any orbital m, the correction due to the n^{th} orbital's presence is equal to the correction due to m^{th} orbital which indeed is true if the orbitals are so close that they almost completely overlap or if the boson energy scale (ω_o) is really large compared to the orbital energy difference ('t').

The power series correction for the for the electron in n^{th} orbital after using the contrac-

tion relation [4.15] is ;

$$\mathcal{P}(t) = 1 - ig^2 \int_0^t dt_1 \int_0^{t_1} d\tau e^{i\varepsilon_n \tau} \Sigma_o(\tau) \mathcal{P}(t_1) \tag{4.30}$$

If we solve the above equation for the lower energy orbital $n = (+)$ with exponential ansatz, we get;

$$\begin{aligned} \mathcal{P}(t) &= 1 + (-ig)^2 \int_0^t dt_1 \mathcal{P}(t_1) \Big[\frac{e^{-i\omega_o t_1} - 1}{-i\omega_o} + \frac{e^{-i\tilde{\omega}_o t_1} - 1}{-i\tilde{\omega}_o} \Big] = e^{g^2 C_1(t)} \quad \text{with,} \\ C_1(k,t) &= \frac{g_+^2}{g^2} \Big(\frac{e^{-i\omega_o t} + i\omega_o t - 1}{\omega_o^2} \Big) + \frac{g_-^2}{g^2} \Big(\frac{e^{-i\tilde{\omega}_o t} + i\tilde{\omega}_o t - 1}{\tilde{\omega}_o^2} \Big) \\ &\text{where}, \tilde{\omega}_o = \omega_o + (\varepsilon_- - \varepsilon_+) = \omega_o + \Delta \end{aligned} \tag{4.31}$$

We can equivalently get the power series correction expression for $n = (-)$ orbital.

$$\begin{aligned} \mathcal{P}(t) &= e^{g^2 C_1(t)} \\ C_1(k,t) &= \frac{g_+^2}{g^2} \Big(\frac{e^{-i\omega_o t} + i\omega_o t - 1}{\omega_o^2} \Big) + \frac{g_-^2}{g^2} \Big(\frac{e^{-i\bar{\omega}_o t} + i\bar{\omega}_o t - 1}{\bar{\omega}_o^2} \Big) \\ &\text{where, } \bar{\omega}_o = \omega_o - (\varepsilon_- - \varepsilon_+) = \omega_o - \Delta \end{aligned} \tag{4.32}$$

4.5.4 The Core-hole Cumulant for Holstein Dimer

In this section, we will sketch the derivation of Core-hole cumulant for Dimer and higher systems in retarded time formalism. In Principle, this cumulant is equivalent to a time-ordered cumulant where the particle and hole levels (here antibonding and bonding levels) are treated by separate branches of Green's function. Hence there is no cross-talk between the two levels i.e. no intra-orbital corrections. In retarded time formalism of Green's function, all this means is that the $(-)$ bosons' effect and therefore terms with $\mathcal{D}(-,t)$ in dimer's self-

energy (4.27) are neglected. The only correction the orbitals get is therefore the inter-orbital corrections due to (+) bosons. The end result is that;

$$\begin{aligned} \mathcal{P}(n,t) &= e^{g^2 C_1(t)} \\ C_1(n,t) &= \frac{g_+^2}{g^2}\Big(\frac{e^{-i\omega_o t} + i\omega_o t - 1}{\omega_o^2}\Big) \end{aligned} \tag{4.33}$$

4.6 Summary:

In this chapter, we started with a general Holstein dimer explaining its real and momenta space Hamiltonian. We then defined the Green's functions of the particles involved as well as the construction of self-energy. We then established the power series ansatz and derived the Power series correction equation highlighting the core principle of self-consistency inherited through the Dyson's equation. Two distinct types of correction terms associated with two different types of bosons were discovered - the self-correction and the inter-orbital correction. We then derived the core-hole and the retarded time cumulant correction by making particular approximations to the power series. In the next chapter, we will explore the numerical results for spectral function from core-hole as well as the retarded-time cumulant and explain their advantages as well as drawbacks. Furthermore, we will investigate the performance of full power series formalism (4.21) on producing the spectral function for the Holstein dimer and benchmark it against the spectral function found through the exact diagonalization technique.

CHAPTER 5

UNDERSTANDING AND GOING BEYOND THE CUMULANT APPROXIMATION: BENCH-MARKING POWER SERIES

So far, we have a power series machinery that in principle computes the interacting system's electron Green's function from the non-interacting system's Green's function. And it has performed fairly well analytically in the limiting cases of core-hole and retarded time cumulant. However, our end goal is to produce a method that works not only in the limiting cases but is easy to implement, inexpensive and reliable. In this chapter, we will outline the numerical implementation of Power series correction. We will then take a detour to investigate the two flavors of cumulant approximations numerically highlighting their technical differences. We will then come back to the numerical implementation of full power series correction formalism (4.21) to produce electron Green's function and spectral function for the interacting system and benchmark it against exact diagonalization result in a finite yet high boson number basis.

5.1 Visualizing the Holstein Dimer : A semi classical interpretation

In order to visualize what the dimer is actually doing, let us look closely to what the bosons actually are in this system. For the electronic orbital, we previously assumed a linear combination of s-like orbitals as shown in figure 4.2. For simplicity, we will limit our discussion to a 1 dimensional vibrations of the system. Here, we assume that each nucleus is a simple 1D harmonic oscillator independent of the oscillation of another nucleus. We can think of this as the nucleus bound to it's equilibrium position with a 'quantum' spring.

5.1.1 *The (±) bosons- quantum mechanics to semi-classical interpretation*

Moving on to the dimer, we now have two separate harmonic traps where two nuclei 'A' and 'B' are trapped respectively. However, we assume that each of these nuclei is only affected by their individual trap. Doing so, we can formulate the bonding and antibonding combination of boson. The bonding combination of wave functions corresponds to (+) bosons and the antibonding combination corresponds to the (−) bosons.

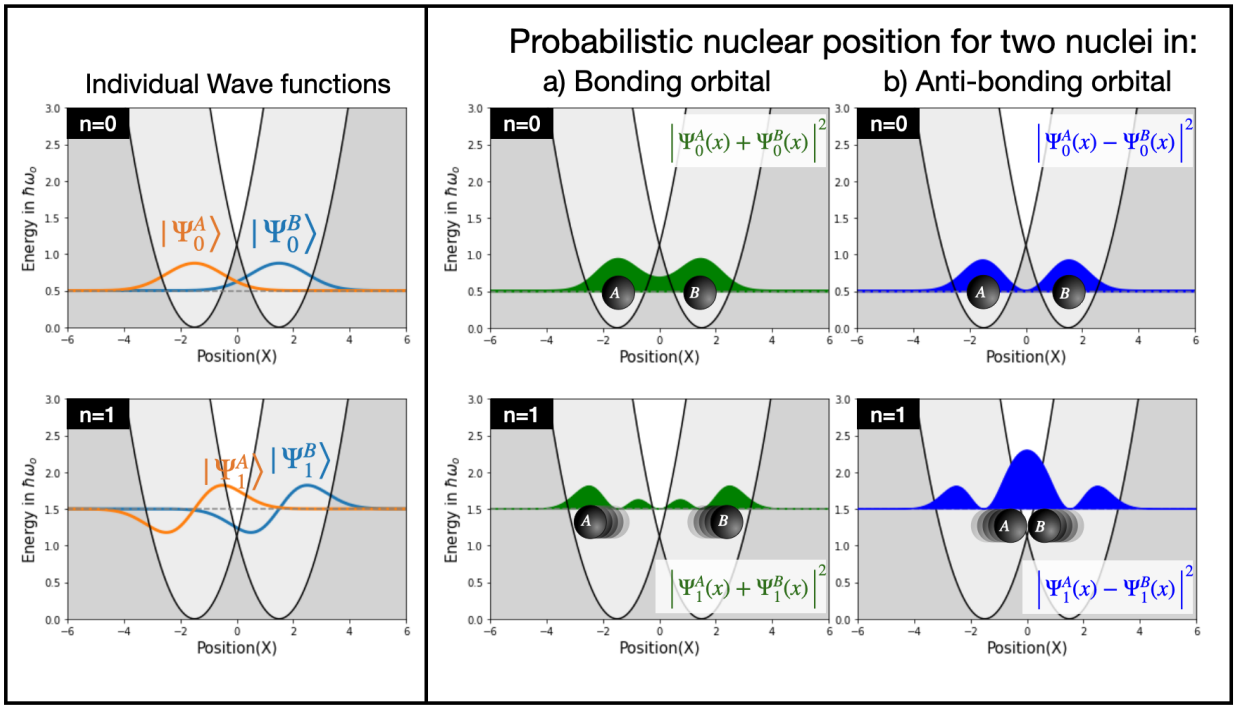

Figure 5.1: Two nuclei in two harmonic traps. The figure on left show the nuclear wave functions for '$n = 0$' and '$n = 1$' states. The mid and the right panels show the probabilistic nuclear position while setting on (+) and (−) bosons respectively. A semi-classical interpretation of this position probability with two nuclei 'A' and 'B' is also provided in the inlay.

We have shown a semi-classical interpretation of the nuclear motion associated with each of the (+) and (−) boson for zero and single boson cases in figure 5.1. The index n here quantifies how many bosons of a given type is present in the system. At '$n = 0$' mode, although the wave functions for both (±) bosons have a finite width due to quantum mechanical effect. However, semi-classically, we can think of the two nuclei as sitting essentially still on average

at the center of the trap - the lattice site. Moreover, there is not much qualitative difference between the two wave functions either and they both have same constant energy. Hence, we can subtract the constant zero boson energy from the Hamiltonian just as previously done.

The nuclei on average move apart while setting up a single quanta of (+) boson and move towards each other while setting up a single quanta of (−) boson. A similar analysis can be done for multi-boson case although we will produce a lot more combination of orbitals. We show the probability density for nuclear position as well as a semi-classical interpretation of what the nuclei are doing when 0 and 1 quanta of (±) bosons are set up in figure 5.1.

5.1.2 Putting together Electronic and Bosonic Physics

Suppose the motion of the nucleus distorts the electron cloud (the orbital) around it. This is not too loose of an assumption in this case because of the fact that there is a single electron in the problem and it is attracted to the two nuclei. We also suppose that this distortion is adiabatic on the pure electronic orbitals with frozen nuclei in that the general of the orbitals don't change much other than stretching or compressing to accommodate for the nuclear motion -the (±) bosons. We can combine this semi classical picture of boson with the electronic bonding/anti-bonding orbital from 4.2 to get a zoo of orbitals and visualize the problem better as shown in figure 5.2. In this picture the (+) boson separates the two nuclei and hence if the electron in in any one of the two lobes (blue or red), it will more likely stay in that lobe. Hence, there is only an overall adiabatic distortion of the orbital shape but bonding orbital remains bonding and anti-bonding orbital remains anti-bonding. In case of (−) boson, since the orbitals are squished together as shown in the semi classical picture 5.2, the electron can hop between the lobes which can result in orbital rearrangement where bonding/anti-bonding orbital could transmute into anti-bonding/bonding orbital. Of course this is just a semi-classical view of what is happening and holds true only when the separation between the nuclei is large. For nuclei that are extremely close to each other, full

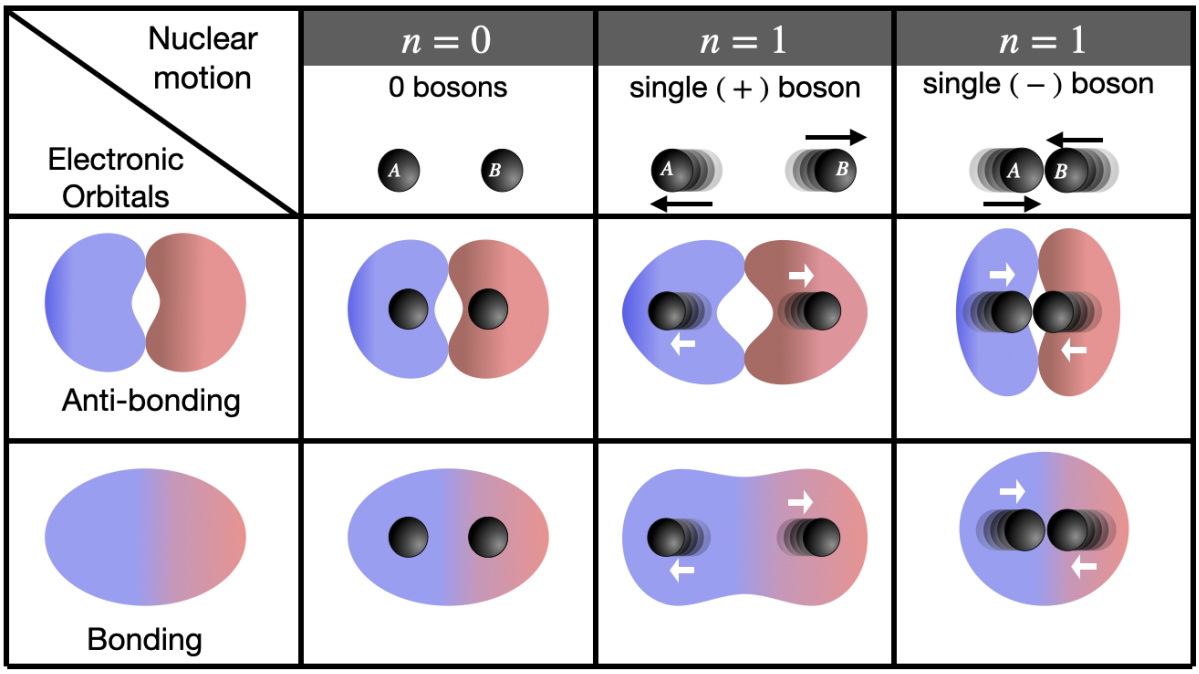

Figure 5.2: Zero (n=0) or a single (n=1) quanta of (±) boson combined with the electronic orbital. The bosons correspond to specific motions of the nuclei(black orbs).

quantum mechanical calculation is desired. For now, we revisit the full dimer problem and look at the electron-boson physics in action in a very semi-classical way.

5.1.3 Visualizing the Electron-Boson Coupling

In the figure 5.3 (A.), we first start with an electron in one of the pure electronic states with energy ε_+. So far, the nuclei are static and thus the system is boson-less. Suppose we pump this system with a single quanta of (+) boson of boson frequency ω_o. This is equivalent to the two nuclei rapidly separating. The question we now ask is what state will this hybrid electron-boson system be in.

As discussed before, the electronic state doesn't change after interaction with (+) boson because the electron close to a nuclei remain close to it even after the two nuclei move apart. However, the coupling with the boson drags and distorts the electron cloud and increases

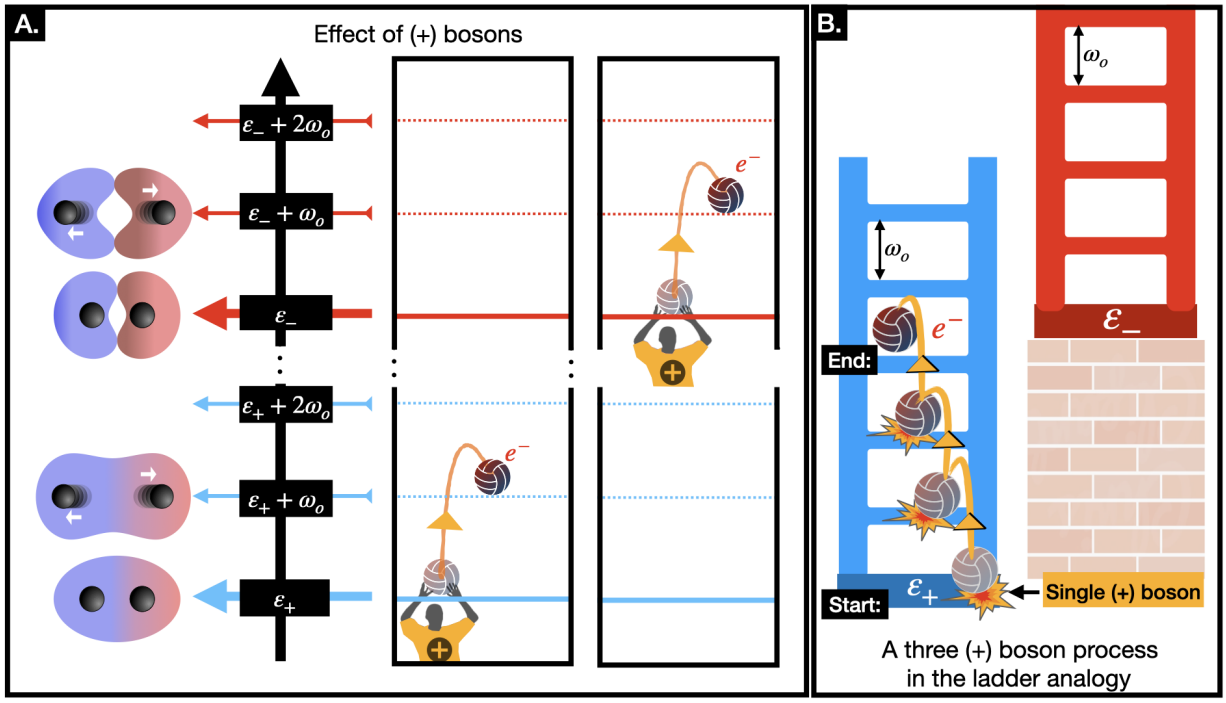

Figure 5.3: (A.) The effect of electron interacting with a single (+) boson in semi classical picture. (B.) A three (-) boson process in an electron starting in state ε_+ in ladder analogy.

it's energy from original pure electronic state energy ε_+ to $(\varepsilon_+ + \omega_o)$. Hence, the total state of the electron-boson system changes from a purely electronic to a hybrid electron-boson state without the qualitative nature of the orbital doesn't change. If this new hybrid state interacts with a second quanta of (+) boson, the system moves to $(\varepsilon_+ + 2\omega_o)$. The electron cloud might distort further but the qualitative nature of it (bonding versus antibonding) doesn't change. The same story also holds true for the ε_- state.

We can therefore visualize these excited states (vibrational states) of the pure electronic states $(\pm)$ after absorbing n quanta of (+) bosons as ladders with lowest rung at $\varepsilon_\pm$ and each higher n^{th} rung at $(\varepsilon_\pm + n\omega_o)$. As seen in figures 5.3 and 5.4(B.), the ε_- ladder (red) starts at an energy above the ε_+ ladder(blue). The electron moves up a rung without jumping between the ladders when it gets a kick from a single quanta of (+) boson. Successive kicks move the electron to higher rungs one rung at a time as shown in figure 5.3 (B.).

The interaction of an electron with a $(-)$ boson is slightly more complicated compared to

(+) boson. This is because absorbing a single quanta of (−) bosons will change the electronic state from bonding to antibonding or vice versa as shown in figure 5.4(A.). By this reasoning, if an electron is starts out at a parent bonding (ε_+) state, absorption of even number (m) of (−) bosons will bring the electron back to a hybrid electron-boson state formed from the parent state and m quanta of (−) bosons. The final state will have the energy ($\varepsilon_+ + m\omega_o$). However, absorption of an odd number(n) quanta of (−) bosons will take the electron to a hybrid state formed by anti-bonding electronic state and n boson quanta. This final state will have the energy $\varepsilon_- + n\omega_o$. Thus the electron jumps back and forth between the energy ladders as it climbs each successive rung giving rise to a more complicated dynamics as shown in figure 5.4(B.).

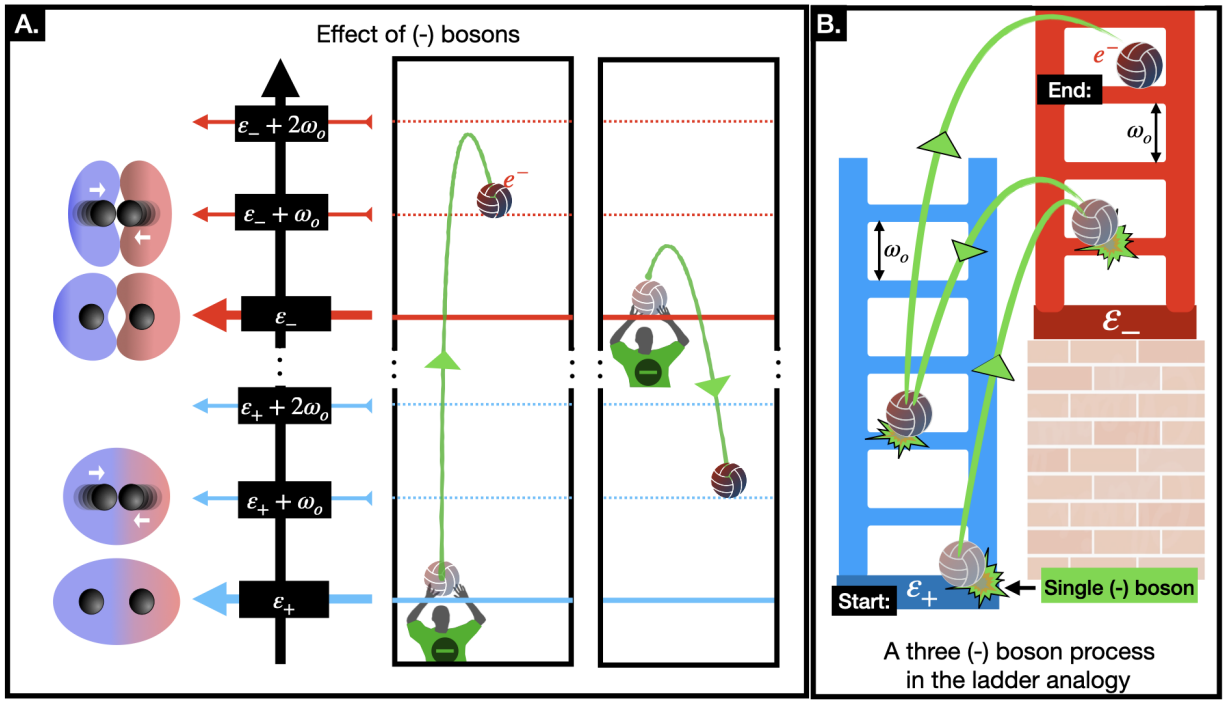

Figure 5.4: (A.) The effect of electron interacting with a single (−) boson in semi classical picture. (B.) Ladder visualization of the electron hopping in a three (-) boson process for an electron starting in state ε_+.

Of course in quantum mechanical probabilistic reality, the strength of the electron-boson interaction g controls how often the electron interacts with a (+) boson when it encounters

one. A larger g means more interaction and thus a larger probability of an electron jumping a rung after the interaction. At the limit of $g \to 0$, the electron is not affected by the boson anymore and it sits at the bottom of the rung for eternity. Furthermore, we have shown a very static picture of a much more intricate dynamical process. In reality, there are infinite numbers of bosons present in the system and the electron can absorb any number of quanta of $(\pm)$ bosons in any order. The final electronic states thus need to be computed self consistently. However, the above semi-classical picture and the analogy hold true qualitatively and are useful in predicting or explaining the spectral features without having to resolve to a fully self-consistent calculation for every given set of parameters.

5.2 Retarded-time and time-ordered cumulant formalisms

In this section, we will discuss the cumulant approximations in more detail. In particular, we will talk about the physical approximations that each cumulant flavor makes internally. We will then explain these approximations in terms of the semi-classical picture we have constructed. Finally, test both of these cumulant-based approximations numerically for a wide range of boson frequencies.

5.2.1 Core-hole like or time-ordered cumulant formalism

The core-hole-like or time-ordered cumulant which is a straightforward generalization of core-hole cumulant formalism only has the self-correction term owing to the absence of $(-)$ boson physics in the problem. Hence, an electron at each parent level only goes to those hybrid electron-boson levels originating from this parent level. Hence, there is no hopping from a ladder to another and the picture is exactly as figure 5.3. In the numerical simulation, we, therefore, expect to get replicas of the boson-less parent level at integers of boson frequency for electron starting at any of the two levels. There is also a renormalization of the pure electronic parent state energy as well as the intensity. The energy renormalization

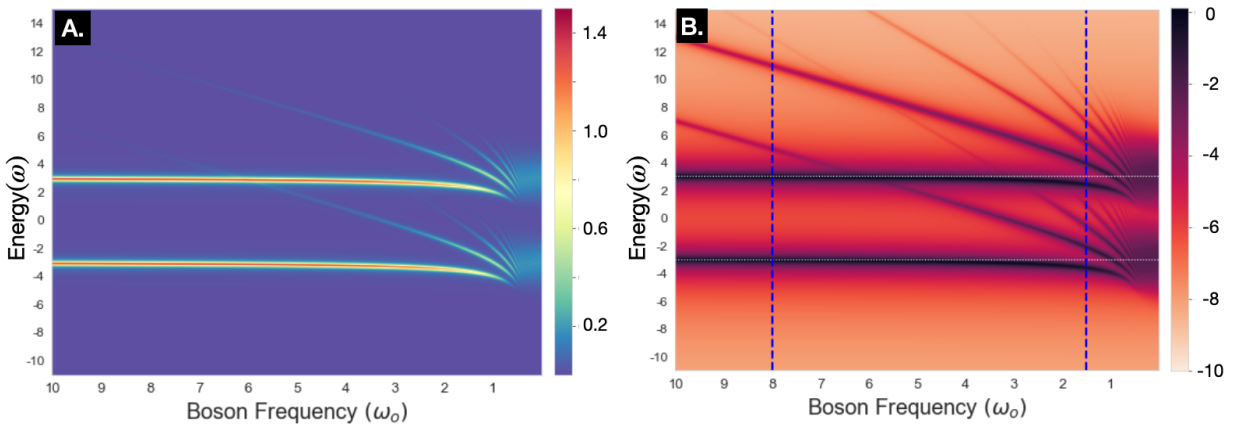

Figure 5.5: A) Spectral function from Core-hole cumulant treatment of Holstein dimer and B) Natural logarithm of figure A. Here, $\varepsilon_{\pm} = \mp 3, \omega_o \in [10, 0)$, and $g = \sqrt{2}$

is simply because the electron transforms from a particle into a quasiparticle due to bosonic 'clothing'. The intensity (or spectral weight) renormalization is for probabilistic reasons. The interacting electron unlike its non-interactive version can be in one of many states originating from a single parent state. The intensity of any energy signifies the probability of the electron being in that energy. Hence, spectral weight flows from the pure electronic parent state to new hybrid states. The magnitude of spectral weight drainage from the parent state is inversely proportional to the magnitude of ω_o and directly proportional to the value of coupling constant g.

5.2.2 Retarded time cumulant formalism

For the retarded time cumulant, in addition to the (+) boson's effect an approximate interaction between the (−) boson and the electron is taken. We begin with the power series correction term for each orbital $\pm$.

$$\mathcal{P}(\pm, t) = 1 + P_{SC}(\pm, t) + P_{IC}(\pm, t) \tag{5.1}$$

In this formalism, the first term is the same on both the bonding orbital's correction(4.31)

and the antibonding orbital's correction (4.32). This makes sense because this self-correction term (P_{SC}) captures the core-hole-like excitation due to (+) bosons which produce satellite features at multiples of boson frequency ω_o. It is simply an upward hopping within a ladder by ω_o regardless of where the electron is in the energy ladder.

$$i.e.\ P_{SC}(+,t) = P_{SC}(-,t) \tag{5.2}$$

The effect of (−) is approximated in the sense that the method internally is assuming the electron hop due to (-) boson from ε_+ to $(\varepsilon_- + \omega_o)$ as being equal to the electron hop from ε_- to $(\varepsilon_+ + \omega_o)$ while calculating the P_{IC} term for + orbital according to equation (4.21).

$$P_{IC}(+,t) = (-ig^2)\int_0^t dt_2 \int_0^{t_2} dt_1 e^{i\varepsilon_+\tau}\Sigma(-,\tau)\mathcal{P}(-,\tau)\mathcal{P}(+,t_2-\tau) \qquad \text{(Full equation)}$$

$$\text{Assume } P_{IC}(-,\tau) \approx P_{IC}(+,\tau)$$

$$\because P_{SC}(-,\tau) = P_{SC}(+,\tau) \qquad \text{From equation (5.2)}$$

$$\therefore 1 + P_{SC}(-,\tau) + P_{IC}(-,\tau) \approx 1 + P_{SC}(-,\tau) + P_{IC}(-,\tau)$$

$$\Rightarrow \mathcal{P}(-,\tau) \approx \mathcal{P}(+,\tau) \tag{5.3}$$

Making this approximation we get,

$$\therefore P_{IC}(+,t) \approx (-ig^2)\int_0^t dt_2 \int_0^{t_2} dt_1 e^{i\varepsilon_+\tau}\Sigma(-,\tau)\mathcal{P}(\overset{+}{\nearrow},\tau)\mathcal{P}(+,t_2-\tau)$$

$$\approx (-ig^2)\int_0^t dt_2 \int_0^{t_2} dt_1 e^{i\varepsilon_+\tau}\Sigma(-,\tau)\mathcal{P}(+,t_2) \quad \text{Using relation (4.15)}$$

Using this form of inter-orbital correction instead of the actual equation (4.21) gives us the RC cumulant for bonding orbital (4.31). Exactly same recipe for the antibonding orbital produces (4.32). From this we get two boson frequencies that combine the orbital energy gap(Δ) as well as the natural boson frequency (ω_o) to approximately capture the inter-orbital

corrections respectively in bonding and anti-bonding electronic levels: $\tilde{\omega}_o = |\Delta + \omega_o|$ and $\overline{\omega}_o = |\Delta - \omega_o|$.

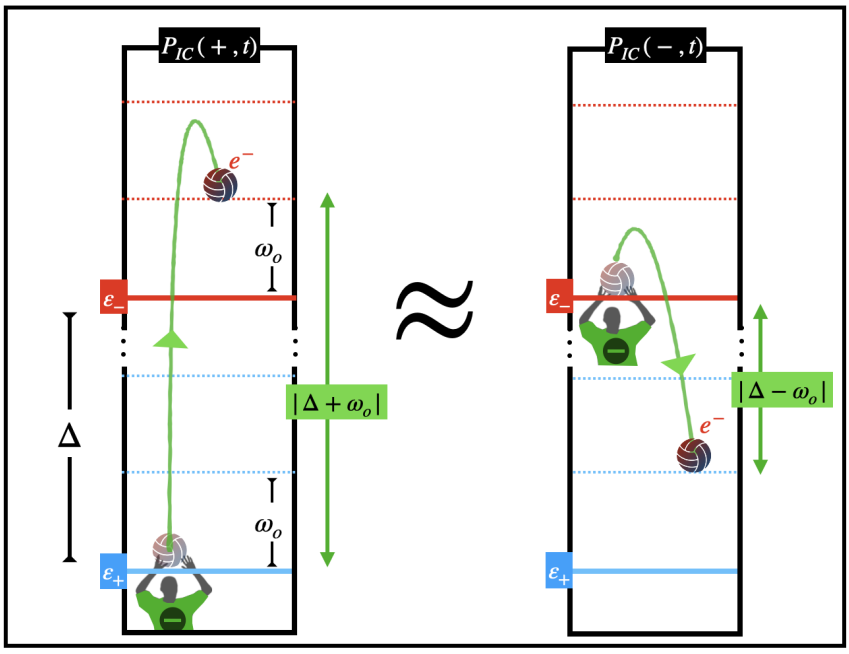

Figure 5.6: In retarded time cumulant, two very different electronic transitions are approximated as being equal. This is valid only when electronic energy scale (Δ) is much smaller than boson frequency (ω_o).

However, the difference in these two new frequencies $\tilde{\omega}_o$ vs $\overline{\omega}_o$) in these two corrections, leads us into a contradiction as shown in figure 5.6. These two distinct electronic transitions become equal only when $|\omega_o - \Delta| \to \infty$. There, either the boson frequency is so large that for the electron which has gulped a boson quanta and made a transition, the electronic energy gap (Δ) becomes irrelevant in this physics. Or, the electronic scale is so large compared to the boson frequency and associated transition that the inter-orbital coupling effect is negligibly small. Most of the physics is then governed by (+) boson's physics - the self-correction.

Hence, this description works well only when $\omega_o \gg \Delta$ here shown in figure 5.7B. However, in this regime, both vibrational state signature shake-offs due to (+) and (-) bosons are small. So, the non-interacting system picture becomes an easier working representation of the system anyways.

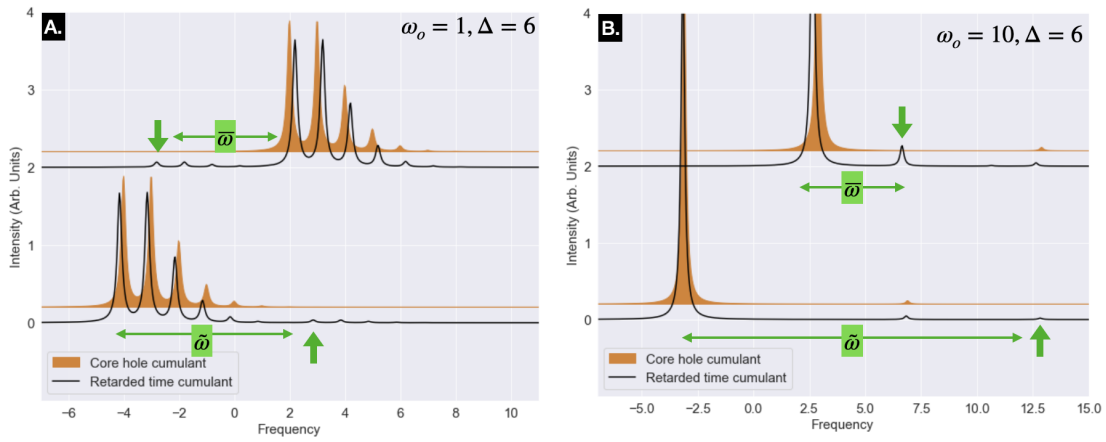

Figure 5.7: Spectral functions from core hole vs retarded time cumulant for A.$\omega_o \ll \Delta$ and B. $\omega_o > \Delta$. The lower spectra are for the bonding orbital and the upper spectra are for the anti-bonding orbitals. The first shake-off due to (-) boson is marked with a green vertical arrow.

In regime $\omega_o \ll \Delta$, we see a close match-up of the core-hole as well as the RC result because self-correction physics is the dominant effect. However, we also see extremely small signatures of inter-orbital coupling in both bonding and anti-bonding electronic orbitals as labeled with green arrows in figure 5.7A. Some approximate mixing of effects where the electron interacts with a (-) followed by many (+) bosons is also visible as shake-offs at ω_o of the first inter-orbital shake-off. A close look at the intensity of these satellites through the use of a logarithmic scale reveals something more problematic about RC cumulant. Faint artifacts (faux orbitals) are visible when $\omega_o \leqslant \Delta$ as seen in figure 5.9B. These artifacts appear as a faux quasiparticle below the bonding level when $\omega_o < \Delta$ and are the result of the second term ($\overline{\omega}_0$) in the antibonding power series correction (4.32). This is a tell-tale sign of this approximation treating (+) bosons as a cause of net upward hop (which is true) and (-) bosons as a cause of net downward hop (which is not true). There is another insidious issue with $\overline{\omega}_o$ - when ω_o and Δ become equal, perfect cancellation occurs which makes $\overline{\omega}_o$ zero. A naive numerical implementation of this retarded cumulant flavor (4.32) therefore diverges as $\overline{\omega}_o \to 0$. However, since this is a '0/0' form, the use of the L'hospital rule twice in the

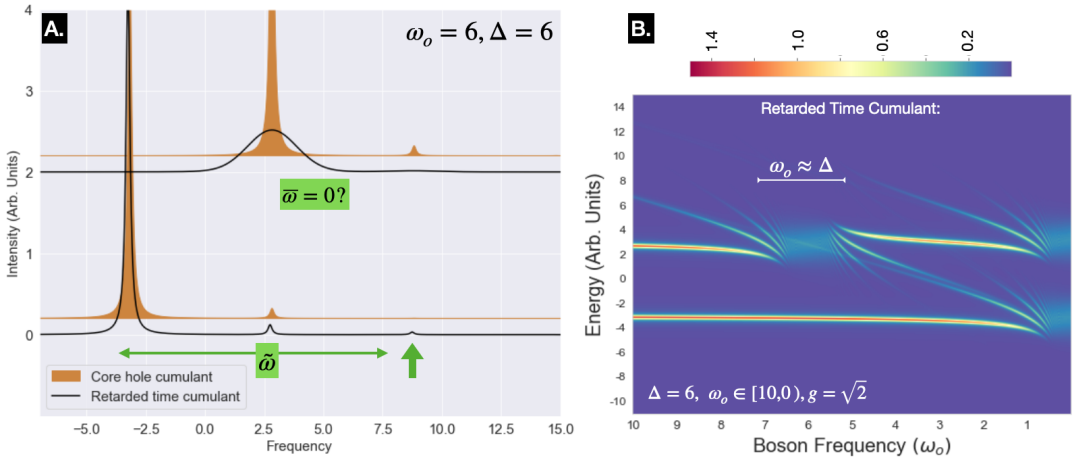

Figure 5.8: A. Spectral function at $\omega_o = \Delta$ for Core hole vs RC cumulant. B. Spectral function for a wide range of boson frequency from RC cumulant for $\varepsilon_\pm \mp 3$ and $g = \sqrt{2}$.

divergent second term of (4.32) gets rid of this divergence. This is because the numerator containing the exponential goes to zero much faster than the quadratic denominator.

$$\lim_{\bar{\omega}_o \to 0} \left(\frac{e^{-i\bar{\omega}_o t} + i\bar{\omega}_o t - 1}{\bar{\omega}_o^2} \right) = \lim_{\bar{\omega}_o \to 0} \frac{(-it)^2}{2} e^{-i\bar{\omega}_o t}$$

The inclusion of this exception is central to the numerical implementation of retarded-time cumulant formalism. However, even after this, the RC cumulant is unable to resolve the shape of the antibonding level when $\omega_o \approx \Delta$ as seen in figure 5.8. The antibonding orbital is represented as an averaged lump of the zero boson parent electronic orbital and all of its higher order orbital offsprings.

5.3 Comparison between Power Series, Exact Diagonalization and Cumulant Expansion

In comparison to any cumulant flavor, we can of course do a better job (here 'better' means assumption-free) of computing the Holstein dimer's spectral function by using the general power series correction. However, does 'better' also mean a better agreement with the actual

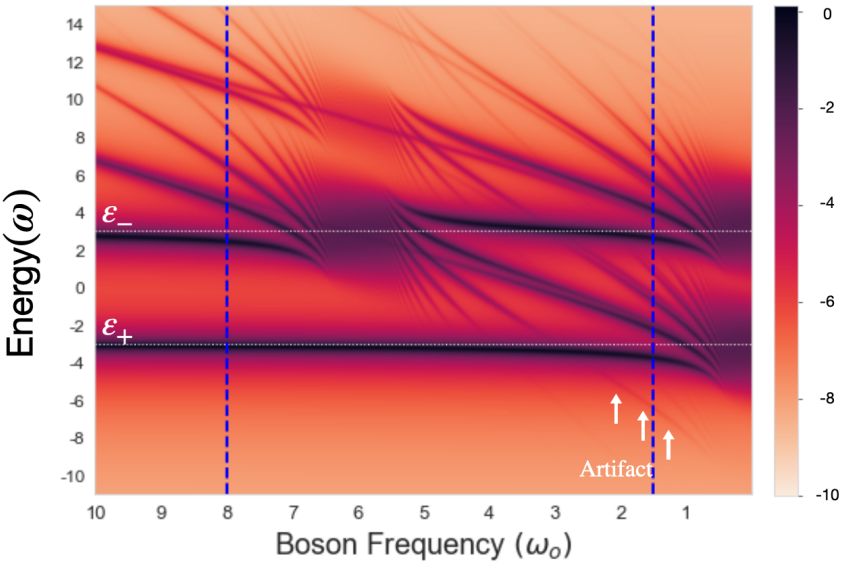

Figure 5.9: Natural log of retarded time cumulant corrected spectral function for Holstein dimer at a wide range of frequency (5.8B.) shows the artifacts (faux quasiparticle states) below the bonding energy quasiparticle at small boson frequency. Furthermore, RC cumulant cannot properly resolve the antibonding level or its higher order shake-offs when $\Delta \approx \omega_o = 6$.

solution? In this section, we show the spectral function produced using full power series correction and core-hole cumulant correction against exact diagonalization with 50 bosons per site. In figure 5.10, we compare the natural logarithm of the spectral function generated from the three methods for a wide range of boson frequency $\omega_o \in [10, 0.1]$ for a strong coupling constant of $g = \sqrt{2}$. The natural logarithm is used here to deduce the finer features which would otherwise get lost in the color scheme. We observe that power series correction is in excellent agreement with the exact diagonalization for the entire frequency range. The small discrepancies between the two in intensity (color) are of the order of $e^{-3} \approx 0.05$ units or smaller. The cumulant however works only when there is a clear separation between the bosonic energy scale (ω_o) and the electronic energy scale ($\Delta = \varepsilon_- - \varepsilon_+$).

Based on the comparison of energy scales , we can separate the figure 5.10 into three distinct regimes.

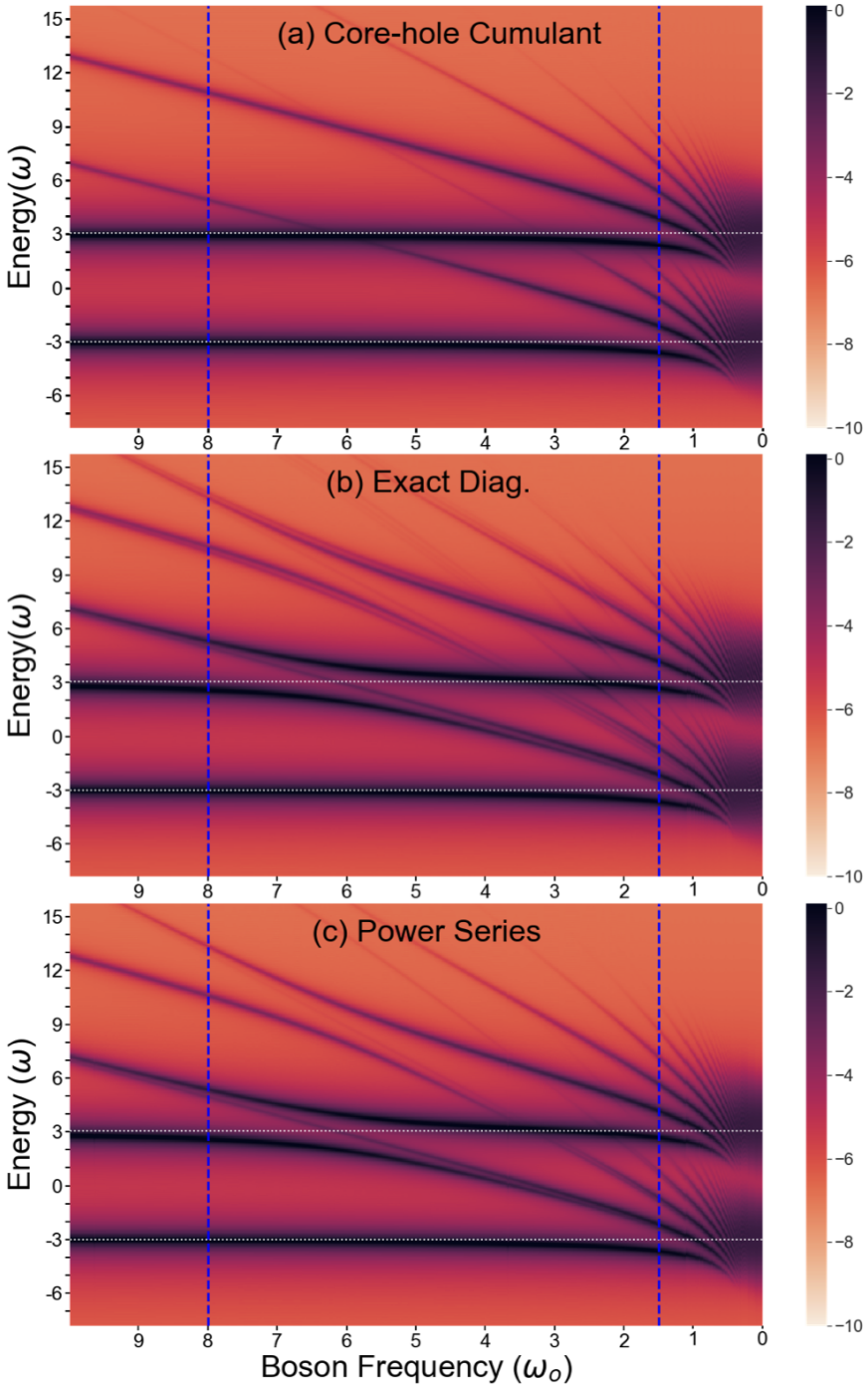

Figure 5.10: Natural log of spectral function from a) core-hole cumulant, b) exact diagonalization, and c) power series for $\varepsilon_{\pm} = \mp 3$ (horizontal white dotted lines) and ω_o between 10 and 0.1. Blue vertical lines separate the three distinct regions. Unlike core-hole cumulant, Power Series is in excellent agreement with the exact diagonalization at all three regions.

5.4 Three Regimes of this Problem

Regime I: $\Delta \ll \omega_o$

The first regime is the weak coupling regime of $\omega_o \gg \Delta$ - here $\omega_o > 8$. Here, both $(\pm)$ plasmon satellites are far away from the quasiparticle and therefore their effect on the quasiparticle energy and weight is negligible. This is most prominently seen from the negligible change in quasiparticle energies from the non-interacting energies $\varepsilon_{\pm}$. Here, the core-hole cumulant adequately captures all the exact spectral features correctly.

Regime II: $\Delta \approx \omega_o$

The second regime has $\omega_o \approx \Delta$ - here $8 > \omega_o > 1.5$. A huge shift of spectral weight occurs from bonding to the anti-bonding orbital effectively splitting the anti-bonding orbital into two (between ω_o of 4 and 7). The shake-off replicas of this split level also come in pairs as seen in the exact spectra in figure 5.11. These are captured exactly by the power series but not by core hole cumulant because it lacks proper accounting of inter-band interaction. Furthermore, as shown in figure 5.7 and 5.9, the retarded time-cumulant cannot resolve the antibonding orbital in this regime.

Regime III: $\Delta \gg \omega_o$

The third regime is when $\omega_o \ll \Delta$ - here $\omega_o < 1.5$. Here the bosonic events are extremely localized around the non-interacting energy and $(+)$ bosons dominate the process. Therefore, inter-band correction is vanishingly small and the solution is dominated by self-correction i.e. core-hole-like cumulant. We observe this in all three spectral functions although both exact and power series solutions become computationally expensive- the former due to large boson number necessary and the latter due to large convergence order. RC cumulant is correct for the most part but it has extra small intensity features because of the treatment of (-) bosons

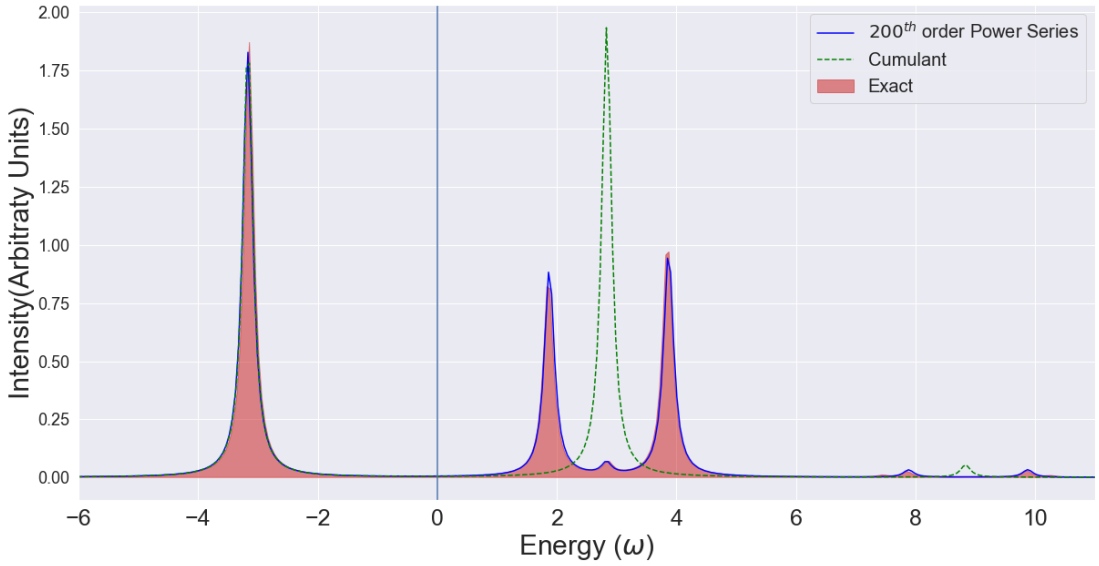

Figure 5.11: Spectral function for Holstein dimer at regime II with $\varepsilon_{\pm} = \mp 3, \Delta = \omega_o = 6$ and $g = \sqrt{2}$ computed from three different methods. Power Series captures the splitting of antibonding orbital but core hole cumulant cannot produce this feature.

as backward hop and the (+) boson as forward hop.

5.5 Numerical Implementation of Power Series Formalism

Rather than talking about Power Series implementation for Holstein dimer, we will talk about applying Power series correction in a general two-band structure framework as shown in figure 5.12. The boson-mediated excitation of the electron in the valence band can cause it to do one of four things as shown in the figure 5.12. For events labeled (a) and (c), there is no change in electron's momenta, and for events of type (a) and (b), there is no hopping between different bands. The event (a) takes into account the effect of (+) bosons in the context of Holstein dimer and this is always accounted for in the general power series as well as all the cumulant approximations. Power series as it stands, cannot handle events of type (d)- the inter-band non-vertical transitions where both electron momentum as well as the electron band index change. But power series, through P_{IC} term can handle (b) in theory and (c) in theory and in implementation. We will discuss this issue at the end of this

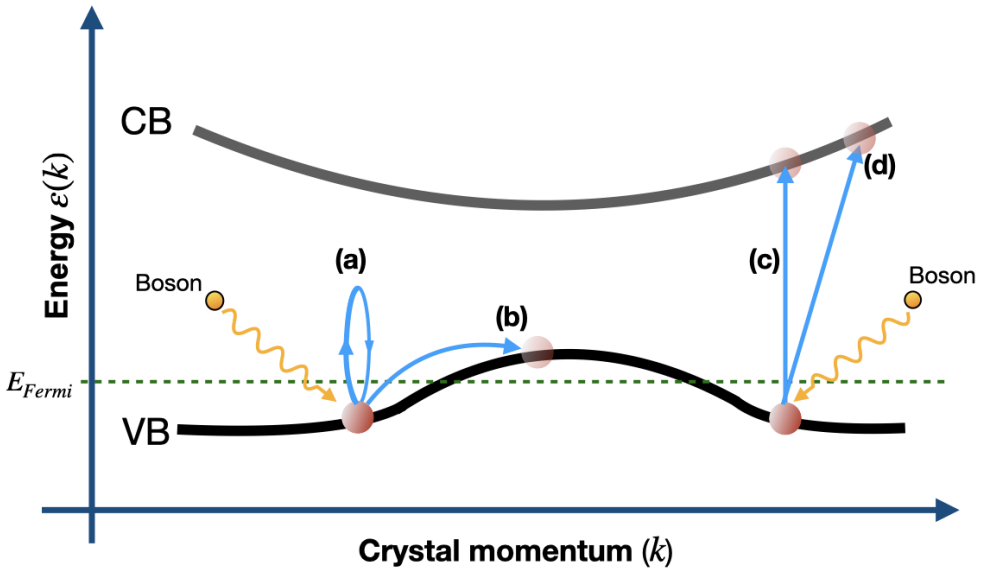

Figure 5.12: Schematic of different kinds of boson mediated losses in excitation spectra of material. a) Self transitions, b) Inter-orbital transition, c) Inter-band vertical transition, and d) Inter-band non-vertical transition between conduction and valence band (CB and VB). These losses show up as shake-off features in the charged excitation spectra.

chapter.

If the boson energy scale ω_o is much larger than the band gap, then classically, the dominant boson-mediated transition will be between bands and not within different orbitals (k-points) in the same band. In this case, the self-correction alone is a good approximation of the total same-band transitions and the IC piece is then used to capture the inter-band transitions.

On the other hand, if ω_o is much smaller than the band gap, then classically, the boson simply doesn't have enough energy to cause inter-band transitions of electrons. The IC piece is then used to capture the transitions within the same band but between different orbitals(k-points). The self-correction piece will capture transition within the same band and same k vector.

Interesting physics takes place when $\omega_o \approx$ band-gap. Now, both inter-band and inter-orbital transitions within the same band become equally relevant. In such cases, a more

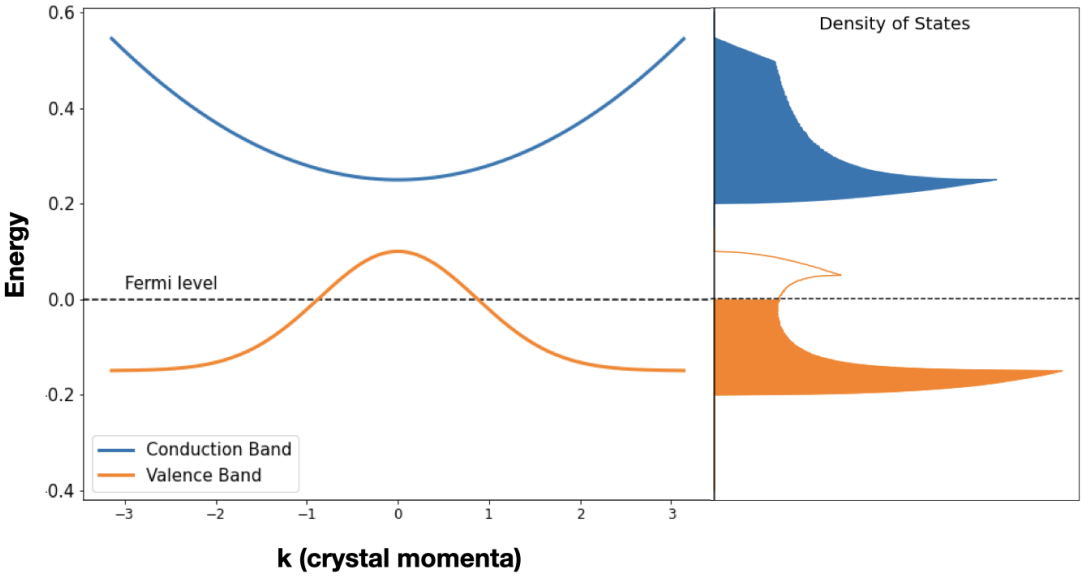

Figure 5.13: Model two band system and its density of states

complex calculation is required in which we don't make any distinctions between the bands but rather treat everything in terms of orbitals. The calculation then becomes cumbersome even using this approach since we cannot make any classical assumptions like before.

Once relevant approximation between the inter-band and the inter-orbital transition is selected, using the fermion propagator and the boson propagator, we can then compute the power series corrected band or orbital self-energy for a given band or orbital and construct the total self-energy. Doing this incorporates the boson-mediated electronic inter-band/orbital transitions in the system through the P_{IC} piece of the Power Series.

Coming back to the implementation, Suppose we treat the electronic part of the Hamiltonian at some DFT or GW level to get an appropriate electronic band structure $\epsilon(n, k)$. Depending on the density of charge carriers (n), the effective mass of charge carriers (m^*), the charge associated with the charge carrier (Q), and the permittivity of free space (ϵ_o), we can also calculate the bare plasma frequency(ω_o) - the energy quanta associated with a

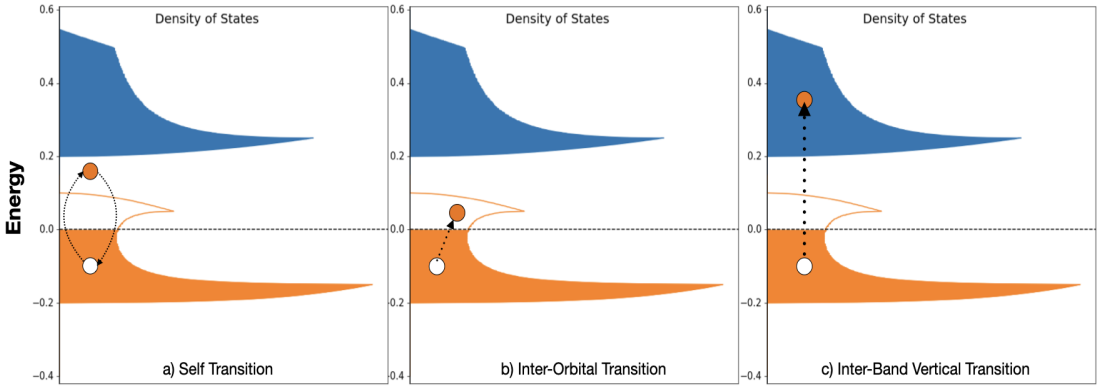

Figure 5.14: Sketch of a) Self-transition, b) Inter-orbital transition, and c) Inter-band transition in model band shown in figure 5.13. Figures a) and b) constitute transition within the same band.

single plasmon process.

$$\omega_o = \sqrt{\frac{nQ}{m^* \epsilon_o}}$$

Given the band gaps from the purely electronic band structure and $omega_o$ and using the decision chart 5.15, suppose we come to the conclusion that the relevant transitions are vertical transitions only i.e events of type (a) and (c). We then proceed by looking at each vertical slice of the electronic band structure as shown in figure 5.16 and treating them as 'orbitals' in (4.21). We construct relevant non-interacting electron Green's function for electron in these orbitals as well as non-interacting Boson (in this case plasmon) Green's function. Using these two objects, we then construct the 'orbital' electron self-energy. We then replace all of these in the Power series machinery we constructed in the previous chapter. Starting with $\mathcal{P}(n,t) = 1$ for all 'orbital', we iterative compute a better approximation of power series on the left-hand side of equation (4.21) by replacing the previous iteration's power series on the right-hand side of this equation. We do so until the solution stops changing i.e. the difference between the power series computed in the x^{th} and $(x-1)^{th}$ iteration is less than some small chosen quantity δ. Of course, one needs to be careful about not letting valence bands correct other valence bands in multi-electron systems. But

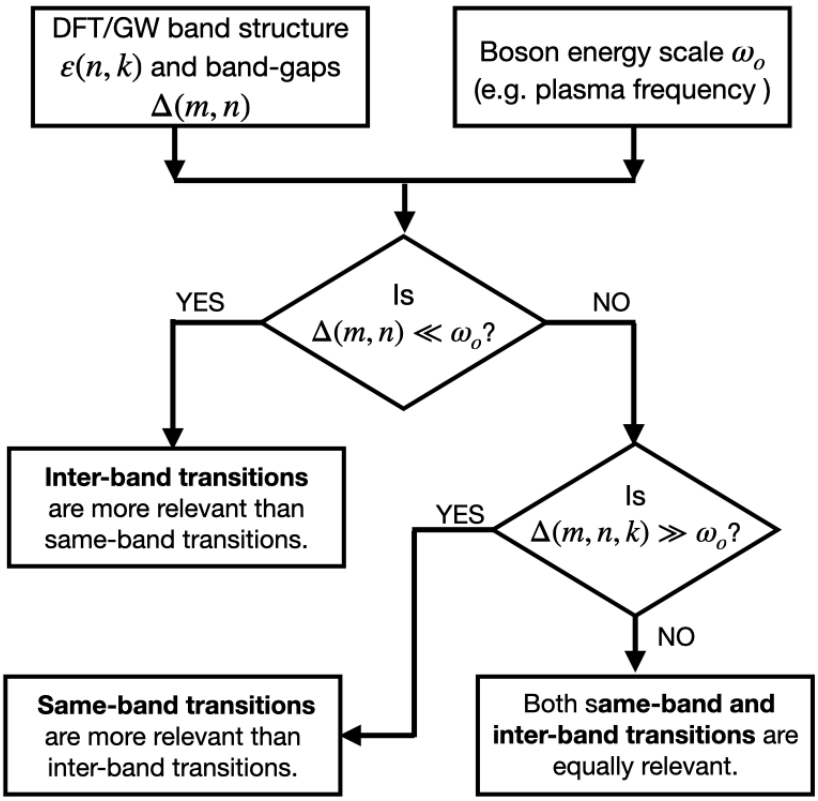

Figure 5.15: Left: Decision chart to decide between inter-orbital and inter-band vertical transition and the flow chart of our method

this can be done by modifying the summation in the inter-orbital correction term for the valence bands. This will effectively stop double occupancy processes where another electron from a lower valence band might jump into a higher valence band that is already filled. A schematic of implementation is presented in figure 5.17. For Holstein dimer, $n = \pm$ and ω_o is the phonon frequency. We now implement this to a simple case of silicon spectra. We first perform a Density functional theory calculation for the electronic band structure of silicon. We compute the theoretical value of plasma frequency in silicon which approximately is 16.9 eV. We then construct dispersionless plasmon propagators with this energy. Given that we are in a large boson frequency limit, we choose to account for vertical transition as shown in figure 5.16. We compute the power series correction as well as the cumulant correction

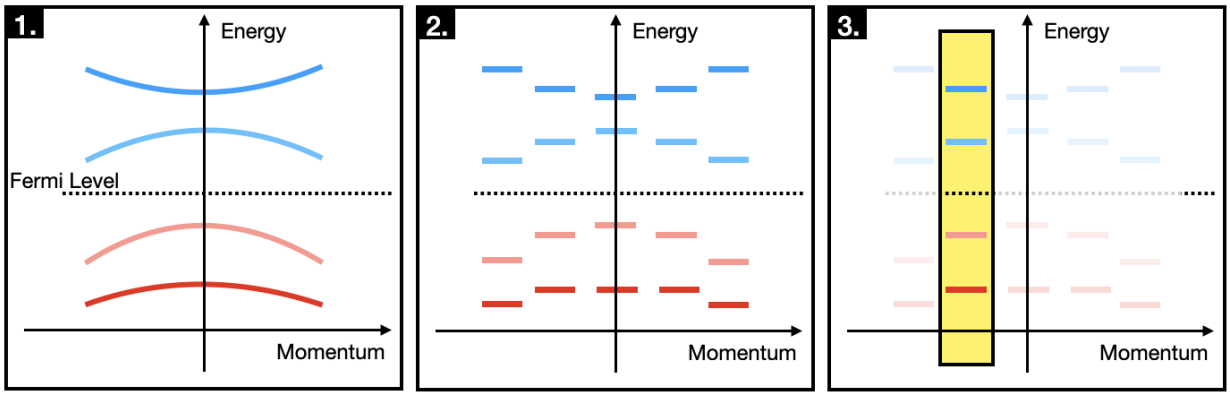

Figure 5.16: Implementation of vertical transition Power Series in the multi-band system. Step 1. We generate an appropriate electronic band structure. Step 2. We segment the band structure into a sequence of short flat band structures. Step 3. We only look at one vertical slice (here yellow box) at a time.

with $g = 1$ and compare that with the DFT spectra along with a replica of the band structure drawn plasma frequency away from the electronic band structure. The cumulant result looks almost like the DFT + replica result. However, the power series as shown in figure 5.18 produces drastically different results as compared to cumulant. It produces novel features in the band gap, splits the electronic band structures at multiple places as well as spreads the boson replica satellites over a wider range.

The point here is not that the Power series is producing the correct result. We still don't know what the appropriate value of 'g' is. The point we make here is that given the same initial input, the enforcement of self-consistency in Green's function through power series produces a drastically different compared to the non-self-consistent cumulant approximations.

5.6 Summary

In this chapter, through a semi-classical interpretation of Holstein dimer we explained two flavors of cumulant visually as well as through rigorous numerical implementations highlighting what approximations they make internally, when are they useful, and when they

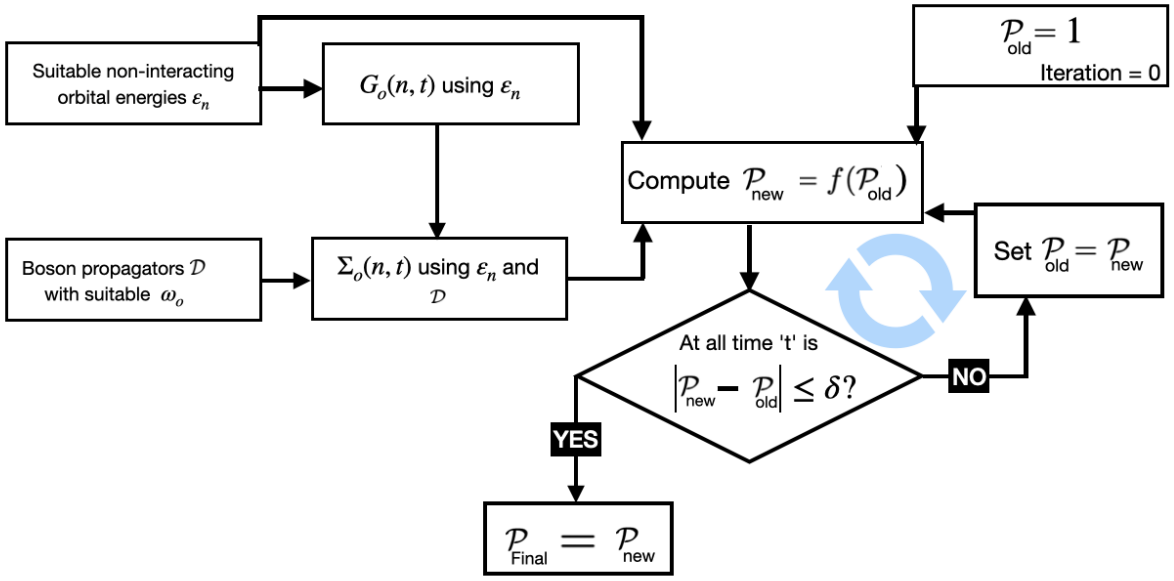

Figure 5.17: Numerical Implementation of Integral Power Series Formalism. δ is a chosen small parameter that governs the self-consistency criteria.

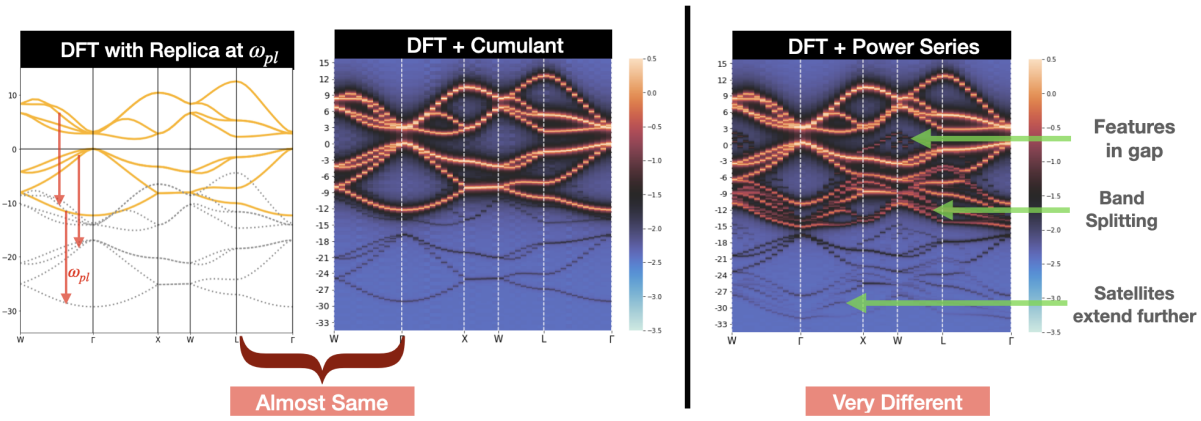

Figure 5.18: Vertical transitions in Silicon. Power series produces drastically different results than cumulant for the same parameters.

become incorrect. Then a full power series calculation was done and bench-marked against exact diagonalization for a wide range of boson frequencies. This led us to three regimes of the problem - two where cumulant works and one where cumulant fails. However, the power series is in excellent agreement with the exact diagonalization result. Finally, we developed

a recipe for the application of power series to improve band structures of actual material systems and showed that power series, by enforcing self-consistency criteria, produces a drastically different spectrum compared to cumulant.

CHAPTER 6

DERIVATION OF SINGLE AND DOUBLE DIFFERENTIAL POWER SERIES FORMALISM AND IMPLEMENTATION IN HOLSTEIN CHAIN

6.1 Why develop a new formalism?

In this chapter, we will extend the power series method we developed on a dimer to a Holstein chain. Computing the power series correction on Dimer through the integral formalism was a relatively straightforward calculation because we were only solving for two correction functions - $\mathcal{P}(+,t)$ and $\mathcal{P}(-,t)$. The whole calculation can be described as a series of computing and checking steps with a starting guess of $\mathcal{P} = 1$ for both orbitals as shown in figure 6.1. Now let us imagine a scenario where we have more than one orbital- say N

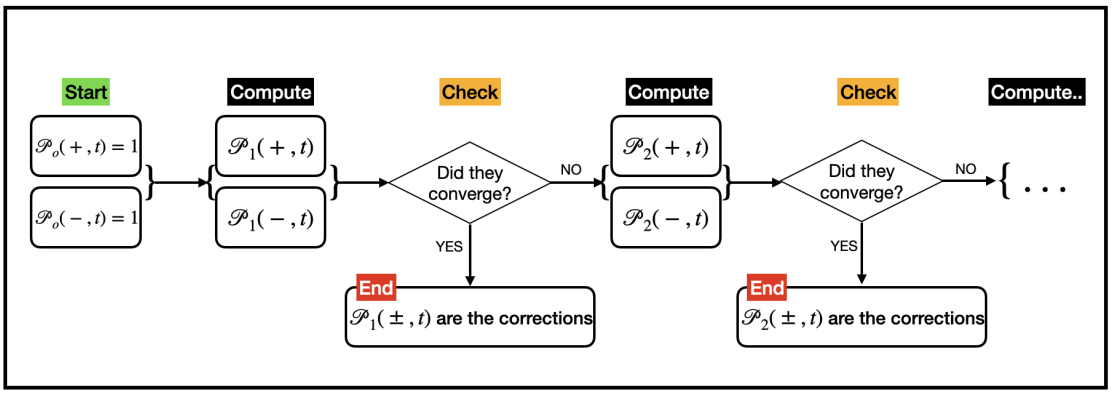

Figure 6.1: Schematic of Integral Power Series Formalism in Holstein dimer.$\mathcal{P}_n(\pm,t)$ is the power series computed at n^{th} compute step.

orbitals and we want to compute the power series correction for each orbital. Firstly, there are N different power series functions to be computed. This gives rise to N different coupled integral equations one for each orbital's power series $\mathcal{P}(n,t)$. Because of this coupling, at strong coupling or small boson frequency, we need a very high resolution in the time grid for

the error in each power series to be small. Otherwise, the power series values diverge quickly and the calculation never completes.

Say our time grid has M time steps each of which is appropriately small and starts from 0 going up to some time 't'. Since we are calculating power series for the entire time length $[0, t]$ at any given computing step, we need to store $(N \times M)$ values at any given computing step and $(2 \times N \times M)$ values at any given checking step (we need to compare the previous iteration as well as current iteration power series for convergence) in the working memory. This is still not as big a hurdle given modern computers.

Finally, we also encounter cases where the computed power series corrections do not converge but rather a cycle with different periodicity as shown in the figure 6.2. Naively following through the compute-check algorithm with only the current and the solution of the previous iteration will not be able to detect this if the solution family has a period of 2. Hence, we often need to store every single iteration and check if the solution produced at the current iteration matches any other past solution. If a match is detected, all of the solutions in that cycle can be averaged and fed as a new guess to the power series machinery. Needless to say, this is really expensive because:

- The time grid should be very fine.
- We need to store correction built at every iteration.
- We need to check the currently produced power series with every power series produced in each previous iteration.
- Using the averaged power series does not guarantee convergence. We simply might jump to a different family of oscillating solutions.

Due to these reasons, we developed the differential formalism of power series which is much more efficient, robust, and fast.

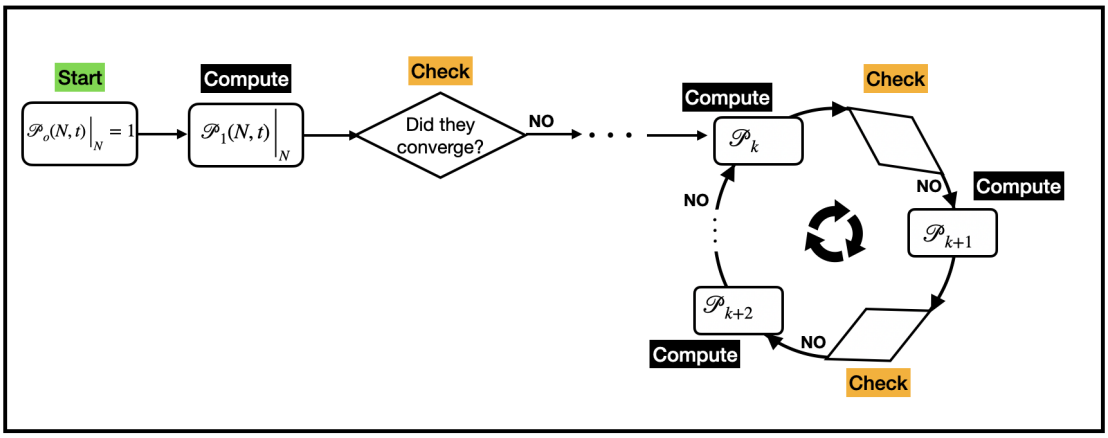

Figure 6.2: During the integral scheme, the solution produced at iteration k -$\mathcal{P}_k$ may repeat after cycling through many iterations.

6.2 The Holstein Chain

For ease of discussion, we present again the second quantized Hamiltonian for the N site Holstein chain with a single electron. Let 'a' be the lattice spacing between any two connected sites. There are three separate parts of the Hamiltonian - the purely electronic (H_e), the purely bosonic (H_{bos}), and the electron-boson interaction (H_{e-bos}). The electronic Hamiltonian is of the tight binding form with ϵ_o being the on-site energy and $-t$ being the hopping energy. Previously, we assumed a constant boson frequency(ω_o) for the boson associated with each site. But this time, rather than making all the bosons independent of each other, we assume a bare boson frequency of ω_o nearest neighbor interaction between them with strength t_d. This means that vibration from a site k can travel to its nearest neighbor site $(k \pm 1)$ and vice versa. This gives rise to an overall boson dispersion and the boson energy spectra resemble an optic phonon spectrum. With $< i, j >$ representing that the interaction is between the nearest neighbor sites and $c_i^\dagger/c_i$ and $b_i^\dagger/b_i$- the electron and the boson ladder operators at any site 'i' respectively, the real space Holstein Hamiltonian for N site chain

can be written as;

$$\begin{aligned} H_{total} &= H_e + H_{bos} + H_{e-bos} \\ H_e &= \epsilon_o \sum_{i=1}^{N} c_i^\dagger c_i + (-t) \sum_{<i,j>} (c_i^\dagger c_j + c_j^\dagger c_i) \\ H_{bos} &= \omega_o \sum_{i=1}^{N} b_i^\dagger b_i + (t_d) \sum_{<i,j>} (b_i^\dagger b_j + b_j^\dagger b_i) \\ H_{e-bos} &= g \sum_{i=1}^{N} (b_i + b_i^\dagger) c_i^\dagger c_i \end{aligned} \tag{6.1}$$

We can Fourier transform this Hamiltonian into momenta space where the purely electronic and the purely bosonic Hamiltonians are exactly diagonalizable. The hopping between electronic states of different momenta is handled by electron-boson coupling. The momenta space Holstein Hamiltonian for the N site chain is as follows.

$$\begin{aligned} H_{total} &= H_e + H_{bos} + H_{e-bos} \\ H_e &= \sum_k \varepsilon_k c_k^\dagger c_k \qquad \varepsilon_k = \epsilon_o - 2t\, cos(ka) \\ H_{bos} &= \sum_q \omega_q b_q^\dagger b_q \qquad \omega_q = \omega_o + 2t_d\, cos(qa) \\ H_{e-bos} &= \frac{g}{\sqrt{N}} \sum_k \sum_q c_{k+q}^\dagger c_k (b_q^\dagger + b_{-q}) \end{aligned} \tag{6.2}$$

Hopping of electron in real space gives a non-trivial momenta-dependent electronic band structure ε_k. But since momenta space electronic Hamiltonian is purely diagonal, the single electron in the system sits at the lowest energy state ε_o. Similarly, because of the boson-boson interaction, there are N different momenta-dependent boson frequencies ω_q. Because there are N different sites in real space, there are N different values of electron and boson momenta ranging from $\pi/(Na.)$ to $\pi/(N.a)$ excluding one of these two endpoints. The purely electronic and the purely bosonic band structures are shown in figure 6.3.

The electron-boson term takes an electron of momenta 'k' and kicks it with a boson of

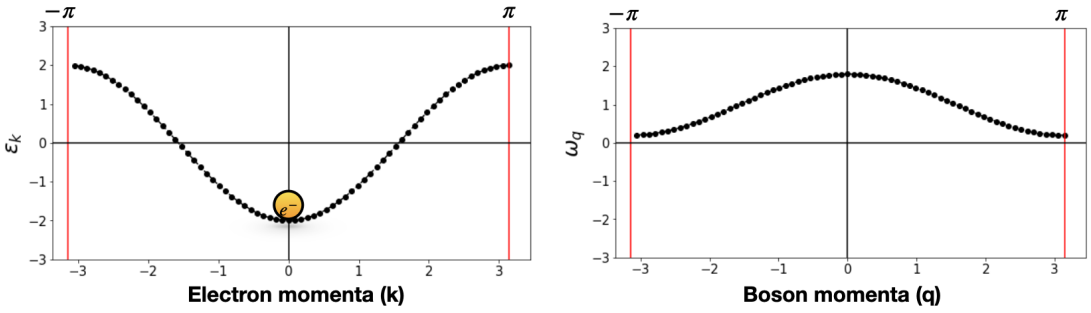

Figure 6.3: The purely electronic (left) and the purely bosonic band structure(right) for 70 site Holstein chain. Both X-axes are in units of $1/N.a$ with N = 70.

moments 'q' to make it an electron of momenta 'k+q' as shown in figure 6.4. This makes the electron hop around in the momenta space band structure and in this process, the non-interacting band structure renormalizes into an interacting band structure. Although at first glance it might seem like the electron boson coupling constant decreases in the momenta space with an increasing number of sites in the chain because of the divisor $\sqrt{N}$, this is not the case. The number of interaction terms also increases proportionally with large N and hence the factor of $\sqrt{N}$ appears just as a normalization to accommodate for this increase. Given the non-interacting electronic and bosonic band structures ε_k and ω_q and the electron-boson coupling constant g, our goal is to find the interacting electronic band structure.

6.2.1 Green's function, Self Energy and the Dyson's equation

As discussed in (11; 6; 51; 15; 52) we will use the retarded Green's function formalism. The quantity of interest is the finite temperature (T) electron and the boson green's functions (G and $\mathcal{D}$ respectively)for a single electron system with the thermal trace over states with zero electron but unrestricted boson number. At zero temperature, the only state that survives in this trace is the electron-boson Fock vacuum $|0\rangle$. We will denote this thermal average by

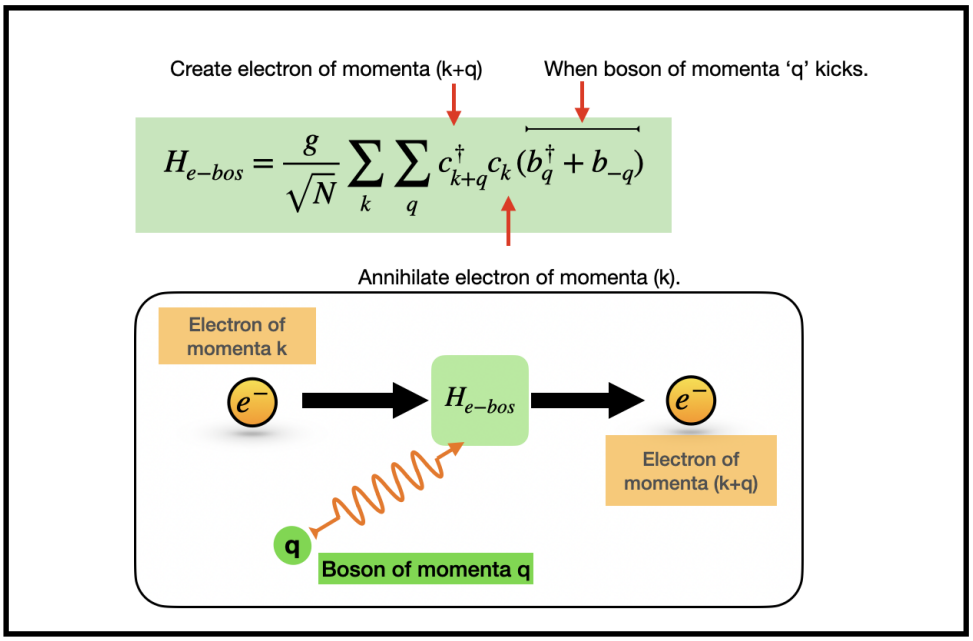

Figure 6.4: The electron-boson coupling term allows electron to hop around in momenta space through interaction with bosons.

angle brackets with inverse temperature β in the subscript ($\langle\ \rangle'_\beta$) (53).

$$
\begin{aligned}
G(k,t) &= -i\theta(t)\frac{Tr[e^{-\beta H}\{c_k(t), c_k^\dagger\}]}{Tr(e^{-\beta H})} \\
&= -i\theta(t)\langle\{c_k(t), c_k^\dagger\}\rangle_\beta \\
\mathcal{D}(q,t) &= -i\theta(t)\langle[A_q(t), A_{-q}]\rangle_\beta \quad \text{where,} \\
A_q(t) &= (b_q e^{-i\omega_q t} + b^\dagger_{-q} e^{i\omega_q t})
\end{aligned}
\tag{6.3}
$$

The non-interacting (g=0) electron and the boson Green's function for a single electron system with finite temperature(T) and the Bose occupation factor N_q^T are defined as follows

(53):

$$
\begin{aligned}
G_o(k,t) &= -i\theta(t)e^{-i\varepsilon_k t} \\
\mathcal{D}_o(q,t) &= -i\theta(t)\big[(N_q^T+1)e^{-i\omega_q|t|} + N_q^T e^{i\omega_q|t|}\big] \\
N_q^T &= \frac{1}{(e^{\omega_q/k_bT}-1)}
\end{aligned}
\tag{6.4}
$$

The first term in $\mathcal{D}_o$ with prefactor (N_q^T+1) model stokes scattering processes which are possible at any temperature while the second term with prefactor N_q^T model anti-stokes processes which are possible only at finite temperature (68). The spectral function $A(k,\omega)$, which is the quantity measured in experiments is defined following our previous convention (51) as,

$$
A(k,\omega) = \frac{1}{\pi}|Im\, G(k,\omega)| \tag{6.5}
$$

At zero coupling (q=0), there is no electron-phonon interaction in the system and hence the electronic state has an infinite lifetime with energy ε_k. However, once the interaction is turned on, the electron-phonon coupling can kick the electron out of its current state into any other state energetically available in the momenta space. Furthermore, depending on the coupling strength, a proportional correction to the pure electronic state's energy and lifetime occurs. This transmutes the infinitely long-lived electron/holes into quasi electron/holes with a finite lifetime. In this method, we assume that the non-interacting electron Green's function (G_o) smoothly transforms to the interacting Green's function (G) through a general power series $\mathcal{P}_k$ of the coupling constant squared $(\frac{g^2}{N})$.

$$
G(k,t) = G_o(k,t)\sum_{n=0}^{\infty}\big(\frac{g^2}{N}\big)^n C_n(k,t) = G_o(k,t)\mathcal{P}_k(t) \tag{6.6}
$$

In this expansion, $C_0 = 1$ and all other $C_{n\neq 0}$ are assumed to be independent functions that vanish at $t = 0$. Similar to the dimer problem, for a given momentum k, the associated

power series correction inherits the temporal contraction relation from the interacting and non-interacting Green's function.

$$\mathcal{P}_k(t_2 - t_1) = \mathcal{P}_k(t_2 - t)\mathcal{P}_k(t - t_1) \quad ; t_1 \leqslant t \leqslant t_2 \tag{6.7}$$

This relation is valid only for power series pieces of the same momenta and is essential in producing the cumulant diagrams. All the information about the possible interactions that can change the energy as well as shorten the lifetime of pure electronic states is packaged together in electron self-energy. This electron self-energy also has an electron Green's function inside it by definition and hence it too gets a power series correction piece as shown below. With the Green's functions (4.7),the first order self energy $\Sigma(k,t)$ is defined as;

$$\begin{aligned} -i\Sigma(k,t) &= \frac{g^2}{N}\sum_q \mathcal{D}_o(q,t)G(k-q,t) \\ &= \frac{g^2}{N}\sum_q \mathcal{D}_o(q,t)G_o(k-q,t)\mathcal{P}_{k-q}(t) \\ &= -i\frac{g^2}{N}\sum_q \Sigma_{k,q}(t)\mathcal{P}_{k-q}(t) \end{aligned} \tag{6.8}$$

The Dyson's equation governs the evolution of the electron green's function by repeated application of self-energy to itself.

$$G(k,\omega) = G_o(k,\omega) + G_o(k,\omega)\Sigma(k,\omega)G(k,\omega) \tag{6.9}$$

6.3 Defining the coupling strength

There are three energy scales in this problem - the electronic, the bosonic, and the coupling scale. The electronic energy is captured by the bandwidth ($2t_{el}$). The bosonic energy scale is captured by the average boson energy (geometric average of extreme ω_q in (6.2) to capture

boson dispersion). And the coupling scale is captured by the coupling constant 'g'. The coupling strength (λ) captures how big the coupling scale is compared to electronic and the bosonic scales and is the metric of importance for electron-boson interaction in such systems(69; 17).

$$\begin{aligned}\lambda &= \frac{\text{Coupling scale}}{\text{electronic scale}} \times \frac{\text{Coupling scale}}{\text{bosonic scale}} \\ &= \frac{g}{2t_{el}} \times \frac{g}{\sqrt{\tilde{\omega}^2 - (2t_d^2)}}\end{aligned} \tag{6.10}$$

6.4 Integral Power Series Formalism for the chain

In this section, we briefly outline the general power series method and direct the reader's attention to previous chapter 4 for more details on the derivation of the power series integral equation as well as chapter 5 for discussion on the drawbacks of popular methods. Following the same logic as chapter 4, we derive the integral power series equation (6.11) for this problem. The self-correction term P_k^{SC} incorporates the correction due to the $q = 0$ bosons that do not cause an electronic state change after electron-boson interaction. The effect of these bosons is like that of bosons in the core-hole problem where diminishing replicas of the electronic peak are produced at the boson frequency. The inter-orbital correction term P_k^{IC} incorporates the correction due to all other $q \neq 0$ bosons which change the electronic state during the interaction.

$$\begin{aligned}\mathcal{P}_k(t) &= 1 + P_k^{SC}(t) + \sum_{q\neq 0} P_k^{IC}(q,t) \\ P_k^{SC}(t) &= -i\frac{g^2}{N}\int_0^t dt_2 \int_0^{t_2} d\tau e^{i\varepsilon_k \tau}\Sigma_{k,q=0}(\tau)\mathcal{P}_k(t_2) \\ P_k^{IC}(q,t) &= -i\frac{g^2}{N}\int_0^t dt_2 \int_0^{t_2} d\tau e^{i\varepsilon_k \tau}\Sigma_{k,q}(\tau)\mathcal{P}_{k-q}(\tau)\mathcal{P}_k(t_2-\tau)\end{aligned} \tag{6.11}$$

6.5 First Differential Formalism of Power Series

The first differential formalism of power series correction is obtained by applying the fundamental theorem of calculus to (6.11).

$$\begin{aligned}\frac{d\mathcal{P}_k(t)}{dt} &= \left(\frac{-ig^2}{N}\right)\left[\int_0^t d\tau e^{i\varepsilon_k\tau}\Sigma_{k,q=0}(\tau)\right]\mathcal{P}_k(t) \quad + \\ &\left(\frac{-ig^2}{N}\right)\sum_{q\neq 0}\int_0^t d\tau e^{i\varepsilon_k\tau}\Sigma_{k,q}(\tau)\mathcal{P}_{k-q}(\tau)\mathcal{P}_k(t-\tau) \\ \mathcal{P}_k(t=&0) = 1 \qquad \text{(Initial condition)}\end{aligned} \tag{6.12}$$

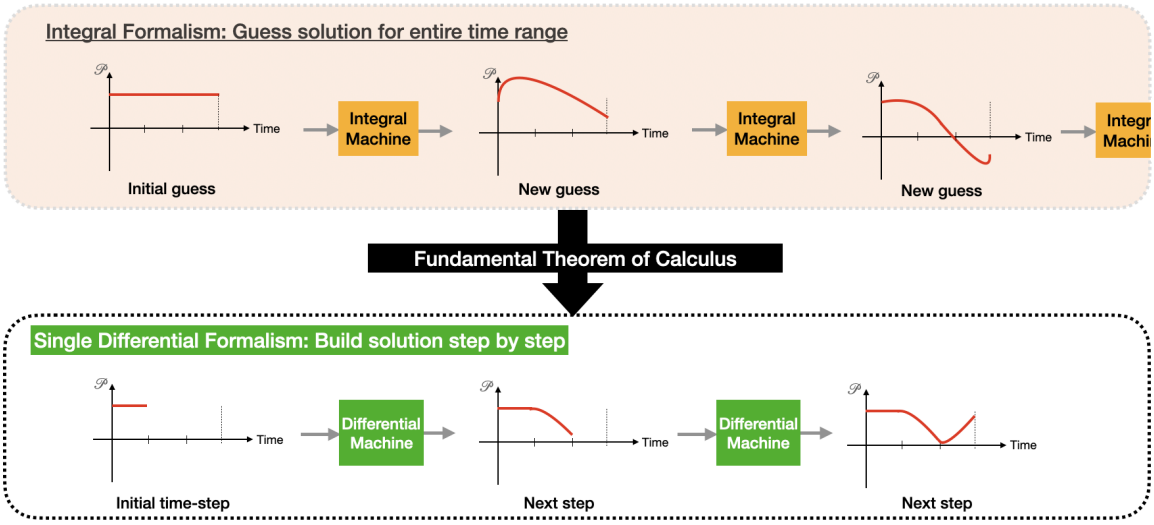

Figure 6.5: Unlike the integral formalism where the correction for the entire time range is guessed, single differential formalism builds the correction time-step by time-step.

The initial condition above is set by letting $t = 0$ in the definition of Power series correction (6.6). This is consistent with our assumption that the mapping of G_o to G is adiabatic and smooth. The integro-differential equation thus obtained is called a continuous delay differential equation because the value of the correction function at a time-instant depends on its past values - here the $\mathcal{P}_k(t-\tau)$ at the end of (6.12). This term $\mathcal{P}_k(t-\tau)$ linking the past value of itself to the equation governing its present value is called a memory

kernel.

So far, the equations (6.11) and (6.12) are formally equivalent. But, (6.12) provides the advantage of computing $\mathcal{P}_k$ for each time step gradually (method of step) by recycling its previous values for the delayed coupling rather than having to optimize for an appropriate value of $\mathcal{P}_k$ for the entire time domain at once. We cannot reduce this equation further without severe approximations to the delay term. Assuming that the delay term $\mathcal{P}_k(t-\tau)$ is splittable into $\mathcal{P}_k(t)/\mathcal{P}_k(\tau)$ using relation (6.7), we can further simplify the power series into a second differentiable formalism which is much closer in spirit with the self-consistent cumulant formalism (15). But due to the severity of this approximation, this second-order formalism is marred with sudden onset of divergence in the correction function.

6.6 Second Differential Formalism of Power Series

We can make one more approximation to the (6.12) by inserting the temporal contraction property (6.7) to simplify the delay term $\mathcal{P}_k(t-\tau)$ as $\mathcal{P}_k(t)/\mathcal{P}_k(\tau)$ in equation (6.12). This simplification allows for the use of the fundamental theorem of calculus again to generate a second differential formalism of power series correction. Inspired by the cumulant approximation where the cumulant correction derivative is zero at $t = 0$, we get a second initial condition where the power series derivative is zero at $t = 0$.

$$\frac{d\mathcal{P}_k(t)}{dt} = \Big(\frac{-ig^2}{N}\Big)\Big[\int_0^t d\tau e^{i\varepsilon_k\tau}\Sigma_{k,q=0}(\tau)\mathcal{P}_k(t) + \sum_{q\neq 0}\int_0^t d\tau e^{i\varepsilon_k\tau}\Sigma_{k,q}(\tau)\mathcal{P}_{k-q}(\tau)\frac{\mathcal{P}_k(t)}{\mathcal{P}_k(\tau)}\Big]$$

$$\frac{1}{\mathcal{P}_k(t)}\frac{d\mathcal{P}_k(t)}{dt} = \Big(\frac{-ig^2}{N}\Big)\Big[\int_0^t d\tau e^{i\varepsilon_k\tau}\Sigma_{k,q=0}(\tau)\Big] + \Big(\frac{-ig^2}{N}\Big)\sum_{q\neq 0}\int_0^t d\tau e^{i\varepsilon_k\tau}\Sigma_{k,q}(\tau)\frac{\mathcal{P}_{k-q}(\tau)}{\mathcal{P}_k(\tau)}$$

$$\frac{d}{dt}ln[\mathcal{P}_k(t)] = \Big(\frac{-ig^2}{N}\Big)\Big[\int_0^t d\tau e^{i\varepsilon_k\tau}\Sigma_{k,q=0}(\tau)\Big] + \Big(\frac{-ig^2}{N}\Big)\sum_{q\neq 0}\int_0^t d\tau e^{i\varepsilon_k\tau}\Sigma_{k,q}(\tau)\frac{\mathcal{P}_{k-q}(\tau)}{\mathcal{P}_k(\tau)}$$

Applying fundamental theorem of calculus, we get:

$$\frac{d^2}{dt^2} ln[\mathcal{P}_k(t)] = \Big(\frac{-ig^2}{N}\Big) \sum_{\forall q} e^{i\varepsilon_k t} \Sigma_{k,q}(t) \ \frac{\mathcal{P}_{k-q}(t)}{\mathcal{P}_k(t)}$$

The initial conditions are; (6.13)

$$\mathcal{P}_k(t=0) = 1 \quad \text{and,} \quad \frac{d\mathcal{P}_k(t)}{dt}\bigg|_{t=0} = 0$$

We can abridge this further by setting the correction to be cumulant-like i.e $\mathcal{P}_k(t) = e^{C_k(t)}$.

$$\frac{d^2 C_k(t)}{dt^2} = \Big(\frac{-ig^2}{N}\Big) \sum_{\forall q} e^{i\varepsilon_k t} \Sigma_{k,q}(t) \ e^{C_{k-q}(t) - C_k(t)}$$

The initial conditions transform to, (6.14)

$$C_k(t=0) = 0 \quad \text{and,} \quad \frac{dC_k(t)}{dt}\bigg|_{t=0} = 0$$

The expressions (6.13), (6.14) are closer in spirit to the expression derived by (15) in their theory of self-consistent cumulants in that in both expressions, the delay term has been severely modified by assuming that the temporal contraction relation (6.7) can be inverted. However, during numerical implementation, both (6.13) and (6.14) as well as the self-consistent cumulant formalism (15) are susceptible to sudden onset of divergence in solution. This is because of the correction term on the right- $\mathcal{P}_k(t)$ inversely relating to the second derivative of its own logarithm on the left in equation (6.13). Therefore a slight increase in the correction term from its equilibrium value amplifies its second derivative and the correction soon diverges. This is seen as we take smaller and smaller grid sizes because the divergence also gets pushed further in time.

6.7 Numerical results on Holstein Dimer

In this section, we revisit the dimer problem and produce the spectral function for the Holstein dimer using the aforementioned two methods. Here, we use $\varepsilon_{\pm} = \mp 3$ which gives an orbital energy gap of $\Delta = 6$. The real space coupling constant is set to $\sqrt{2}$ which in momenta space gives a normalized coupling constant of 1. The boson frequency is taken to be $\omega_o \in [10, 0)$. So far there is no boson dispersion in this problem.

Firstly, we show the natural logarithm of the electron spectral function constructed through the first differential method against the exact diagonalization result. We have al-

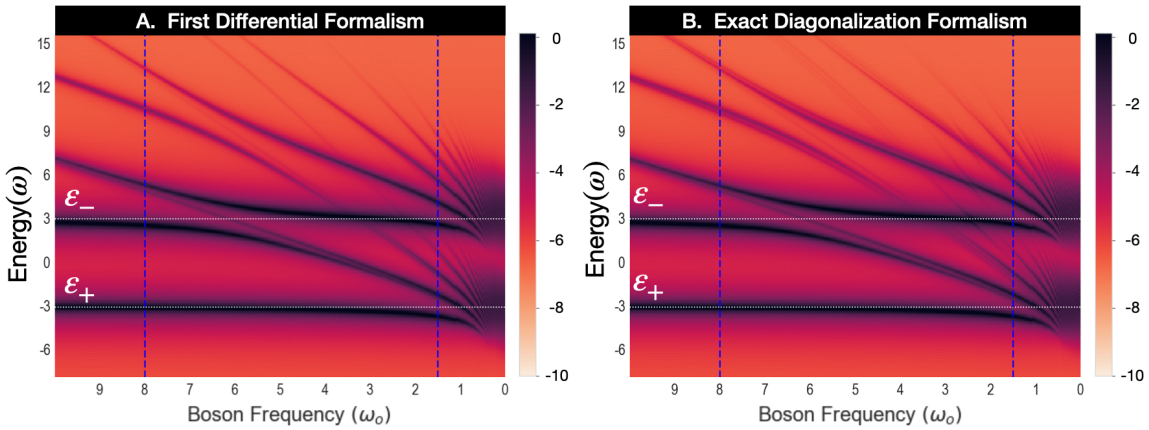

Figure 6.6: Natural log of electron spectral function produced from A)First differential formalism and B)Exact diagonalization for $\Delta = 6$, $g = \sqrt{2}$ and $\omega_o \in [10, 0)$. The blue vertical lines separate the three regimes of the problem.

ready shown in chapter 5 that the integral formalism produces excellent results that match the exact diagonalization result in all three regimes. Because the first differential formalism is formally equivalent to the integral formalism it too is in excellent agreement with the exact diagonalization in all three regimes of this problem.

The second differential formalism, however, is not formally equivalent to the integral power series formalism and internally makes a drastic approximation to simplify and localize the memory kernel $\mathcal{P}_k(t-\tau)$ in time. At first glance, the approximation produces the severe

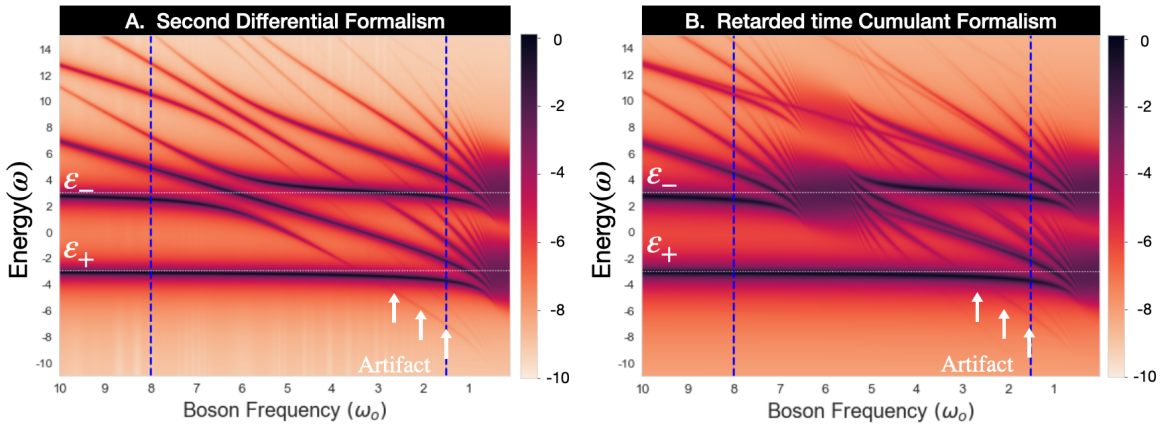

Figure 6.7: Natural log of electron spectral function produced from A)Second differential formalism and B)Retarded time cumulant for $\Delta = 6$, $g = \sqrt{2}$ and $\omega_o \in [10, 0)$. The blue vertical lines separate the three regimes of the problem.

antibonding orbital splitting in regime II ($\omega_0 \approx \Delta$) of this problem 5.4. Although this the splitting structure does not exactly match the exact diagonalization, there is a qualitative match. Furthermore, the replicas of this splitting are also split. However, in regime I, where $\omega_o \gg \Delta$, we see extra features which closely resemble the extra features produced by the retarded time cumulant. In regime III, where $\omega_o \ll \Delta$, the overall shape of the actual quasiparticle orbitals resemble the exact result very well. However, the logarithm of the spectral function shows the faux orbitals in the second differential formalism just like in the retarded time cumulant.

The advantage of using second differential formalism of course is in speed since there are no integrals involved. It is orders of magnitude faster than both integral and the first differential formalism. At first glance, this formalism is a better version of retarded time cumulant in that it doesn't diverge when $\omega_o \approx \Delta$ but rather produces the dimer's antibonding splitting that looks good qualitatively but fails quantitatively as shown in figure 6.8. This is because although the split is present, the second differential formalism still puts most of the spectral weight at the center of the splitting. As we will see in the later chapter, the second differential formalism will diverge when $\omega_o \approx \Delta$ when scaled up to compute spectral

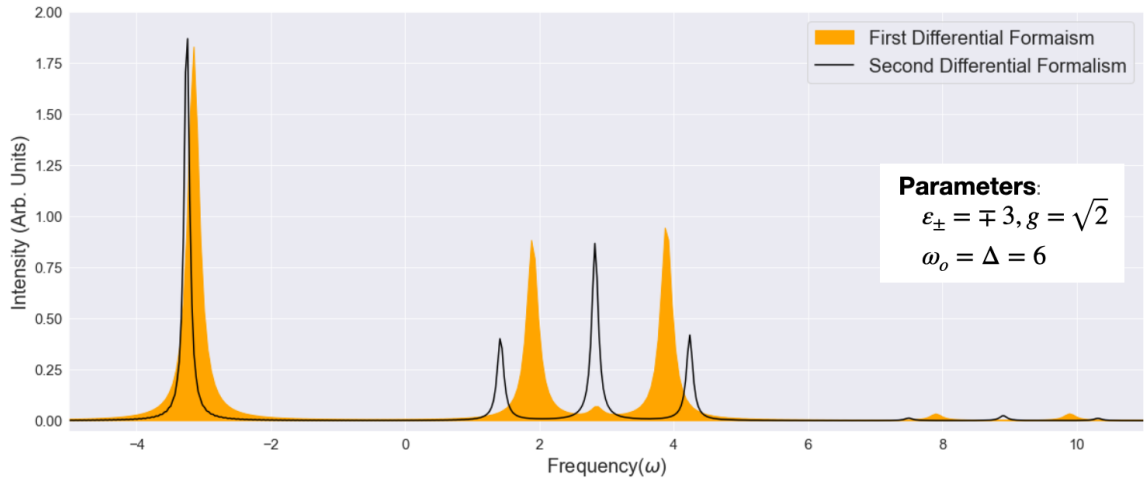

Figure 6.8: First and second differential formalism at strongest antibonding orbital splitting. The second differential formalism splits the antibonding orbital but still assigns most of the spectral weight at the center of the split (Frequency =3).

function on a Holstein chain.

6.8 Summary:

In this chapter, we derived the first and the second differential formalism of Power series correction. The first differential formalism is formally equivalent to the integral power series and thus produces results that are in excellent agreement with the exact diagonalization. The second differential formalism although captures the strong antibonding orbital splitting (Regime II), it still assigns most of the spectral weight to the parent level. Thus it is only qualitatively true in regime II. At regimes I and III, the second differential formalism is equivalent to retarded time cumulant formalism. In the next chapter, we will implement the first and second differential formalism to the Holstein chain at the thermodynamic limit at zero temperature and discuss the effect of the coupling constant. We will then show the first differential formalism result for finite temperature and discuss the effect of temperature. Finally, we will construct a heuristic argument to explain the structures observed.

CHAPTER 7

ZERO AND FINITE TEMPERATURE ELECTRON SPECTRAL FUNCTION FOR HOLSTEIN CHAIN

In this chapter, we compute the electron Green's function for a single electron N site Holstein chain in 1 dimension using the first differential formalism of the Power series. Although in principle, a one-dimensional Holstein chain can only have lattice vibrations in acoustic mode, we assume an optic phonon-like boson band structure by including a boson dispersion. The first reason for this is that this shows that the method is valid for a wide class of bosons and not just for a simple dispersionless boson. The second reason is of practical nature - other existing methods in literature also assume a similar boson band structure and we compare our method against other existing methods.

We show that, at zero temperature, compared to cumulant the power series spectral function shows a richer satellite structure. We then discuss the effect of coupling strength on carrier properties. We also show the validation of power series against literature as well as exact diagonalization. We then investigate the effect of extreme coupling in the electronic band structure and translate this result to effects in the quasiparticle. We then move on to the numerical calculation of finite temperature spectral function and elucidate the effect of temperature in this system.

Building intuition from the exercise above, we then construct a Heuristic argument that explains the features in the interacting electron spectra with simple static arguments. We will show that this intuition is built by collecting relevant exponential terms from the power series equations. We also briefly discuss the divergence in second differential formalism with a numerical example and point out when can we use this method.

7.1 Electron Spectral Function at Zero Temperature

In this problem, unlike the case of the dimer, we have a momenta varying initial electronic band structure ε_k and a momenta varying boson band structure ω_q. Therefore, rather than discussing our results in terms of the coupling constant g, we will discuss our results in terms of the coupling strength - 'λ' as defined in 6.10. Doing so, we effectively combine the three scales of the problem into a single parameter making it easier to compare across cases. We use the first differential formalism to compute the electronic Green's and spectral functions.

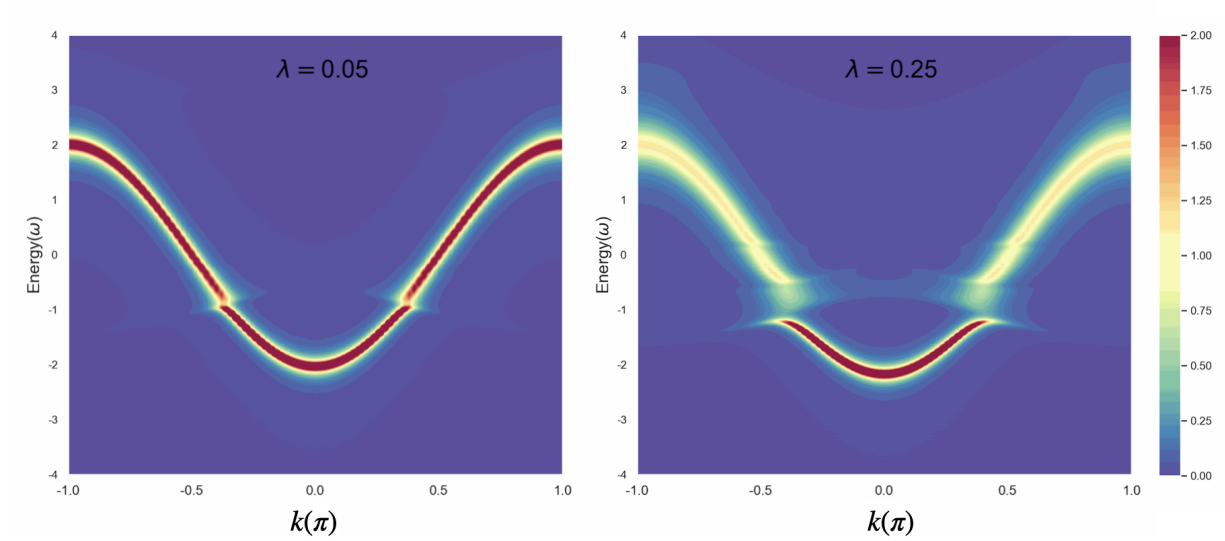

Figure 7.1: Electron spectral function at weak coupling strength

At weak coupling ($\lambda = 0.05$), the non-interacting sinusoidal electronic band fractures roughly at bare phonon energy $\tilde{\omega_o}$ from the band bottom separating the head from the two arms on each side as seen in figure 7.1(left). As the coupling strength increases, the fracture becomes more prominent growing in thickness and extent. The spectral weight from the fractured region folds over towards the center creating a satellite structure over the head. Although at zero temperature, the head remains sharp and pristine in terms of spectral weight spread, there is an onset of bloating of the fractured arms which broadens the arms making it less intense. This can be observed in figure 7.1(right). Although faint, we also

observe the onset of second-order fracturing of the arms at an approximate Energy value of $\omega = 0$. These two boson events, as we will see in the later sections, are the single boson processes originating from the newly minted single boson event satellite structure.

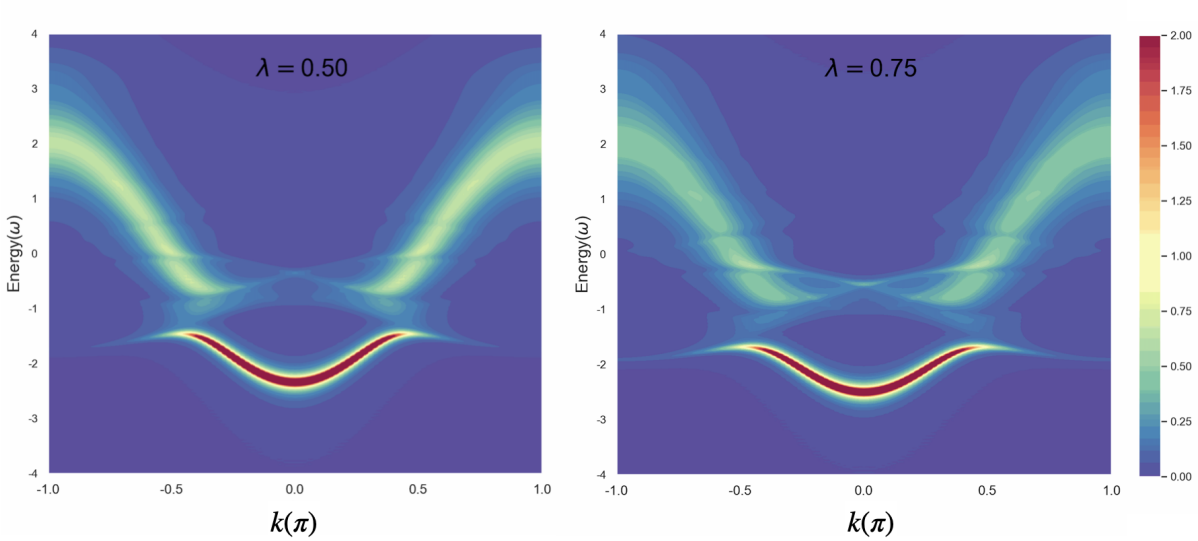

Figure 7.2: Electron spectral function at intermediate coupling strength

As we increase the coupling strength further, we observe a clear elongation of the ends of the head along the first satellite peak. We also observe the inward folding of the lower ends of the fractured arms along this satellite structure. Because the intensity of the single boson satellite structure now is significant, previously described single boson events originating from this structure also intensify. The satellite structure develops crosses due to the merging of these structures originating from the two sides of $k = 0$.

Although very faint, we also observe a further fracturing of the fractured arm around the energy of $\omega = 1$ which is a two-boson event originating from the head of the fermion band. There is a significant and drastic bloating of the fractured arms but the fractured head still remains pristine. A clear difference in the intensity of the arms can be seen between the $\lambda = 0.5$ and $\lambda = 0.75$ cases. All this can be observed in the figure 7.2.

At strong and extreme coupling, counter-intuitively, most of the structure in the first

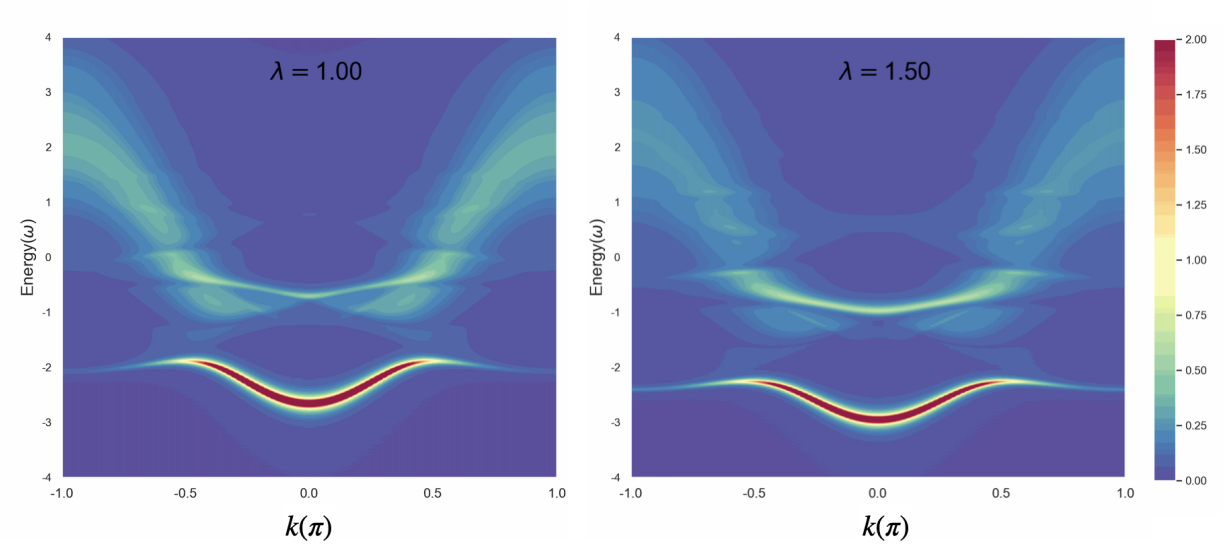

Figure 7.3: Electron spectral function at strong coupling strength

satellite structure (crosses and folds) vanishes away leaving only a strong cusp-like structure that somewhat resembles the head of the band. The fractured arms become wide and dim. We also see higher-order satellite structures above $k = 0$. Although a stretch, the head of the band still remains pristine. These effects can be observed in figure 7.3.

7.1.1 Richer Structure in the Satellites

Due to boson-mediated electronic excitations spectral weight diffuses from the fermion band to form faint satellites above the head with intricate crossing structures due to the non-interacting fermion band folding along fracture at the single boson excitation level on both sides as seen in figure 7.4.

The cumulant expansion, in the end, is the very first-order approximation of the power series (51; 52). Hence, it is only able to produce an averaged structure, unlike the full Power series. Therefore, it is not surprising that cumulant only puts an averaged lump to represent a satellite with much richer structures and spread. Furthermore, the extent of the lower head is also severely restricted by the cumulant and the intensity of the fractured arms is

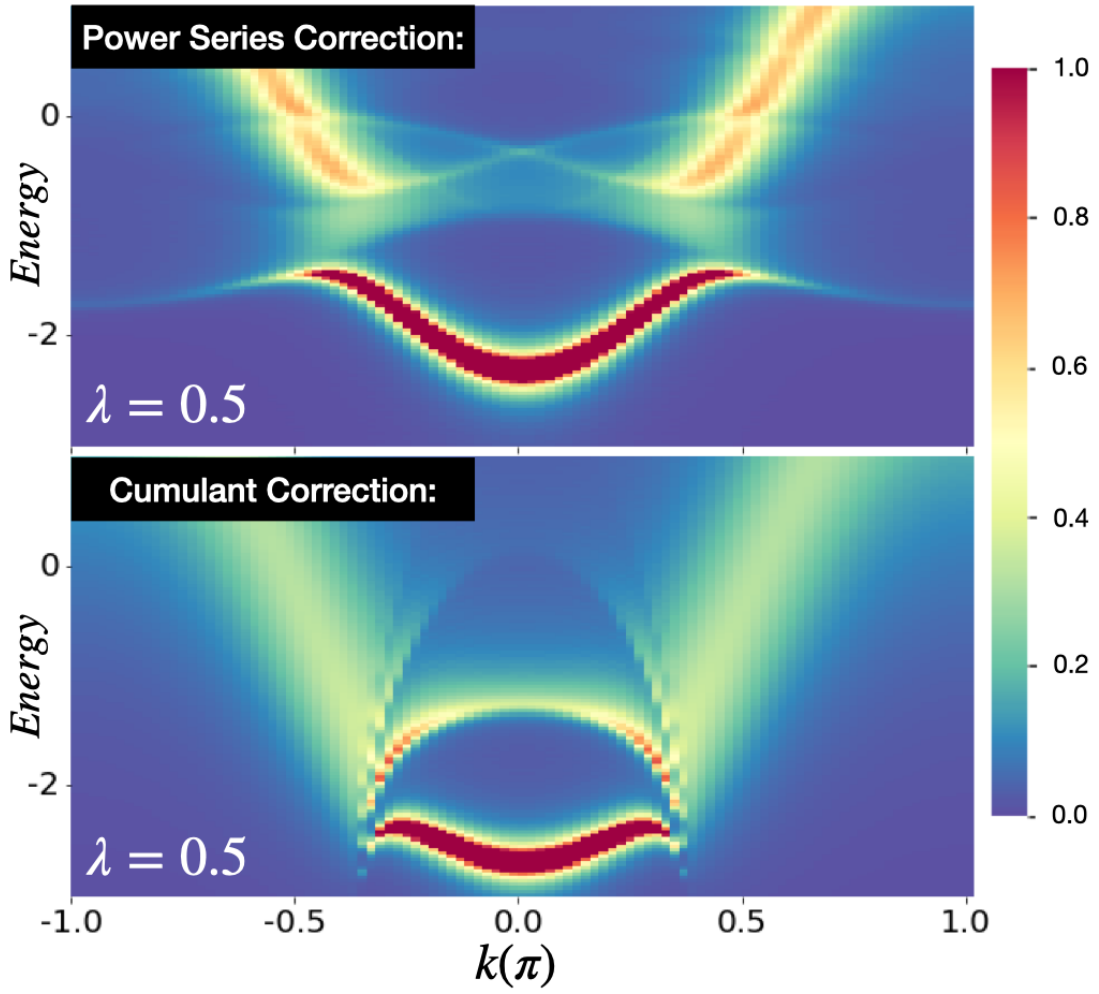

Figure 7.4: The head and the first satellite structure as produced by power series and cumulant expansion for $\lambda = 0.5$, $\epsilon_o = 0, t_{el} = 1, \tilde{\omega} = 1$ and $t_d = 0.2$. The curvature and the extent of the head are very different for the two approximations. The power series satellite also shows a richer structure with multiple crossings and variations in spectral weight as compared to the cumulant.

also significantly lower in cumulant corrected band structure.

7.1.2 Effect of coupling strength on carrier properties

The coupling to the boson also significantly affects the electronic band's curvature as well as the location of the band bottom. As seen in figure 7.8, stronger electron-boson coupling (λ) proportionally flattens and pushes the fractured head of the electronic band away from the

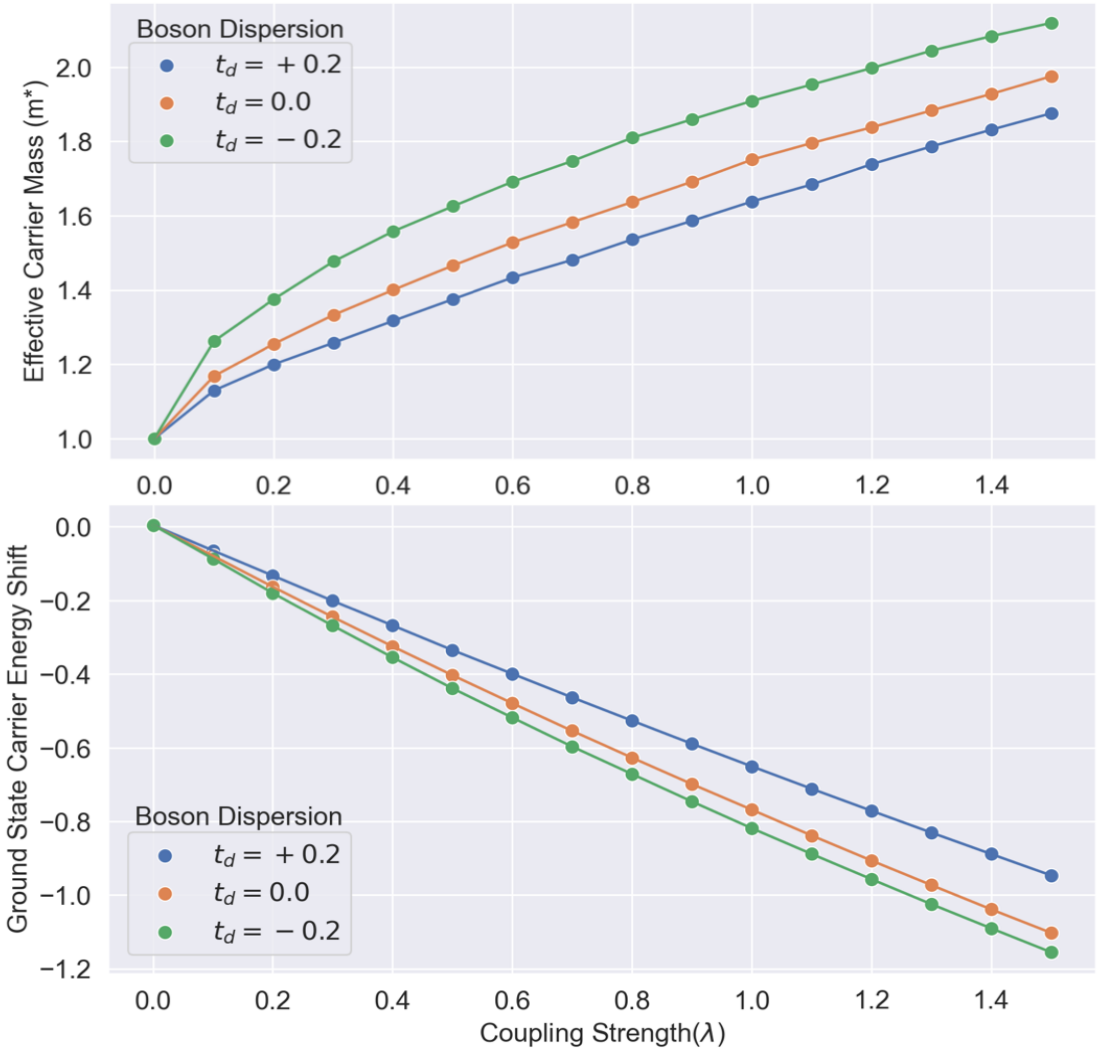

Figure 7.5: Effective carrier mass (top) shows initially grows rapidly but quickly becomes linear with coupling strength λ. The ground state carrier energy (band bottom) also gets displaced linearly to lower energy as a function (λ). The rates of change of both properties depend on boson dispersion(t_d).

non-interacting parabolic fermionic band. The carrier's effective mass is given by the inverse of the band curvature. This effective mass initially grows rapidly but quickly becomes linear with growing coupling strength λ. The head of the band which gives the carrier's ground state energy linearly increases with the coupling strength. That being said, there are differences in the effective mass growth rate as well as the band displacement rate depending on the boson dispersion 't_d' as seen in figure 7.5. A larger carrier effective mass and a smaller carrier

energy displacement is observed for smaller $|\omega_{q=0}|$ mode in (6.2) because of the single boson excitation level (and thus band splitting) being closer to the non-interacting band bottom.

7.2 Validation of Power Series correction

In order to validate our results, we rely upon exact diagonalization results in the same system. The problem with exact diagonalization is its steeply rising cost with each new site and/or each additional boson in the system. This is because of the quadratic dependence of the Hamiltonian matrix on both these factors. Hence, we perform exact diagonalization on 8 site Holstein chain on a finite boson basis. The convergence of features is estimated by increasing the number of bosons. For intermediate coupling of $\lambda = 0.5$ and 3 bosons for each momenta value q, the majority of the features converge and the differences remain only in the smaller features. As seen in figure 7.6, the power series captures the overall

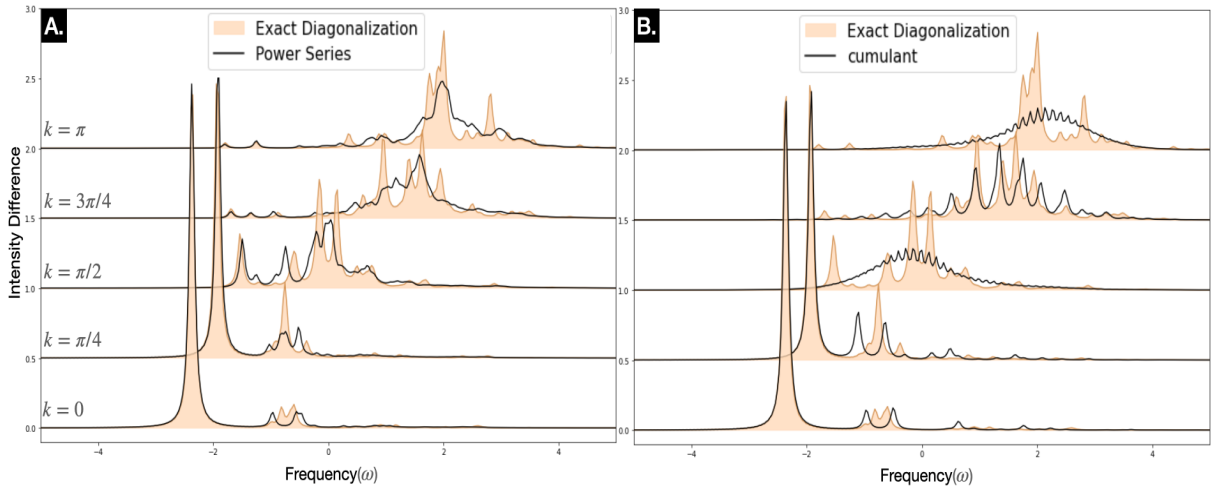

Figure 7.6: (A)Power series (line) closely matches most of the exact diagonalization features (solid) for 8 site Holstein chain at $\lambda = 0.5$. (B)Cumulant matches the exact diagonalization only near $k = 0$.

shape of the spectra as well as most of the larger details of the exact diagonalization. This is especially true of the head of the spectra where the power series almost matched exact diagonalization. Here, the power series performs this calculation within a few minutes while

the exact diagonalization takes numerous hours to complete. In contrast, the cumulant only captures the features well at small momenta (i.e. around $k = 0$). Cumulant spectacularly fails to capture the features at large momenta and represents the spectral features as broad averaged lumps (example $k = \pi/2$ and $k = \pi$ in figure 7.6). Furthermore, the cumulant also fails to capture the curvature at the bottom of the band (features at the negative frequency).

We can of course ask if this 8-site Holstein model with 3 bosons suffers from some finite size effect and if the power series only works for small systems. Now, we present power series results bench-marked against two other methods from the literature. These methods are variational Hilbert space Monte Carlo method (17) and self-consistent cumulant expansion (15). The variational Monte Carlo method suffers from scaling issues just like exact

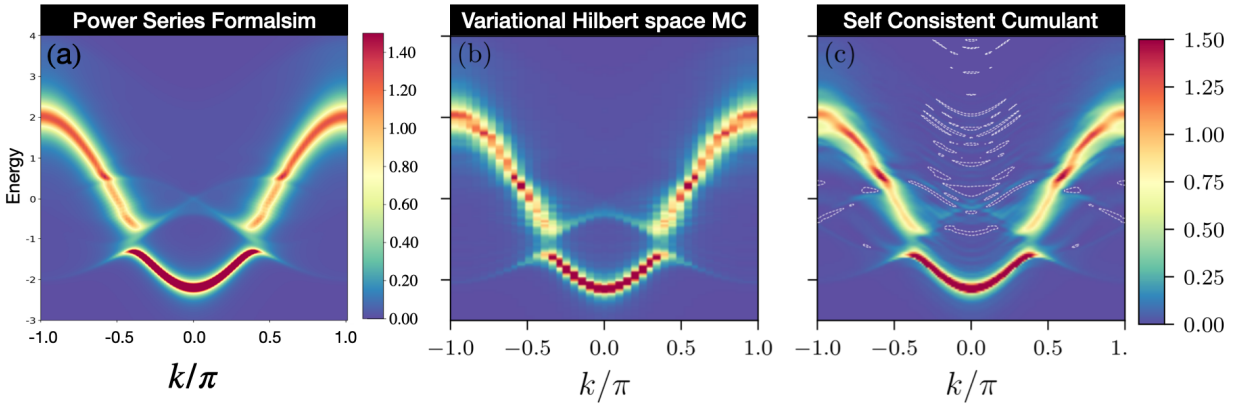

Figure 7.7: Power Series spectra are in excellent agreement with variational Hilbert space Monte Carlo method. Self-consistent cumulant also produces similar results but suffers from artifacts like blooms and negative spectral weights. Here,$\lambda = 0.5, t_d = 4$, and $t_e = \omega_o = 1$

diagonalization. This is because with a larger number of sites, the electron and boson momenta grids become finer making the calculation extremely expensive. The self-consistent cumulant which is closer in spirit to second differential formalism suffers from the sudden onset of divergent in the correction function whenever $\omega_q < \Delta$ is true. Because of this, the correction scheme is truncated before the divergence occurs. This premature truncation leads to artifacts such as blooms and flares and negative spectral weight.

The First differential formalism of power series doesn't suffer from any such drawbacks,

is scalable to incorporate a large number of sites and technically has an infinite number of bosons because of the self-consistency criteria.

7.3 Electron spectral function at extreme coupling strengths

With increasing coupling strength, the system adiabatically moves to a region where Migdal's theorem (61; 12) becomes invalid. This is because by approximating the self-energy with only the very first irreducible self-energy diagram, we neglect many higher-order irreducible diagrams onward of the second order. These diagrams at higher coupling have a non-negligible contribution to particle dynamics. Hence, because of their absence, the spectral function computed with the first-order self-energy is deficient with missing features, incorrect feature sizes, and incorrect separations between features. This also is the reason why exact diagonalization is not feasible in this regime because an extremely high number of bosons is necessary for the validity of the calculated spectra.

Nevertheless, using power series correction with first order self-energy we can assess general features and trends the actual spectra should follow at extreme coupling ($\lambda = 1-1.5$) for zero or finite temperature as shown in figure 7.8. It is surprising that at extreme values of coupling, rather than being more intricate, the satellite structure coagulates and simplifies to look more like a 'replica' of the fermion band's head. Apart from this, there is a significant damping of the fractured arms and a significant increase in the spectral weight of this replica, and a flattening of the band head. Of course, these results must be taken with a grain of salt because of the aforementioned reasons regarding the validity of Migdal's approximation. But this exercise proves that the differential power series method is inherently stable even at extreme values of coupling. Therefore given a more exhaustive set of self-energy diagrams, power series machinery can always produce a better electron spectral function.

7.4 Electron Green's Function at Finite Temperature

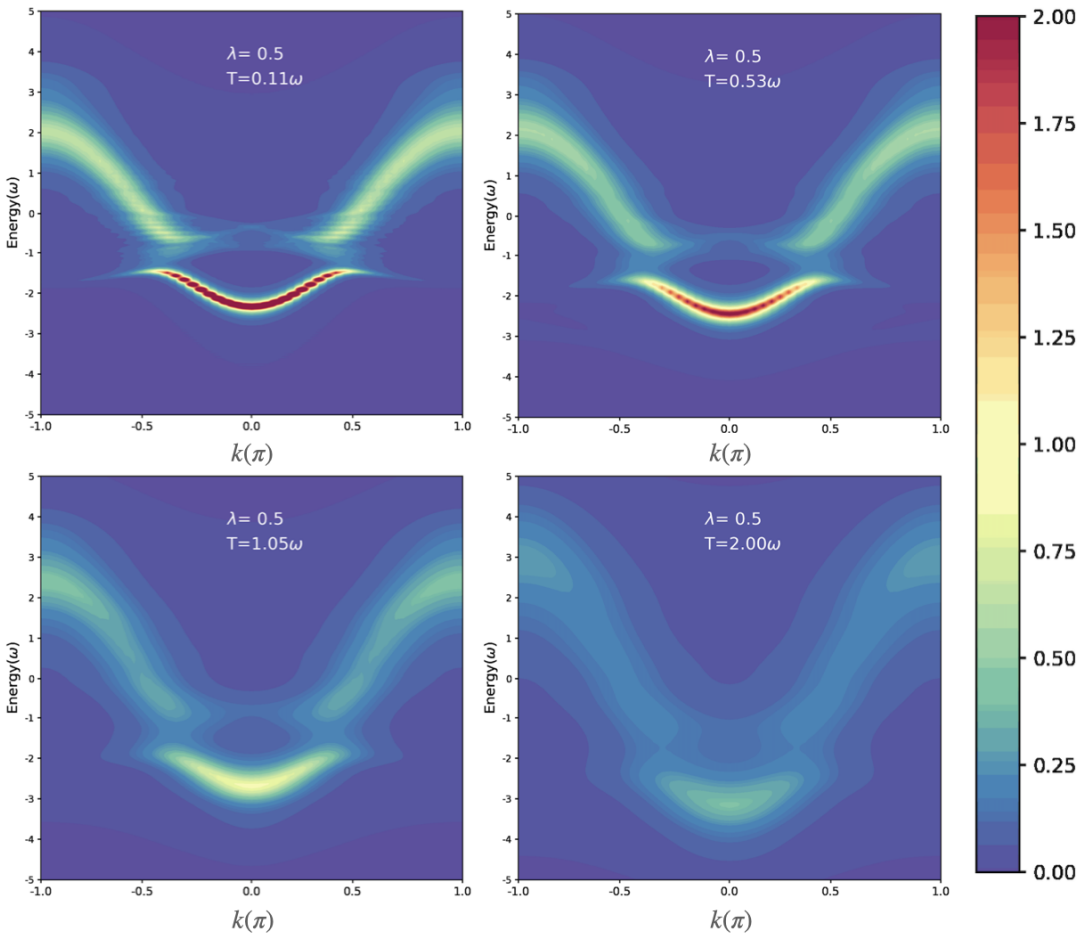

Figure 7.8: Electron spectral function evolution as a function of temperature(T). Here the temperature is in the units of bare boson frequency.

For finite temperature, the main advantage of our method is that the onus of carrying the thermal information lies on the non-interacting Green's functions rather than the power series machinery. Hence, the computation speed and resources required to calculate the finite temperature interacting Green's function remain more-or-less same as that in zero temperature interacting Green's function. This is far from the case of Monte Carlo methods (70; 17) or exact diagonalization because of the thermal trace over infinitely many states in (4.7) due to finite temperature. Here we present the interacting Green's function for finite temperature ($T = 0.5\tilde{\omega}$) at different coupling regimes for N=50 site Holstein chain as shown

in the second row of figure 7.8.

The main effect of temperature is to broaden and stretch the overall band structure on both sides of the fracture because of the onset of finite temperature anti-stokes scattering processes. As shown in figure 7.8, at a very high temperature of $2\omega_o$, there remains no coherent structure in the band structure and hence the distinction between the main band structure and the satellites becomes meaningless given the thickness of the structures.

7.5 Some notes on Second Differential Formalism:

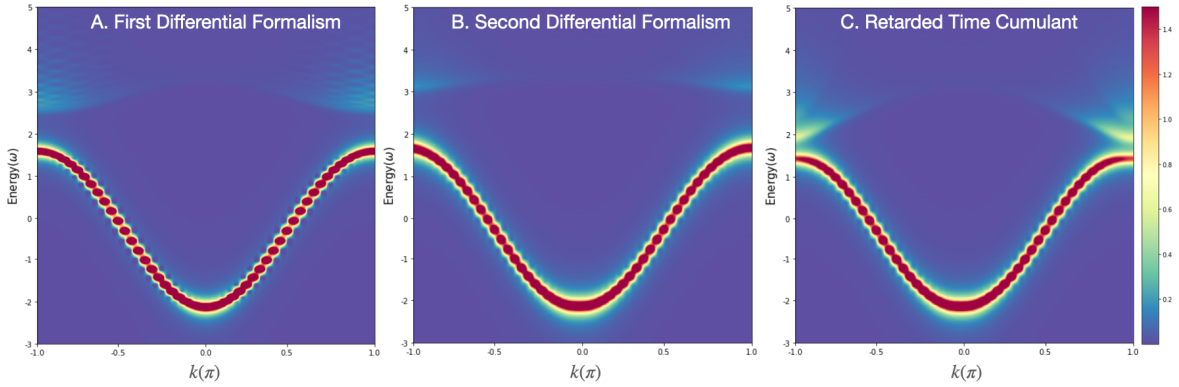

Figure 7.9: Comparison of electron spectral function generated from three different methods. All figures are drawn with the same color scheme.

With regards to the second differential formalism, we show the application on a system with $\omega_o = 5$ and the electronic bandwidth of 4 ($\varepsilon_0 = -2$ and $\varepsilon_\pi = 2$). In this case, the vibrational levels all occur outside the electronic band. Here, in figure 7.9, we show the numerical result from the first differential, second differential, and the retarded cumulant formalism for a 50-site Holstein chain. The first differential formalism takes about 20 minutes to complete. The second differential formalism takes about 3 minutes to complete and the retarded cumulant takes around 20 seconds to complete this calculation.

The cumulant formalism produces a significantly different result with strong boson signatures around the edges of the band structure at $k \approx \pi$. However, the first differential and

the second differential formalism results look qualitatively very similar with broader bosonic satellite features.

Although fast, the second differential formalism diverges whenever the boson frequency ω_q is smaller than the width of the electronic band structure ($\Delta = \max|\varepsilon_k - \varepsilon_{k'}|$). This is the case of strong antibonding-like splitting of some non-interacting electronic energy. Whenever this happens, the temporal contraction relation can no longer be inverted reliably which is at the heart of derivation of second differential formalism (6.13).

$$\mathcal{P}_k(t-\tau) \neq \frac{\mathcal{P}_k(t)}{\mathcal{P}_k(\tau)} \tag{7.1}$$

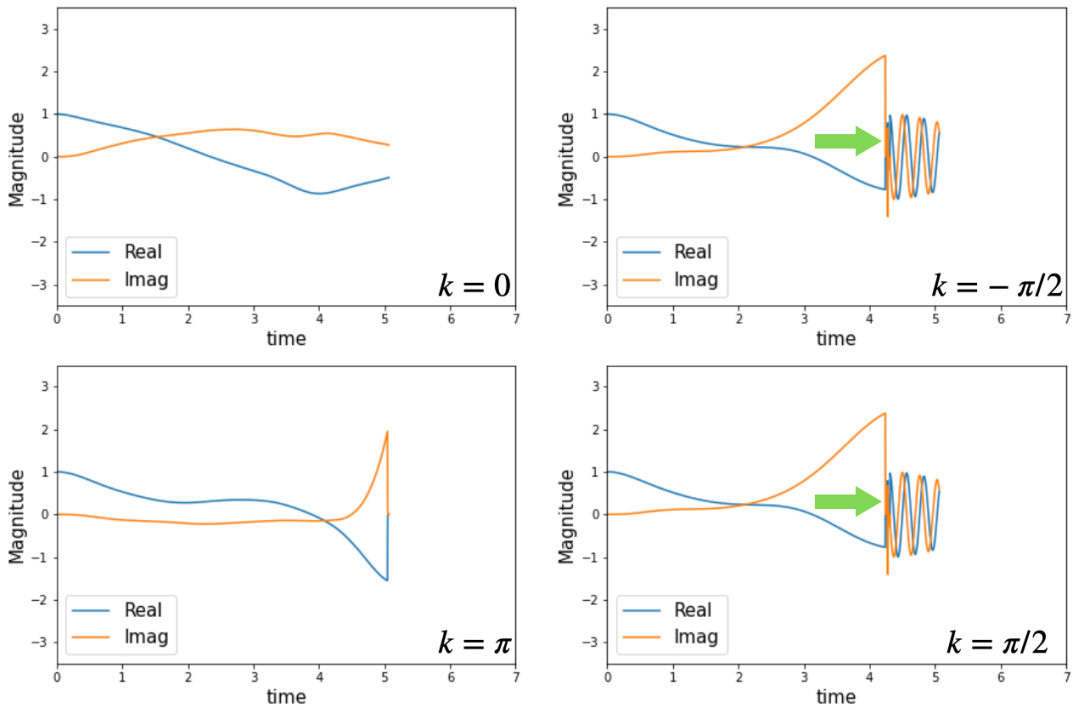

Figure 7.10: Divergence in Power series correction in 4 site Holstein model when $\omega_o < \Delta$ happens.

This happens because the power series term rapidly starts to oscillate in magnitude to account for a stark change in the electronic spectra when splitting happens. At some

point, both the real and the imaginary parts of the power series drop in magnitude to near zero. This makes the power series fraction above (7.1) undefined. At this point, the second derivative on the left-hand side diverges in equation (6.13) and the calculation stops. We show the power series corrections for 4 site Holstein model with $\epsilon_o = 0$, $t_e = 1.5$, $\omega_o = 1$ and $g = 1$ in figure 7.10. The green arrows show the moment when both real and imaginary parts of the power series at $k = \pm\pi/2$ drop rapidly to zero. This then causes the power series piece at $k = \pi$ to also rapidly drop to zero. After this, the calculation terminates because of the inability of computers to handle a '0/0' function.

7.6 Heuristic Argument for the origin of structures

In the context of first differential formalism, we now ask ourselves an ill-defined question - can we predict the features in the interacting system's electronic spectra without actually doing the dynamic temporal correction through the use of power series? In the content of figure 7.11, we ask ourselves the following question. what is the effect of the presence of spectral structures at 'B' and 'C' on the spectral structure at A in the non-interacting electronic band structure?

The answer to this can be found using the following steps:

1. Draw the non-interacting band structure and label points 'A', 'B', and 'C'.

2. Draw the boson band structure centered over points 'B' and 'C' at $\omega_{q=0}$ distance from these points.

3. Draw a vertical line going through 'A' and find its intersection with the previously drawn boson bands. Put spectral weight from 'A' at these intersections with a larger share going to the closer intersection.

More formally, we claim that we can predict most of the locations where spectral weight from any non-interacting ε_k flows towards as well as identify regions where novel structures

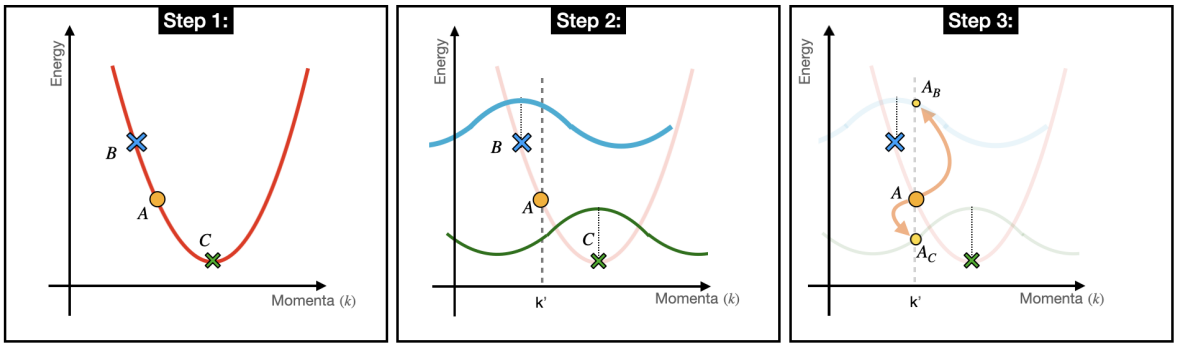

Figure 7.11: Three steps to discern effects of spectral structures at 'B' and 'C' on a spectral structure at 'A'.

(fractures, crosses in satellite structures) occur by simply collecting the complex exponential terms from (6.5) and (4.7).

$$\text{Structures over } \varepsilon_k \approx \sum_q (-ie^{-i\varepsilon_k t})\left[e^{i\varepsilon_k t} e^{-i(\varepsilon_{k-q}+\omega_{k-q})t}\right]$$

The first term $(-ie^{-i\varepsilon^k t})$ is just the non-interacting band structure at momenta k. The second term here represents the erasure some of spectral weight from the non-interacting band at k. The third term $e^{-i(\varepsilon_{k-q}+\omega_{k-q})t}$ represents the effect of the rest of the band structure at momenta k where the aforementioned erased spectral weight flows to. This term is equivalent to drawing a boson band structure centered at every point on the non-interacting band at a distance $\omega_{q=0}$ away as shown in figure 7.11. If we uniformly sample the non-interacting(NI) electronic band structure and follow the recipe above, we see that the spectral weights from a single boson event originating from the non-interacting band coagulates to form a front shown in 7.12. At zero temperature, the electronic band structure is pristine below this front and heavily modified above this front. The electronic band fractures and folds along the creases formed by this coagulated front in our calculation. Single boson events originating from this front create the rich structure of the satellite as discussed in 7.1.1.

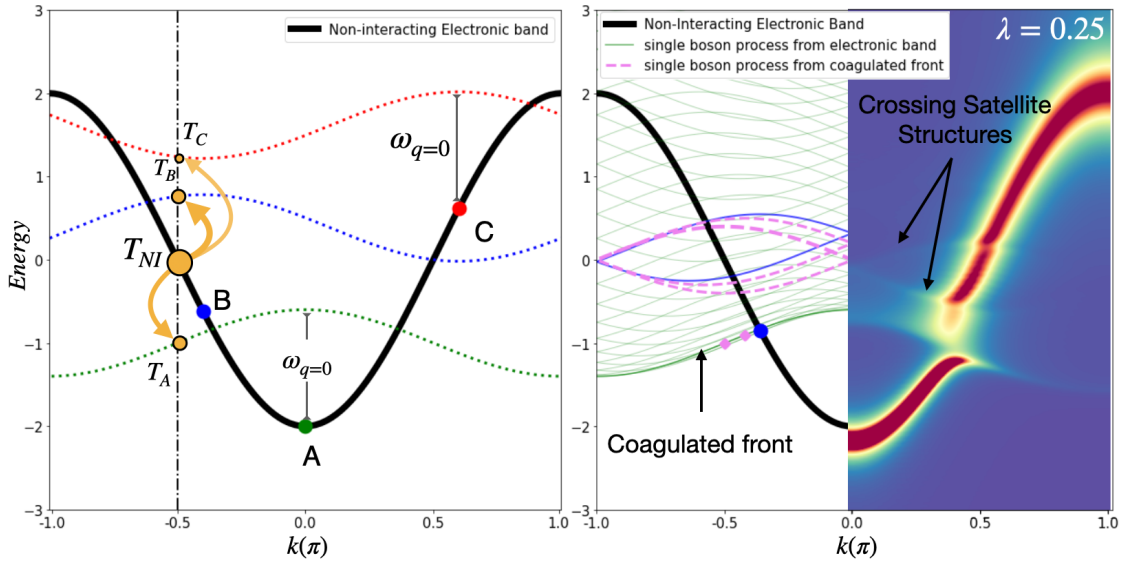

Figure 7.12: (On left)The spectral weight from non-interacting (NI) target point T_{NI} flows to T_A and T_B as described in 7.11. (On right) The Boson band structure drawn over a uniform sampling of a non-interacting electronic band reveals the coagulated front of spectral weights from a single boson process from the NI band. The NI band fractures and bends around this coagulated front. Single boson process from this front forms the crossing satellite structures.

7.7 Summary:

In this chapter, we numerically studied the two power series methods. We found that the first differential formalism produces excellent agreement with exact diagonalization as well as other existing methods in the literature. The second differential formalism only works when the boson energy scale is much larger than the electronic energy scale. We also developed a heuristic argument that explains most of the features in the electronic spectra without having to do the actual calculation.

CHAPTER 8

CONCLUSION AND OUTLOOK

By now, we hope we have convinced the reader of the importance of self-consistency in Green's function calculation. We started with the Dyson's equation and through the aid of a power series function we enforced self-consistency in the Green's function calculation. This was done by making sure that the Green's function inside the self-energy was also corrected through this power series. Doing so, in Holstein Dimer, we revealed the three regimes of the problem. Based on this, we can sketch out a phase diagram along with the applicability regimes of cumulant. Cumulants can only be used when there is a clear

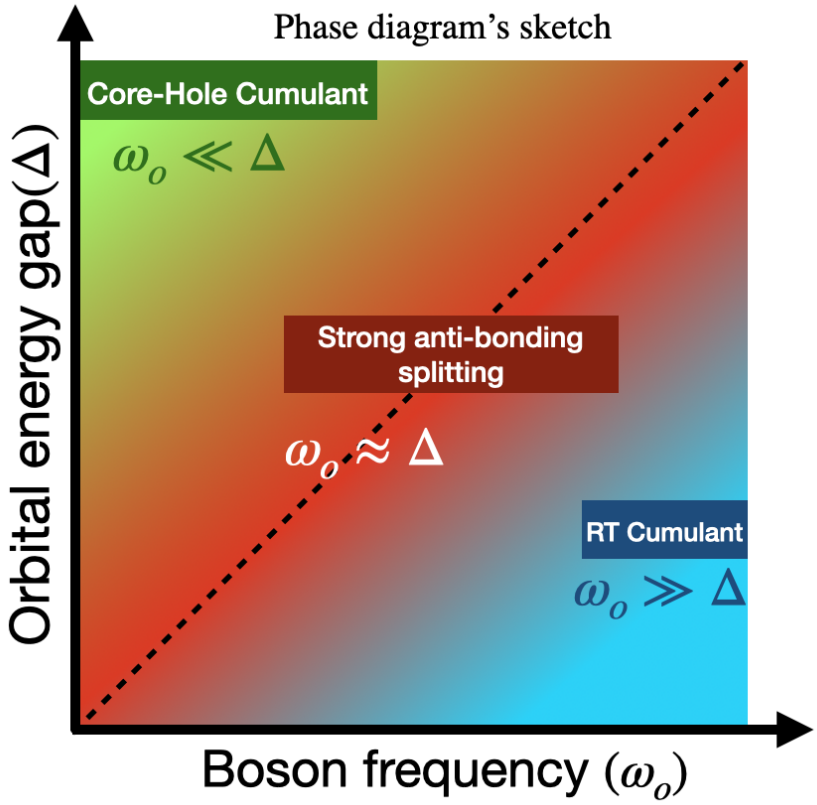

Figure 8.1: A sketch of the phase diagram of Holstein dimer

separation of electronic and bosonic energy scales in the problem. In the middle, of this

phase diagram, the electron boson coupling significantly alters the electronic spectra and cumulants spectacularly fail to capture this. However, the power series works in all regimes without any approximation.

With regards to the cost associated with the Power series, of course, it is more expensive than Cumulant. For the cumulant, the implementation time is almost instantaneous (in seconds for large systems). Each cycle of the integral power series is almost as expensive as the cumulant. Hence for Holstein dimer, the calculation takes about a couple of minutes. At the thermodynamic limit of large number of sites, the differential power series can produce spectral functions with an implementation time of roughly 20 minutes for 100 sites. And this is independent of the value of the coupling constant. Given that exact diagonalization is impossible at this limit without the aid of a supercomputer and there too one faces severe scaling limitations due to the requirement of large boson numbers at large g, tens of minutes is a very reasonable time. Furthermore, power series results are in excellent agreement when compared to literature as well as exact diagonalization in a smaller number of sites.

Given all of these benefits, this method, in our opinion, is ripe enough to be implemented in real systems. We of course showed a preliminary implementation on silicon. But performance in GW for crystals as well as in molecular spectroscopy is a topic worthy of future investigation. In problems with multiple boson species (say plasmons and phonons), this method allows for the inclusion of both bosons' physics without needing to know the microscopic details of the problem.

Of course, this method has to break at some very high value of g. This is the limit where the problem is boson dominant and the fermionic quasiparticle picture completely breaks down. In such problems where bosonic physics is dominant, we could turn this method upside down and ask what is the effect of the presence of fermion or other minor bosons on boson spectra. Given the current surge of interest in polariton physics, this is another path worthy of exploration.

A final direction we would like to point out is to use power series as a Machine Learning example generator in model systems in order to learn what these interaction operators are doing in such problems. Given the performance and flexibility in parameter choice, a large number of examples can easily be generated using this technique and the interaction operator's effect can effectively be learned for various values of parameter. Once this is done, this Machine learned operator can be set free on band structures obtained from purely electronic calculations in order to capture the bosonic effects in an even faster way regardless of the band structure complexity.

REFERENCES

[1] D. S. Pines, "A collective description of-electron interactions: III. coulomb interactions in a degenerate electron gas," *Physical Review*, vol. 92, pp. 609–625, 1953.

[2] R. L. Dally, A. J. Heng, A. Keselman, M. M. Bordelon, M. B. Stone, L. Balents, and S. D. Wilson, "Three-Magnon Bound State in the Quasi-One-Dimensional Antiferromagnet $\alpha - \mathrm{NaMnO_2}$," *Physical Review Letters*, vol. 124, p. 197203, May 2020. Publisher: American Physical Society.

[3] M. C. T. D. Müller, S. Blügel, and C. Friedrich, "Electron-magnon scattering in elementary ferromagnets from first principles: Lifetime broadening and band anomalies," *Phys. Rev. B*, vol. 100, p. 045130, Jul 2019.

[4] X. Ma, Z. Cheng, M. Tian, X. Liu, X. Cui, Y. Huang, S. Tan, J. Yang, and B. Wang, "Formation of Plasmonic Polarons in Highly Electron-Doped Anatase $\mathrm{TiO_2}$," *Nano Letters*, Dec. 2020. Publisher: American Chemical Society.

[5] C. Lemell, S. Neppl, G. Wachter, K. Tőkési, R. Ernstorfer, P. Feulner, R. Kienberger, and J. Burgdörfer, "Real-time observation of collective excitations in photoemission," *Physical Review B*, vol. 91, p. 241101, June 2015. Publisher: American Physical Society.

[6] M. Guzzo, G. Lani, F. Sottile, P. Romaniello, M. Gatti, J. J. Kas, J. J. Rehr, M. G. Silly, F. Sirotti, and L. Reining, "Valence Electron Photoemission Spectrum of Semiconductors: Ab Initio Description of Multiple Satellites," *Physical Review Letters*, vol. 107, p. 166401, Oct. 2011. Publisher: American Physical Society.

[7] J. P. Perdew, "Density functional theory and the band gap problem," *International Journal of Quantum Chemistry*, vol. 28, no. S19, 1985.

[8] X. Gonze, "Adiabatic density-functional perturbation theory," *Physical Review A*, vol. 52, pp. 1096–1114, Aug. 1995. Publisher: American Physical Society.

[9] J. Deslippe, G. Samsonidze, D. A. Strubbe, M. Jain, M. L. Cohen, and S. G. Louie, "BerkeleyGW: A massively parallel computer package for the calculation of the quasiparticle and optical properties of materials and nanostructures," *Computer Physics Communications*, vol. 183, no. 6, pp. 1269–1289, 2012.

[10] M. Govoni and G. Galli, "Large Scale GW Calculations," *Journal of Chemical Theory and Computation*, vol. 11, pp. 2680–2696, June 2015. Publisher: American Chemical Society.

[11] J. J. Kas, J. J. Rehr, and L. Reining, "Cumulant expansion of the retarded one-electron Green function," *Physical Review B*, vol. 90, p. 085112, Aug. 2014.

[12] O. Gunnarsson, V. Meden, and K. Schönhammer, "Corrections to Migdal's theorem for spectral functions: A cumulant treatment of the time-dependent Green's function," *Physical Review B*, vol. 50, pp. 10462–10473, Oct. 1994.

[13] J. S. Zhou, M. Gatti, J. J. Kas, J. J. Rehr, and L. Reining, "Cumulant Green's function calculations of plasmon satellites in bulk sodium: Influence of screening and the crystal environment," *Physical Review B*, vol. 97, p. 035137, Jan. 2018. Publisher: American Physical Society.

[14] F. Caruso, H. Lambert, and F. Giustino, "Band Structures of Plasmonic Polarons," *Physical Review Letters*, vol. 114, p. 146404, Apr. 2015. Publisher: American Physical Society.

[15] P. J. Robinson, I. S. Dunn, and D. R. Reichman, "Cumulant methods for electron-phonon problems. II. The self-consistent cumulant expansion," *Physical Review B*, vol. 105, p. 224305, June 2022. Publisher: American Physical Society.

[16] P. J. Robinson, I. S. Dunn, and D. R. Reichman, "Cumulant methods for electron-

phonon problems. I. Perturbative expansions," *Physical Review B*, vol. 105, p. 224304, June 2022. Publisher: American Physical Society.

[17] J. Bonča, S. A. Trugman, and M. Berciu, "Spectral function of the Holstein polaron at finite temperature," *Physical Review B*, vol. 100, p. 094307, Sept. 2019. Publisher: American Physical Society.

[18] O. S. Barišić, "Calculation of excited polaron states in the Holstein model," *Physical Review B*, vol. 69, p. 064302, Feb. 2004. Publisher: American Physical Society.

[19] G. De Filippis, V. Cataudella, V. M. Ramaglia, and C. A. Perroni, "Static and dynamic polaron features in a coherent-state basis," *Physical Review B*, vol. 72, p. 014307, July 2005. Publisher: American Physical Society.

[20] J. L. M. van Mechelen, D. van der Marel, C. Grimaldi, A. B. Kuzmenko, N. P. Armitage, N. Reyren, H. Hagemann, and I. I. Mazin, "Electron-phonon interaction and charge carrier mass enhancement in $SrTiO_3$," *Phys. Rev. Lett.*, vol. 100, p. 226403, Jun 2008.

[21] J. T. Devreese, S. N. Klimin, J. L. M. van Mechelen, and D. van der Marel, "Many-body large polaron optical conductivity in $SrTi_{1-x}Nb_xO_3$," *Phys. Rev. B*, vol. 81, p. 125119, Mar 2010.

[22] Z. Wang, S. McKeown Walker, A. Tamai, Y. Wang, Z. Ristic, F. Y. Bruno, A. de la Torre, S. Riccò, N. C. Plumb, M. Shi, P. Hlawenka, J. Sánchez-Barriga, A. Varykhalov, T. K. Kim, M. Hoesch, P. D. C. King, W. Meevasana, U. Diebold, J. Mesot, B. Moritz, T. P. Devereaux, M. Radovic, and F. Baumberger, "Tailoring the nature and strength of electron–phonon interactions in the $SrTiO_3$(001) 2D electron liquid," *Nature Materials*, vol. 15, Aug. 2016.

[23] A. G. Swartz, H. Inoue, T. A. Merz, Y. Hikita, S. Raghu, T. P. Devereaux, S. Johnston,

and H. Y. Hwang, "Polaronic behavior in a weak-coupling superconductor," *Proceedings of the National Academy of Sciences*, vol. 115, no. 7, pp. 1475–1480, 2018.

[24] A. Edelman and P. B. Littlewood, "Normal state correlates of plasmon-polaron superconductivity in strontium titanate," 2021.

[25] O. Rösch, O. Gunnarsson, X. J. Zhou, T. Yoshida, T. Sasagawa, A. Fujimori, Z. Hussain, Z.-X. Shen, and S. Uchida, "Polaronic behavior of undoped high-T_c cuprate superconductors from angle-resolved photoemission spectra," *Phys. Rev. Lett.*, vol. 95, p. 227002, Nov 2005.

[26] A. Damascelli, Z. Hussain, and Z.-X. Shen, "Angle-resolved photoemission studies of the cuprate superconductors," *Reviews of Modern Physics*, vol. 75, pp. 473–541, Apr. 2003. Publisher: American Physical Society.

[27] E. Baldini, M. A. Sentef, S. Acharya, T. Brumme, E. Sheveleva, F. Lyzwa, E. Pomjakushina, C. Bernhard, M. v. Schilfgaarde, F. Carbone, A. Rubio, and C. Weber, "Electron–phonon-driven three-dimensional metallicity in an insulating cuprate," *Proceedings of the National Academy of Sciences*, vol. 117, pp. 6409–6416, Mar. 2020.

[28] S. Yang, J. A. Sobota, D. Leuenberger, A. F. Kemper, J. J. Lee, F. T. Schmitt, W. Li, R. G. Moore, P. S. Kirchmann, and Z.-X. Shen, "Thickness-dependent coherent phonon frequency in ultrathin FeSe/$SrTiO_3$ films," *Nano Letters*, vol. 15, no. 6, pp. 4150–4154, 2015. PMID: 26027951.

[29] P. Pingel and D. Neher, "Comprehensive picture of p -type doping of P3HT with the molecular acceptor F 4 TCNQ," *Physical Review B*, vol. 87, p. 115209, Mar. 2013.

[30] R. Ghosh, A. R. Chew, J. Onorato, V. Pakhnyuk, C. K. Luscombe, A. Salleo, and F. C. Spano, "Spectral Signatures and Spatial Coherence of Bound and Unbound Polarons

in P3HT Films: Theory Versus Experiment," *The Journal of Physical Chemistry C*, vol. 122, pp. 18048–18060, Aug. 2018. Publisher: American Chemical Society.

[31] Y. Chen, S. Ghosh, X. Liu, I. V. Zozoulenko, M. Fahlman, and S. Braun, "Experimental and Theoretical Investigation into the Polaron Structure of K-Doped Polyfluorene Films," *The Journal of Physical Chemistry C*, vol. 125, pp. 937–945, Jan. 2021.

[32] R. Ghosh and F. C. Spano, "Excitons and Polarons in Organic Materials," *Accounts of Chemical Research*, vol. 53, pp. 2201–2211, Oct. 2020. Publisher: American Chemical Society.

[33] G. Acbas, K. A. Niessen, E. H. Snell, and A. G. Markelz, "Optical measurements of long-range protein vibrations," *Nature Communications*, vol. 5, p. 3076, Jan. 2014. Number: 1 Publisher: Nature Publishing Group.

[34] N. L. Ing, M. Y. El-Naggar, and A. I. Hochbaum, "Going the Distance: Long-Range Conductivity in Protein and Peptide Bioelectronic Materials," *The Journal of Physical Chemistry B*, vol. 122, pp. 10403–10423, Nov. 2018. Publisher: American Chemical Society.

[35] D. R. Hekstra, K. I. White, M. A. Socolich, R. W. Henning, V. Šrajer, and R. Ranganathan, "Electric-field-stimulated protein mechanics," *Nature*, vol. 540, pp. 400–405, Dec. 2016. Number: 7633 Publisher: Nature Publishing Group.

[36] V. Cataudella, G. De Filippis, A. S. Mishchenko, and N. Nagaosa, "Temperature Dependence of the Angle Resolved Photoemission Spectra in the Undoped Cuprates: Self-Consistent Approach to the t J Holstein Model," *Physical Review Letters*, vol. 99, p. 226402, Nov. 2007.

[37] L. Rettig, R. Cortés, H. S. Jeevan, P. Gegenwart, T. Wolf, J. Fink, and U. Bovensiepen, "Electron–phonon coupling in 122 Fe pnictides analyzed by femtosecond time-resolved

photoemission," *New Journal of Physics*, vol. 15, p. 083023, Aug. 2013. Publisher: IOP Publishing.

[38] A. N. Das and S. Sil, "Small to large polaron transition in a strongly correlated system," *Physica C: Superconductivity*, vol. 207, pp. 51–57, Mar. 1993.

[39] A. J. Millis, P. B. Littlewood, and B. I. Shraiman, "Double Exchange Alone Does Not Explain the Resistivity of $La_{1-x}Sr_xMnO_3$," *Physical Review Letters*, vol. 74, pp. 5144–5147, June 1995. Publisher: American Physical Society.

[40] A. Millis, B. Shraiman, and R. Mueller, "Dynamic jahn-teller effect and colossal magnetoresistance in $La_{1-x}Sr_xMnO_3$," *Physical Review Letters*, vol. 77, no. 1, pp. 175–178, 1996.

[41] J. Zaanen and P. B. Littlewood, "Freezing electronic correlations by polaronic instabilities in doped La_2NiO_4," *Physical Review B*, vol. 50, pp. 7222–7225, Sept. 1994.

[42] M. Mohamed, M. M. May, M. Kanis, M. Brützam, R. Uecker, R. v. d. Krol, C. Janowitz, and M. Mulazzi, "The electronic structure and the formation of polarons in Mo-doped $BiVO_4$ measured by angle-resolved photoemission spectroscopy," *RSC Advances*, vol. 9, no. 27, 2019.

[43] X.-C. Ma, Y. Dai, L. Yu, and B.-B. Huang, "Energy transfer in plasmonic photocatalytic composites," *Light: Science & Applications*, vol. 5, pp. e16017–e16017, Feb. 2016. Number: 2 Publisher: Nature Publishing Group.

[44] I. N. Hulea, S. Fratini, H. Xie, C. L. Mulder, N. N. Iossad, G. Rastelli, S. Ciuchi, and A. F. Morpurgo, "Tunable Fröhlich polarons in organic single-crystal transistors," *Nature Materials*, vol. 5, pp. 982–986, Dec. 2006. Number: 12 Publisher: Nature Publishing Group.

[45] M. Kang, S. W. Jung, W. J. Shin, Y. Sohn, S. H. Ryu, T. K. Kim, M. Hoesch, and K. S. Kim, "Holstein polaron in a valley-degenerate two-dimensional semiconductor," *Nature Materials*, vol. 17, Aug. 2018.

[46] H. Tang, C.-J. Chen, Z. Huang, J. Bright, G. Meng, R.-S. Liu, and N. Wu, "Plasmonic hot electrons for sensing, photodetection, and solar energy applications: A perspective," *The Journal of Chemical Physics*, vol. 152, p. 220901, June 2020. Publisher: American Institute of Physics.

[47] S. K. Cushing and N. Wu, "Progress and Perspectives of Plasmon-Enhanced Solar Energy Conversion," *The Journal of Physical Chemistry Letters*, vol. 7, pp. 666–675, Feb. 2016. Publisher: American Chemical Society.

[48] C. Melnick and M. Kaviany, "Phonovoltaic. I. Harvesting hot optical phonons in a nanoscale $p-n$ junction," *Physical Review B*, vol. 93, p. 094302, Mar. 2016. Publisher: American Physical Society.

[49] C. Melnick and M. Kaviany, "Phonovoltaic. III. Electron-phonon coupling and figure of merit of graphene:BN," *Physical Review B*, vol. 94, p. 245412, Dec. 2016. Publisher: American Physical Society.

[50] J. M. Riley, F. Caruso, C. Verdi, L. B. Duffy, M. D. Watson, L. Bawden, K. Volckaert, G. van der Laan, T. Hesjedal, M. Hoesch, F. Giustino, and P. D. C. King, "Crossover from lattice to plasmonic polarons of a spin-polarised electron gas in ferromagnetic EuO," *Nature Communications*, vol. 9, p. 2305, June 2018. Number: 1 Publisher: Nature Publishing Group.

[51] B. Pandey and P. B. Littlewood, "Going beyond the Cumulant Approximation: Power Series Correction to the Single-Particle Green's Function in the Holstein System," *Physical Review Letters*, vol. 129, p. 136401, Sept. 2022.

[52] B. Pandey and P. B. Littlewood, "Going Beyond the Cumulant Approximation II :Power Series Correction to Single Particle Green's Function in 1D Holstein Chain," Mar. 2023. arXiv:2303.03503 [cond-mat].

[53] G. D. Mahan, *Many-Particle Physics*. Boston, MA: Springer US, 2000.

[54] E. K. Gross and E. Runge, *Many-particle theory*. Adam Hilger Ltd, 1986.

[55] P. Coleman, *Introduction to Many-Body Physics*. Cambridge University Press, 2015.

[56] N. W. Ashcroft and N. D. Mermin, *Solid State Physics*. Holt-Saunders, 1976.

[57] T. Azumi and K. Matsuzaki, "What does the term "vibronic coupling" mean?," *Photochemistry and Photobiology*, vol. 25, no. 3, pp. 315–326, 1977.

[58] J. P. Perdew and A. Ruzsinszky, "Fourteen easy lessons in density functional theory," *International Journal of Quantum Chemistry*, vol. 110, no. 15, pp. 2801–2807, 2010.

[59] A. Klamt, "Tight-binding polarons. i. a new variational approach to the molecular-crystal model," *Journal of Physics C: Solid State Physics*, vol. 21, p. 1953, apr 1988.

[60] R. D. Mattuck, *A guide to Feynman diagrams in the many-body problem*. Courier Corporation, 1992.

[61] A. B. Migdal, "Interaction Between Electrons and the Lattice Vibrations in a normal Metal," *Zhur. Eksptl'. i Teoret. Fiz.*, vol. Vol: 34, June 1958. Institution: Moscow Inst. of Engineering Physics.

[62] D. C. Langreth, "Singularities in the X-Ray Spectra of Metals," *Physical Review B*, vol. 1, pp. 471–477, Jan. 1970.

[63] O. Burrau, "Berechnung des Energiewertes des Wasserstoffmolekel-Ions (H2+) im Normalzustand," *Naturwissenschaften*, vol. 15, Jan. 1927.

[64] E. J. Heller, E. B. Stechel, and M. J. Davis, "Molecular spectra, Fermi resonances, and classical motion: Example of CO_2," *The Journal of Chemical Physics*, vol. 71, Dec. 1979.

[65] E. J. Heller, E. B. Stechel, and M. J. Davis, "Molecular spectra, Fermi resonances, and classical motion," *The Journal of Chemical Physics*, vol. 73, Nov. 1980.

[66] J. Ranninger and U. Thibblin, "Two-site polaron problem: Electronic and vibrational properties," *Phys. Rev. B*, vol. 45, pp. 7730–7738, Apr 1992.

[67] F. Aryasetiawan, L. Hedin, and K. Karlsson, "Multiple Plasmon Satellites in Na and Al Spectral Functions from Ab Initio Cumulant Expansion," *Physical Review Letters*, vol. 77, pp. 2268–2271, Sept. 1996.

[68] K. Luchner and H. Micklitz, "Phonon sidebands (stokes and anti-stokes) in the optical spectra of rare earth atoms in rare gas matrices," *Journal of Luminescence*, vol. 18-19, pp. 882–886, Jan. 1979.

[69] D. J. J. Marchand and M. Berciu, "Effect of dispersive optical phonons on the behavior of a Holstein polaron," *Physical Review B*, vol. 88, p. 060301, Aug. 2013. Publisher: American Physical Society.

[70] J. Bonča and S. A. Trugman, "Dynamic properties of a polaron coupled to dispersive optical phonons," *Physical Review B*, vol. 103, p. 054304, Feb. 2021. Publisher: American Physical Society.

[71] T. Holstein, "Studies of polaron motion: Part I. The molecular-crystal model," *Annals of Physics*, vol. 8, pp. 325–342, Nov. 1959.

[72] M. D. Kaplan and G. O. Zimmerman, "Mechanism of colossal magnetoresistance and the role of electron correlations by virtual phonon exchange," *Journal of Physics and Chemistry of Solids*, vol. 59, pp. 2218–2219, Oct. 1998.